THE COLLAPSE OF COMPOSITE CYLINDRICAL PANELS WITH VARIOUS THICKNESS USING FINITE ELEMENT ANALYSIS

THESIS

Christopher P. Chaplin, Second Lieutenant, USAF

AFIT/GA/ENY/94D-4

DEPARTMENT OF THE AIR FORCE
AIR UNIVERSITY
AIR FORCE INSTITUTE OF TECHNOLOGY

Wright-Patterson Air Force Base, Ohio

AFIT/GA/ENY/94D-4

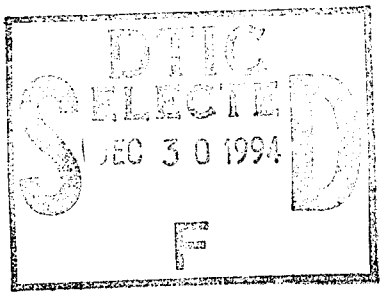

THE COLLAPSE OF COMPOSITE CYLINDRICAL PANELS WITH VARIOUS THICKNESS USING FINITE ELEMENT ANALYSIS

THESIS

Christopher P. Chaplin, Second Lieutenant, USAF

AFIT/GA/ENY/94D-4

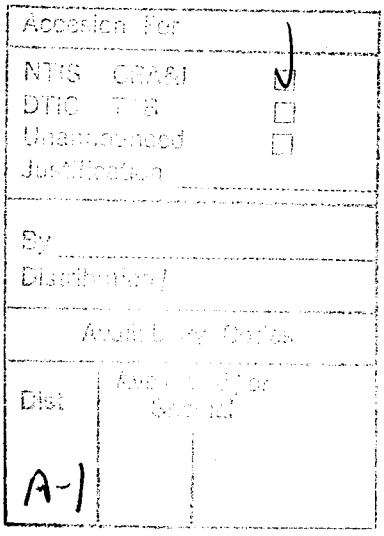

Approved for public release; distribution unlimited

The views expressed in this thesis are those

of the author and do not reflect the official policy or

position of the Department of Defense or the U. S. Government

AFIT/GA/ENY/94D-4

THE COLLAPSE OF COMPOSITE CYLINDRICAL PANELS WITH VARIOUS THICKNESS USING FINITE ELEMENT ANALYSIS

THESIS

Presented to the Faculty of the Graduate School of Engineering

of the Air Force Institute of Technology

Air University

In Partial Fulfillment of the

Requirements for the Degree of

Master of Science in Astronautical Engineering

Christopher P. Chaplin

Second Lieutenant, USAF

December, 1994

Acknowledgments

I would like thank my family for their support throughout this entire endeavor. I am especially grateful for having my grandparents, Bob and Margaret Haney, and my aunt and uncle, Sue and Rob Haney, in the area. I want to thank them for including me in their daily affairs and making me feel so welcome in their homes. I will especially miss little Ryan Haney, who always kept a smile on my face. As for my parents, I want to thank them for encouraging me and pushing me to finish. Also, I must praise my roommate, David Keener, for putting up with me.

I am grateful to all the helpful people at the Air Force Institute of Technology and the Flight Dynamics Lab. No matter what the problem, there was always someone who could help. First, there was Captain Jim Greer who helped introduce me to the SHELL program. Then there was Captain Scott Shimmels who patiently endured with me as I struggled to increase the capabilities of the program CLASSIC. I also must thank Captain Scott Morton for sitting down with me and teaching me how to use the Tecplot software. As a Second Lieutenant, I can consider my self fortunate to have role models such as these to look to for their professionalism and their extreme willingness to go out of their way to help. In addition, I am extremely grateful to my thesis advisor, Dr. Anthony Palazotto for his guidance and encouragement throughout the entire thesis process.

Finally, I acknowledge Jesus Christ as the most important influence in my life. No one else has done as much for me as Him. During this time, no one else has been as great a source of strength or encouragement to me. Without Him, I could not have made it.

Table of Contents

List of Figures

List of Tables

Abstract

This study compared numerical collapse results of graphite/epoxy cylindrical panels with free vertical edges undergoing axial compression for three different shell theories. Symmetric quasi-isotropic laminates were investigated using solid panels and panels with five different centralized cutouts with three thicknesses. The theories compared in the study were the Simplified Large displacement moderate Rotation (SLR) theory, the Donnell Cylindrical Shell (Modified Donnell) theory, and the Classical Donnell theory. The purpose of the study was to determine when large rotations and through-the-thickness shear become important in the numerical collapse analysis of cylindrical composite shells. The SLR theory takes into account large rotations in its sophisticated higher order strain terms and coupling of the u, v, and w displacements into the rotational terms. Both the SLR and Modified Donnell theories incorporate a parabolic transverse shear strain distribution through the thickness. The Classical Donnell theory neglects both rotations and shear strain. By observing cases where the numerical collapse results differed noticeably (>3%), it could be determined when large rotations and through-the-thickness shear were important. The effects of large rotations were noticed in nearly all of the panels with large cutouts (>3% panel area). Large rotations were also found to be important for thicker panels with either no cutout or a small cutout. The effects of through-the-thickness shear were only noticed in the thickest panels with large cutouts. Also, a trend was noticed in some of the large cutouts in which the effects of through-the-thickness shear increases with increasing thickness while the effects of large rotations appeared to become less dominant.

THE COLLAPSE OF COMPOSITE CYLINDRICAL PANELS WITH VARIOUS THICKNESS USING FINITE ELEMENT ANALYSIS

I. Introduction

1.1 Background

Composite materials are being used increasingly more often in modern aircraft as designers attempt to improve the overall strength to weight ratio of airframes and enhance the stiffness of particular components. These lighter, stronger aircraft allow for higher performance with no increase in fuel consumption. Because of the aerodynamic shapes of aircraft fuselages and wings, shell structures or panels are frequently used. Often, aircraft require openings in these composite shell structures for windows, landing gear doors, or access panels. These holes or imperfections change the collapse characteristics of the structure. Depending on the dimensionality and area of the cutout, the load carrying ability of the structure may be greatly reduced [1].

Axial compression of monocoque cylindrical shells has long been a challenging problem because of the inherent nonlinearities involved due to the curved nature of these structures. This nonlinearity becomes even more predominant as the thickness of the shell panel and the area removed from the shell by a cutout increase [1,2]. Previous research concerning the collapse of composite shell structures with large centrally located cutouts has mostly been done by the Air Force Institute of Technology (AFIT) and the National Aeronautical and Space Administration (NASA) [1]. A great deal of research on geometric instability of composite shells without cutouts has been published [3-6] as has some material on isotropic shells with and without cutouts [7-11].

Initially, most work on composite panels with cutouts focused on shells with smaller sized cutouts (cutout < 3% of panel area). Janisse [12] studied the effects of a small cutout, comparing experimental to analytical results. He found that the collapse characteristics of composite cylindrical panels are dependent upon ply lay-up and size of the cutout. Several investigations made in the area of composite shell structures with large cutouts have been conducted at AFIT. Some of the earliest work utilized the non-linear capability of Lockheed's energy based finite element program Structural Analysis for General Shells (STAGSC-1). Tisler [13,14] compared STAGSC computer results to experimental results and found that STAGSC did not seem capable of handling the large rotations inherent to large cutouts. Schimmels [15,16] compared experimental results for composite shell panels with large cutouts using both STAGSC and the SHELL program developed by Scott Dennis [2] as part of his doctoral dissertation on a large displacement and rotational formulation for composite shells. Schimmels concluded that the SHELL program provided better results for panels with large cutouts with free edge rotations greater than 17 degrees compared to STAGSC results. In addition, Dennis and Palazotto found that experimental test results for panel surface rotations around a 101.6 mm x 101.6 mm (4" X 4") cutout, obtained by Tisler, in comparison with STAGSC-1 results exceeded the intermediate nonlinear capability of the STAGSC-1 program [17].

In other research at AFIT, Captain James Hatfield investigated the effects of thickness, ply layup, and panel axial length on the collapse characteristics of a panel with and without a large cutout, and Captain John Del Barga investigated the effect of cutout dimensionality. Hatfield [18] performed collapse analysis using the SHELL program for a 101.6 mm x 101.6 mm (4" X 4") cutout using a 304.8 mm x 304.8 mm (12" x 12") and

304.8 mm x 508 mm (12" x 20") panel with free vertical edges where the first measurement is in the circumferential direction and the second measurement is in the axial direction. He analyzed both symmetric quasi-isotropic and symmetric cross-ply lay-ups and compared them to experimental results. He verified that quasi-isotropic lay-ups for similar panel configurations had higher collapse loads than the cross-ply lay-ups, and by increasing the axial length from 304.8 mm (12") to 508 mm (20"), it was found the collapse load was reduced for panels with the same number of plies. Hatfield also found that the greatest radial displacements and rotations for a panel with a cutout occurred along the free vertical edges of the panel and the corners of the cutout. The greatest values of radial displacement and rotations tended to occur along the horizontal centerline of the panel at the free vertical edges.

Del Barga [1] examined the effects of cutout dimensionality by using the SHELL program to analyze five different centralized cutout configurations for 8, 16, and 24 ply quasi-isotropic [0/+45/-45/90] lay-ups for 304.8 mm x 304.8 mm (12" x 12") and 304.8 mm x 508 mm (12" x 20") panels with free vertical edges and compared them to experimental results. His results indicated that the magnitudes of the radial displacements along the vertical edge at the horizontal centerline of the panels ranged from 4-12 times the panel thickness, which led him to conclude that a nonlinear theory which addresses large rotations, like SHELL, was required. He also determined that the numerical vaulues of maximum bending rotations (ψ_s) were inclined to occur at the panel vertical edge at or near the panel horizontal centerline. In addition, the numerical values of local maximum radial displacements tended to occur at the vertical cutout edge along the panel horizontal

centerline, while the local maximum bending rotations occurred at or near the cutout corners when transverse shear effects became significant. As for dimensionality, the collapse load and stiffness of a panel were numerically verified to decrease with an increase in cutout area, and the collapse of panels with equivalent cutout areas was characterized by the manner in which axial compressive energy was absorbed by the panel. Also, the collapse load and stiffness of a panel increased with increasing panel thickness when panels of equivalent axial lengths were compared.

The program SHELL mentioned above is a geometric nonlinear finite element program developed by Scott Dennis at AFIT. This program takes into account large displacements and moderately large rotations and incorporates a parabolic distribution of shear through the panel thickness. Unlike isotropic panels, it is necessary to take into account the effects of transverse shear in an analytical model for thick composite shells due to the longitudinal modulus (E_1) being one to two orders of magnitude larger than the transverse shear moduli (G_{12} and G_{13}) [19]. In addition, the effect of transverse shear becomes more important as the thickness of the panel is increased [20].

In addition to Dennis' work, a great deal of research has been devoted to transverse shear in composite cylindrical shells [21-29]. Ren [30] compared results from classical shell theory and Donnell shell theory to exact solutions. He found that the classical shell theory leads to a very poor description of a laminated shell at low radius-to-depth ratios (where $R/h < 20$). Linneman [31,32] also compared Donnell solutions with classical solutions in order to examine the effects of transverse shear deformation in his presentation on the theoretical development of anisotropic cylindrical shell theory. Tighe

[33,34] looked at higher order shear deformation theory and found that curvature plays an important role in the buckling load of cylindrical shells. In a very thorough analysis of higher-order transverse shear theory for composite shells, Smith [35] compared eight variations on the order of the thickness expansions used to approximate the shell shape factors, the order of the assumed linear displacement field, and the nonlinearity of transverse shear strain. He found that a thin, shallow (h = 0.25", R = 100"), isotropic cylindrical shell panel exhibited a more flexible response during collapse when nonlinear transverse shear was included. For deeper shells, the quasi-nonlinear higher-order transverse shear deformation theory produced a more flexible response during collapse when the order of the shell shape factor approximations was increased.

1.2 Objectives

The objective of this research was to study the effects of through-the-thickness shear and moderately large rotations on the instability of quasi-isotropic [0/+45/-45/90] graphite/epoxy cylindrical shell panels. A numerical collapse analysis was performed on panels with varying centrally located cutouts for axial compression. For each configuration, the thickness was varied by using panels of 8, 16, and 32 plies. This analysis was performed using three different shell theories. The most accurate of the three theories is known as the Simplified Large displacement moderate Rotation (SLR) theory [2,17]. This theory takes into account both through-the-thickness shear and moderately large rotations. The second theory used was the Donnell cylindrical shell theory with transverse shear flexibility. As the name implies, this theory takes into account through-

the-thickness shear. However, it tends to produce inaccurate results when large rotations ($> 10^{o}$) are introduced [17]. The third theory used was the classical Donnell cylindrical shell theory, which neglects both through-the-thickness shear and large rotations. The intent of this approach was to determine when large rotations and through-the-thickness shear become significant in the collapse analysis by noting where the three theories diverged for each of the cutout configurations for varying thickness.

The cutout configurations used were the same as Del Barga's [1] except that solid shells with no cutouts were also examined. Del Barga used only SLR theory to analyze 8, 16, and 24 ply panels, whereas this research used two other theories and examined 32 ply panels instead of 24 ply panels. The SHELL computer program was used for both SLR and Donnell analysis. A modified SHELL program called CLASSIC was used for the Classical Donnell analysis. Experimental results from both Hatfield and Del Barga were used to check the accuracy of the computer results for both 8 and 16 ply panels.

The boundary conditions assumed for this analysis were free vertical edges with the horizontal bottom edge of the panel fixed. The top horizontal edge of the panel was assumed to only displace in the axial (u) direction. The panel's horizontal edges were assumed to be fixed circumferentially.

Another objective of this research is to determine the limits of the Donnell and Classical Donnell theories in collapse analysis. The equations used in Donnell allow for a significant decrease in computational work over SLR, and the equations for Classical Donnell are even more simplified. However, these bonuses in computing time may be

negated by inaccuracies caused by the introduction of large rotations and through-the-thickness shear for each respective theory.

1.3 Scope

Three panel configurations for six different size cutouts were analyzed. Both Del Barga and Hatfield agreed that the 304.8 mm x 508 mm (12" x 20") panel was more realistic for practical applications, so no analysis was performed on the 304.8 mm x 304.8 mm (12" x 12") panel. Thus, the three configurations used are 8, 16, and 32 plies for the (12" x 20") panel. The cutout sizes used were:

No cutout
50.8 mm x 50.8 mm (2" x 2")
101.6 mm x 101.6 mm (4" x 4")
127 mm x 127 mm (5" x 5")
50.8 mm x 203.2 mm (2" x 8")
203.2 mm x 50.8 mm (8" x 2")

where the first measurement is in the circumferential direction and the second measurement is in the axial direction.

Using 3 different configurations for 6 different cutout sizes and three different theories resulted in 54 different sets of data, not including additional runs for isotropic comparisons.

2. Theory

2.1 SHELL Theory

Both the SHELL and CLASSIC programs use a geometrically nonlinear static shell theory. The SHELL program has the ability to utilize both SLR and Donnell cylindrical shell theories, while CLASSIC incorporates the equations for Classical Donnell theory. All three of these theories share several assumptions. First, the shell is assumed to be thin so that a state of plane stress is said to exist ($\sigma_3 = 0$). This allows the three dimensional shell problem to be handled as a two dimensional problem, or to be more precise, the entire shell is described by the datum surface. Another assumption shared by the three theories is that the shell consists of linear elastic laminated orthotropic material which implies a small strain assumption or no plasticity. Finally, both SLR and Donnell assume the transverse shear distribution is parabolic through the panel thickness with the transverse shear being equal to zero at the top and bottom surface of the panel.

The application of these theories requires cylindrically shaped finite-elements. These elements capture the shell bending-membrane coupling by matching the curvature of the shell surface. This makes them superior to flat finite-elements used in numerical models where panel responses are predicted for shells with large cutouts.

A brief explanation and description of the more significant equations used in the three theories is presented in the following sections. Palazotto and Dennis [17] provide a more detailed description and derivation of all three theories.

2.1.1 Geometry and Contracted Notation

Both programs use a curvilinear orthogonal coordinate system which is shown in Figure 1. The angle θ depicted in this figure indicates the positive ply lay orientation. The datum surface is formed by the X and S axes and lies at the center of the thickness of the panel. The thickness coordinate on the outer surface is negative and the inner surface is positive. The displacements u, v, and w lie along the X, S, and Z axes respectively. The radius of curvature, which is measured to the outside surface of the panel, is 304.8 mm (12"). Subscripts denoting stress and strain orientation are summarized in Table 1.

Table 1. SHELL Contracted Notation [15]

Stress		Strain		Cylindrical
Explicit	Contracted	Explicit	Contracted	Coordinates
σ_{11}	σ_1	ε_{11}	ε_1	X ⇒ 1
σ_{22}	σ_2	ε_{22}	ε_2	S ⇒ 2
σ_{33}	σ_3	ε_{33}	ε_3	Z ⇒ 3
σ_{23}	σ_4	γ_{23}	ε_4	S-Z ⇒ 4
σ_{13}	σ_5	γ_{13}	ε_5	X-Z ⇒ 5
σ_{12}	σ_6	γ_{12}	ε_6	X-S ⇒ 6

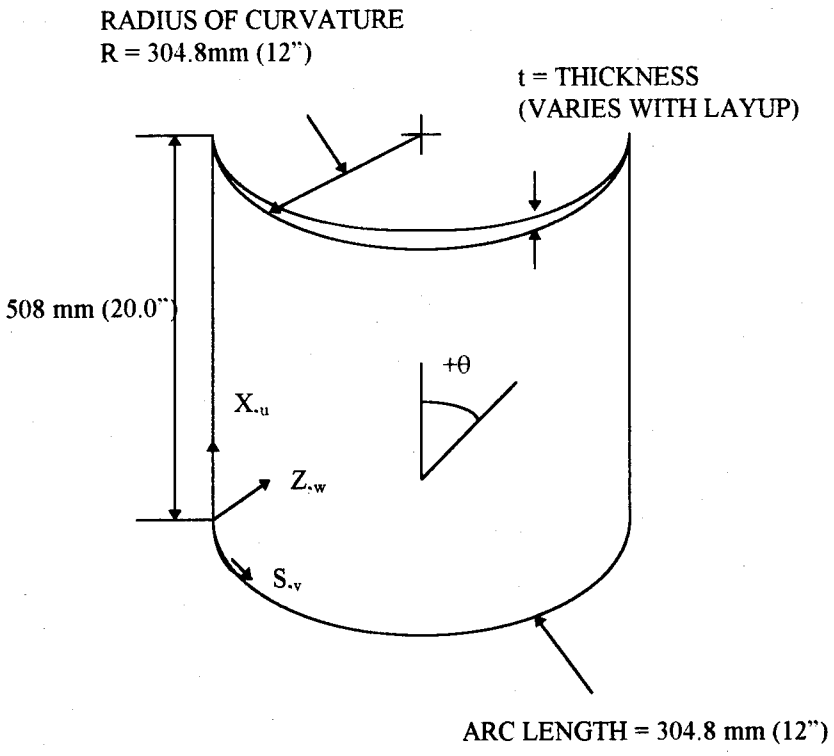

Figure 1. Shell Panel Geometry With Positve Ply Orientation Angle

2.1.2 Constitutive Equations

The SHELL program used for this research assumes a modified plane stress relationship. This modified relationship allows $\sigma_3 = 0$ but it assumes σ_4 and σ_5 are not equal to zero, which incorporates non-zero through-the-thickness shear stress into the finite-element code [2]. A complete derivation can be found in several recent sources [2,15,17]. The reduced stiffness constitutive relation becomes [15] :

$$\begin{Bmatrix} \sigma_1 \\ \sigma_2 \\ \sigma_6 \\ \sigma_4 \\ \sigma_5 \end{Bmatrix} = \begin{bmatrix} Q_{11} & Q_{12} & 0 & 0 & 0 \\ Q_{12} & Q_{22} & 0 & 0 & 0 \\ 0 & 0 & 2Q_{66} & 0 & 0 \\ 0 & 0 & 0 & Q_{44} & 0 \\ 0 & 0 & 0 & 0 & Q_{55} \end{bmatrix} \begin{Bmatrix} \varepsilon_1 \\ \varepsilon_2 \\ \varepsilon_6 \\ \varepsilon_4 \\ \varepsilon_5 \end{Bmatrix} \qquad (1)$$

The reduced stiffness coefficients (Q_{ij}) related in terms of engineering constants are [1]:

$$Q_{11} = E_1/(1-\nu_{12}\nu_{21})$$

$$Q_{12} = \nu_{12}E_2/(1-\nu_{12}\nu_{21}) = \nu_{21}E_1/(1-\nu_{12}\nu_{21})$$

$$Q_{22} = E_2/(1-\nu_{12}\nu_{21}) \qquad (2)$$

$$Q_{66} = G_{12}$$

$$Q_{44} = G_{23}$$

$$Q_{55} = G_{13}$$

where the E_i's are the moduli of elasticity, the G_{ij}'s are the transverse shear moduli, and the ν_{ij}'s are the Poisson's ratios.

These equations (1 and 2) are used for an orthotropic material where stresses and strains are defined with respect to the principal material directions. The next equation is used for a laminate where the fiber directions do not coincide with the global coordinate directions. Therefore, the plies must be referenced to a global axis system and their effects summed [15]. The stress-strain relations with respect to the global X-S coordinate system is defined by:

$$\{\sigma_i\}_k = [T][Q_{ij}]_k[T]^T\{\varepsilon\}_k \tag{3}$$

where,

$$[T] = \begin{bmatrix} c^2 & s^2 & -2cs \\ s^2 & c^2 & 2cs \\ cs & -cs & (c^2 - s^2) \end{bmatrix} \quad \text{for} \quad \begin{bmatrix} Q_{11} & Q_{12} & 0 \\ Q_{12} & Q_{22} & 0 \\ 0 & 0 & 2Q_{66} \end{bmatrix} \tag{4}$$

and

$$[T] = \begin{bmatrix} c & -s \\ s & c \end{bmatrix} \quad \text{for} \quad \begin{bmatrix} Q_{44} & 0 \\ 0 & Q_{55} \end{bmatrix} \tag{5}$$

with c = cosθ and s = sinθ where θ is the rotation from the material to the global stiffness relation. Equation (3), which is the transformed constitutive relation, can be written:

$$\{\sigma_i\}_k = \left[\overline{Q}_{ij}\right]_k \{\varepsilon_i\}_k \tag{6}$$

The k means each kth ply in the laminate is characterized by this equation. The kth ply is defined by its distance form the mid-plane of the laminate. The reduced stiffness can be transformed via equation (4) to $\overline{Q}_{11}$, $\overline{Q}_{12}$, $\overline{Q}_{16}$, $\overline{Q}_{26}$, and $\overline{Q}_{66}$ which are defined in several composite materials texts [36]. Applying equation (5) yields the remaining transformed constitutive equations:

These equations (1 and 2) are used for an orthotropic material where stresses and strains are defined with respect to the principal material directions. The next equation is used for a laminate where the fiber directions do not coincide with the global coordinate directions. Therefore, the plies must be referenced to a global axis system and their effects summed [15]. The stress-strain relations with respect to the global X-S coordinate system is defined by:

$$\{\sigma_i\}_k = [T][Q_{ij}]_k[T]^T\{\varepsilon\}_k \tag{3}$$

where,

$$[T] = \begin{bmatrix} c^2 & s^2 & -2cs \\ s^2 & c^2 & 2cs \\ cs & -cs & (c^2 - s^2) \end{bmatrix} \quad \text{for} \quad \begin{bmatrix} Q_{11} & Q_{12} & 0 \\ Q_{12} & Q_{22} & 0 \\ 0 & 0 & 2Q_{66} \end{bmatrix} \tag{4}$$

and

$$[T] = \begin{bmatrix} c & -s \\ s & c \end{bmatrix} \quad \text{for} \quad \begin{bmatrix} Q_{44} & 0 \\ 0 & Q_{55} \end{bmatrix} \tag{5}$$

with c = cosθ and s = sinθ where θ is the rotation from the material to the global stiffness relation. Equation (3), which is the transformed constitutive relation, can be written:

$$\{\sigma_i\}_k = \left[\overline{Q}_{ij}\right]_k \{\varepsilon_i\}_k \tag{6}$$

The k means each kth ply in the laminate is characterized by this equation. The kth ply is defined by its distance form the mid-plane of the laminate. The reduced stiffness can be transformed via equation (4) to $\overline{Q}_{11}$, $\overline{Q}_{12}$, $\overline{Q}_{16}$, $\overline{Q}_{26}$, and $\overline{Q}_{66}$ which are defined in several composite materials texts [36]. Applying equation (5) yields the remaining transformed constitutive equations:

$$\overline{Q}_{44} = Q_{44}\cos^4\theta + Q_{55}\sin^4\theta$$

$$\overline{Q}_{45} = (Q_{44} - Q_{55})\cos\theta\sin\theta \qquad (7)$$

$$\overline{Q}_{55} = Q_{44}\sin^4\theta + Q_{55}\cos^4\theta$$

The program CLASSIC assumes a plane stress relationship where σ_4 and σ_5 are equal to zero. Thus, the ply constitutive relations are developed similarly to those used above for SHELL except equation (5) is not used because the initial reduced stiffness relation is:

$$\begin{Bmatrix}\sigma_1\\ \sigma_2\\ \sigma_6\end{Bmatrix} = \begin{bmatrix}Q_{11} & Q_{12} & 0\\ Q_{12} & Q_{22} & 0\\ 0 & 0 & 2Q_{66}\end{bmatrix}\begin{Bmatrix}\varepsilon_1\\ \varepsilon_2\\ \varepsilon_6\end{Bmatrix} \qquad (8)$$

and through-the-thickness shear stress is not incorporated into the finite element code.

2.1.3 SLR Strain-Displacement Relations

The main differences in the three theories used for this study can be found in the strain-displacement relations for each theory. The SLR theory includes through-the-thickness shear distribution and uses the exact Green's strain-displacement relations for in-plane strains ε_1, ε_2, and ε_6. The transverse shear strains, ε_4 and ε_5, include only the linear Green's strain-displacement terms. The physical strains (ε_{ij}) are defined by:

$$\varepsilon_{ij} = \gamma_{ij} / (h_i\, h_j) \qquad (9)$$

where (γ_{ij}) are Green's strain-displacement relations presented in Saada [37] and h_i are the shell shape factors. The Green's strain-displacement relations are only valid for small strain situations and are a function of the u_1, u_2, and u_3 displacements and the shell shape factors (h_i). They are defined in terms of the metric tensor of the transformed coordinate

system as a result of deformation (G_{ij}) and the metric tensor of the transformed coordinate system prior to deformation (g_{ij}) through the following equation:

$$2\gamma_{ij} = G_{ij} - g_{ij} \tag{10}$$

The metric tensor links the Cartesian to the curvilinear coordinate system through the invariant property of length. The shell shape factors are a function of the coordinate system scale factors (α_i) and radii of curvature of the shell (R_1 and R_2). For the cylindrical shell, the coordinate system scale factors and radii of curvature are defined as $\alpha_1 = \alpha_2 = 1$ and $R_1 = \infty$ and $R_2 = R$. The general shell shape factor equations yield the values of the shell shape factors that are used in this research:

$$\begin{aligned} h_1 &= \alpha_1(1 - z/R_1) = 1 \\ h_2 &= \alpha_2(1 - z/R_2) = 1 - z/R \\ h_3 &= 1 \end{aligned} \tag{11}$$

A more complete overview of the development of Green's strain displacement equations and their relations to shells can be found in Palazotto and Dennis [17]. The definitions of the coordinate system scale factors and radii of curvature and an in-depth derivation of Green's strain displacement equations is provided in Saada [37].

The kinematics permit the incorporation of the through-the-thickness shear with the thickness variable z in the following displacement equations:

$$\begin{aligned} u_1(x,s,z) &= u^0 + z\psi_x + z^2\phi_x + z^3\gamma_x + z^4\theta_x \\ u_2(x,s,z) &= v^0(1 - z/R) + z\psi_S + z^2\phi_S + z^3\gamma_S + z^4\theta_S \\ u_2(x,s,z) &= w \end{aligned} \tag{12}$$

where u^0, v^0, ψ_i, ϕ_i, γ_i, and θ_i are functions of the coordinates X and S. The displacements u^0 and v^0 are of the shell middle surface. The ψ_i terms are rotations of the surface normals in the X and S planes. The ϕ_i, γ_i, and θ_i terms are functions to be determined such that there is no shear stress (σ_4 and σ_5) on the top and bottom surfaces of the shell, since transverse normal strain (ε_3) is assumed negligible.

The shear effects are accounted for by keeping just the linear displacement terms for Green's strain displacement relations, γ_{23} and γ_{13}. Using equation 10, the transverse shear strains ε_4 and ε_5 can be calculated:

$$\varepsilon_4 = 1/h_2 \, (u_{3,2} + h_2 u_{2,3} - u_2 h_{2,3}) \qquad (13)$$

$$\varepsilon_5 = 1/h_1 \, (u_{3,1} + h_1 u_{1,3} - u_1 h_{1,3})$$

By using the shape factors established previously and substituting the displacements in equation (12) into equation (13), the functions ϕ_i, γ_i, and θ_i can be determined. Assuming zero transverse shear stress, and thus zero transverse shear strain on the top and bottom surface of the shell, ϕ_i, γ_i, and θ_i become:

$$\phi_1 = \phi_2 = 0$$

$$\theta_i = \gamma_i / 2R_i \qquad (14)$$

$$\gamma_i = -4/3h^2(\psi_i + w,_i/\alpha_i)$$

where h is the thickness of the shell. Using these values and ignoring the 4th order term because it is only 1/20th the third-order term [17], equation (12) can be rewritten as:

$$u_1(x,s,z) = u^0 + z\psi_x - (4/h^3)z^3(\psi_x + w_{,x})$$

$$u_2(x,s,z) = v^0(1 - z/R) + z\psi_S + (4/h^3)z^3(\psi_S + w_{,S}) \qquad (15)$$

$$u_3(x,s,z) = w$$

If equation (15) is substituted into equation (13) and neglecting the small order terms (z^3), one obtains the transverse shear strains:

$$\varepsilon_4 = [1/(1 - z/R)](\psi_S + w_{,S})[1 - (4z^2/t^2)] \qquad (16)$$

$$\varepsilon_5 = (\psi_x + w_{,x})[1 - (4z^2/t^2)]$$

The in-plane strain displacement relations are found by substituting equation (15) into equation (9):

$$\varepsilon_1 = \varepsilon_{11} = \frac{\gamma_{11}}{h_1^2} = \varepsilon_1^0 + z\kappa_1^1 + z^2\kappa_1^2 + z^3\kappa_1^3 + z^4\kappa_1^4 + z^6\kappa_1^6$$

$$\varepsilon_2 = \varepsilon_{22} = \frac{\gamma_{22}}{h_2^2} = \varepsilon_2^0 + z\kappa_2^1 + z^2\kappa_2^2 + z^3\kappa_2^3 + z^4\kappa_2^4 + z^6\kappa_2^6 \qquad (17)$$

$$\varepsilon_6 = 2\varepsilon_{12} = \frac{\gamma_{12}}{h_1 h_2} = \varepsilon_6^0 + z\kappa_6^1 + z^2\kappa_6^2 + z^3\kappa_6^3 + z^4\kappa_6^4 + z^6\kappa_6^6$$

By expanding typical scale factor expressions into binomial series and substituting them into equation (17) after truncating past the first order z terms, the following equation results:

$$\varepsilon_i = \varepsilon_i^0 + \sum_{p=1}^{7} z^p \kappa_{ip}$$

$$i = 1, 2, 6 \qquad (18)$$

This equation can also be written in matrix format:

$$\begin{Bmatrix}\varepsilon_1\\ \varepsilon_2\\ \varepsilon_6\end{Bmatrix}=\begin{Bmatrix}\varepsilon_1^0\\ \varepsilon_2^0\\ \varepsilon_6^0\end{Bmatrix}+\begin{bmatrix}\kappa_{11} & \kappa_{12} & \kappa_{13} & \kappa_{14} & \kappa_{15} & \kappa_{16} & \kappa_{17}\\ \kappa_{21} & \kappa_{22} & \kappa_{23} & \kappa_{24} & \kappa_{25} & \kappa_{26} & \kappa_{27}\\ \kappa_{61} & \kappa_{62} & \kappa_{63} & \kappa_{64} & \kappa_{65} & \kappa_{66} & \kappa_{67}\end{bmatrix}\begin{Bmatrix}z\\ z^2\\ z^3\\ z^4\\ z^5\\ z^6\\ z^7\end{Bmatrix} \tag{19}$$

The matrix equation for the transverse shear strains is:

$$\begin{Bmatrix}\varepsilon_4\\ \varepsilon_5\end{Bmatrix}=\begin{Bmatrix}\varepsilon_4^0\\ \varepsilon_5^0\end{Bmatrix}+\begin{bmatrix}\kappa_{42}\\ \kappa_{52}\end{bmatrix}z^2 \tag{20}$$

For the cylindrical shells used in this study, equations (21-24) represent the specific strain-displacement equations, where c = 1/R and k = $-4/2h^2$. The seven degrees of freedom u, v, w, w_x, w_S, ψ_x, and ψ_S are functions of the mid-surface coordinates X and S only.

$$\varepsilon_1 = \varepsilon_1^0 + z^p \kappa_{1p}$$

$$\varepsilon_1^0 = u_{,x} + \frac{1}{2}(u_{,x}^2 + v_{,x}^2 + w_{,x}^2)$$

$$\kappa_{11} = \psi_{x,x} - v_{,x}^2 c + \psi_{x,x} u_{,x} + \psi_{s,x} v_{,x}$$

$$\kappa_{12} = v_{,x}^2 \frac{c^2}{2} - \psi_{s,x} v_{,x} c + \frac{1}{2}(\psi_{x,x}^2 + \psi_{s,x}^2)$$

$$\kappa_{13} = k(w_{,xx} + \psi_{x,x}) + u_{,x}\, k(w_{,xx} + \psi_{x,x}) + v_{,x}\, k(w_{,sx} + \psi_{s,x}) \tag{21}$$

$$\kappa_{14} = -v_{,x}\, kc(w_{,sx} + \psi_{s,x}) + \psi_{x,x} k(w_{,xx} + \psi_{x,x}) + \psi_{s,x} k(w_{,sx} + \psi_{s,x})$$

$$\kappa_{15} = 0$$

$$\kappa_{16} = (\frac{k^2}{2})(w_{,xx}^2 + 2w_{,xx}\, \psi_{x,x} + \psi_{x,x}^2 + w_{,sx}^2 + 2w_{,sx}\, \psi_{s,x} + \psi_{s,x}^2)$$

$$\kappa_{17} = 0$$

$$\varepsilon_2 = \varepsilon_2^0 + z^p \kappa_{2p}$$

$$\varepsilon_2^0 = v_{,s} - wc + \frac{1}{2}(v_{,s}^2 + w_{,s}^2 + u_{,s}^2 + v^2c^2 + w^2c^2) + vw_{,s}\,c - v_{,s}\,wc$$

$$\kappa_{21} = \psi_{s,s} - wc^2 + u_{,s}^2\,c + w_{,s}^2\,c + w^2c^3 - c^2(v_{,s}\,w - vw_{,s}) + v\psi_s c^2 + v_{,s}\,\psi_{s,s} + u_{,s}\,\psi_{x,s} - c(\psi_{s,s}w - \psi_s w_{,s})$$

$$\kappa_{22} = \psi_{s,s}c + \frac{1}{2}(\psi_{s,s}^2 + \psi_{x,s}^2 + \psi_s^2 c^2) + 2\psi_{x,s}u_{,s}\,c + v\psi_s c^3 - 2c^2(\psi_{s,s}w - \psi_s w_{,s}) + \psi_{s,s}v_{,s}\,c$$

$$\kappa_{23} = k(w_{,ss} + \psi_{s,s}) + c(\psi_{s,s}^2 + \psi_{x,s}^2) + ku_{,s}\,(w_{,xs} + \psi_{x,s}) + \psi_s^2 c^3 + kv_{,s}\,(w_{,ss} + \psi_{s,s}) + vkc^2(w_{,s} + \psi_s) - wkc(w_{,ss} + \psi_{s,s}) + w_{,s}\,kc(w_{,s} + \psi_s) \qquad (22)$$

$$\kappa_{24} = kc(w_{,ss} + \psi_{s,s}) + 2u_{,s}\,kc(w_{,xs} + \psi_{x,s}) + vkc^3(w_{,s} + \psi_s) + 2kc^2(-ww_{,ss} - w\psi_{s,s} + w_{,s}^2 + w_{,s}\,\psi_s) + k\psi_{s,s}(w_{,ss} + \psi_{s,s}) + k\psi_{x,s}(w_{,xs} + \psi_{x,s}) + \psi_s kc^2(w_{,s} + \psi_s) + v_{,s}\,kc(w_{,ss} + \psi_{s,s})$$

$$\kappa_{25} = 2kc[\psi_{s,s}(w_{,ss} + \psi_{s,s}) + \psi_{x,s}(w_{,xs} + \psi_{x,s}) + \psi_s c^2(w_{,s} + \psi_s)]$$

$$\kappa_{26} = (k^2/2)[w_{,ss}^2 + 2w_{,ss}\,\psi_{s,s} + \psi_{s,s}^2 + w_{,xs}^2 + 2w_{,xs}\,\psi_{x,s} + \psi_{x,s}^2 + c^2(w_{,s}^2 + 2w_{,s}\,\psi_s + \psi_s^2)]$$

$$\kappa_{27} = k^2 c[(w_{,ss} + \psi_{s,s})^2 + (w_{,xs} + \psi_{x,s})^2 + c^2(w_{,s} + \psi_s)^2]$$

$$\varepsilon_6 = \varepsilon_6^0 + z^p \kappa_{6p}$$

$$\varepsilon_6^0 = u_{,s} + v_{,x} + u_{,x}\, u_{,s} + v_{,x}\, v_{,s} + w_{,x}\, w_{,s} + c(vw_{,x} - v_{,x}\, w)$$

$$\begin{aligned}\kappa_{61} = {} & c(u_{,s} - v_{,x}) + \psi_{x,s} + \psi_{s,x} + u_{,x}\, \psi_{x,s} + \psi_{x,x} u_{,s} + \\ & c(u_{,x}\, u_s - v_{,x}\, v_{,s} + w_{,x}\, w_{,s} - w\psi_{s,x} + w_{,x}\, \psi_s) + v_{,x}\, \psi_{s,s} + v_{,s}\, \psi_{s,x}\end{aligned}$$

$$\begin{aligned}\kappa_{62} = {} & c(\psi_{x,s} + u_{,x}\, \psi_{x,s} + u_{,s}\, \psi_{x,x} - cw\psi_{s,x} - cw\psi_{s,x} + cw_{,x}\, \psi_s) + \\ & \psi_{x,x}\psi_{x,s} + \psi_{s,x}\psi_{s,s}\end{aligned}$$

$$\begin{aligned}\kappa_{63} = {} & 2kw_{,xs} + k\psi_{x,s} + k\psi_{s,x} + ku_{,s}(w_{,xx} + \psi_{x,x}) + ku_{,x}(w_{,xs} + \psi_{x,s}) + \\ & kv_{,x}(w_{,ss} + \psi_{s,s}) + kcw_{,x}(w_{,s} + \psi_s) - kcw(w_{,xs} + \psi_{s,x}) + \\ & c(\psi_{x,x}\psi_{x,s} + \psi_{s,x}\psi_{s,s}) + kv_{,s}(w_{,xx} + \psi_{s,x})\end{aligned}$$

$$\begin{aligned}\kappa_{64} = {} & kc(w_{,xs} + \psi_{x,s}) + kcu_{,s}(w_{,xx} + \psi_{x,x}) + k\psi_{s,x}(w_{,ss} + \psi_{s,s}) - \\ & kc^2(ww_{,xs} + w\psi_{s,x} - w_{,x}\, w_s - w_{,x}\, \psi_s) + \\ & k(\psi_{x,x}w_{,xs} + 2\psi_{x,x}\psi_{x,s} + \psi_{x,s}w_{,xx}) + \\ & k\psi_{s,s}(w_{,xs} + \psi_{s,x}) + kcu_{,x}(w_{,xs} + \psi_{x,s})\end{aligned} \qquad (23)$$

$$\kappa_{65} = kc(\psi_{x,x}w_{,xs} + \psi_{x,s}w_{,xx} + \psi_{s,x}w_{,ss} + \psi_{s,s}w_{,xs} + 2\psi_{x,x}\psi_{x,s} + 2\psi_{s,x}\psi_{s,s})$$

$$\kappa_{66} = k^2[(w_{,xx} + \psi_{x,x})(w_{,xs} + \psi_{x,s}) + (w_{,xs} + \psi_{s,x})(w_{,ss} + \psi_{s,s})]$$

$$\kappa_{67} = k^2 c[(w_{,xx} + \psi_{x,x})(w_{,xs} + \psi_{x,s}) + (w_{,xs} + \psi_{s,x})(w_{,ss} + \psi_{s,s})]$$

$$\varepsilon_4 = (w_{,s} + \psi_s) + z^2 3k(w_{,s} + \psi_s)$$

$$\varepsilon_5 = (w_{,x} + \psi_x) + z^2 3k(w_{,x} + \psi_x) \qquad (24)$$

2.1.4 Modified Donnell Strain-Displacement Relations

The Modified Donnell cylindrical shell strain displacement relations are much more simplified, as seen in the following:

$$\varepsilon_1 = u_{1,x} + \frac{1}{2} w_{,x}^2$$

$$\varepsilon_2 = u_{2,s} - w / R + \frac{1}{2} w_{,s}^2 \qquad (25)$$

$$\varepsilon_6 = u_{1,s} + u_{2,x} + w_{,x} w_{,s}$$

where u_1 and u_2 are given by the kinematics of equation (15). When the kinematics are substituted into equation (25), the strain-displacement relations can be found to be similar to equations (21-24) except that there is a great reduction in the number of terms.

$$\varepsilon_1 = \varepsilon_1^0 + z^p \kappa_{1p}$$

$$\varepsilon_1^0 = u_{,x} + \frac{1}{2} w_{,x}^2$$

$$\kappa_{11} = \psi_{x,x} \qquad (26)$$

$$\kappa_{13} = k(w_{,xx} + \psi_{x,x})$$

$$\kappa_{1p}(p = 2,4,5,6,7) = 0$$

$$\varepsilon_2 = \varepsilon_2^0 + z^p \kappa_{2p}$$

$$\varepsilon_2^0 = v_{,s} - w / R + \frac{1}{2} w_{,s}^2$$

$$\kappa_{21} = \psi_{s,s} - v_{,s} / R \qquad (27)$$

$$\kappa_{23} = k(w_{,ss} - \psi_{s,s})$$

$$\kappa_{2p}(p = 2,4,5,6,7) = 0$$

$$\varepsilon_6 = \varepsilon_6^0 + z^p \kappa_{6p}$$

$$\varepsilon_6^0 = u_{,s} + v_{,x} + w_{,x} w_{,s}$$

$$\kappa_{61} = \psi_{x,s} + \psi_{s,x} - v_{,x}/R \qquad (28)$$

$$\kappa_{63} = k(2w_{,xs} + \psi_{x,s} + \psi_{s,x})$$

$$\kappa_{6p}(p = 2,4,5,6,7) = 0$$

where $k = -4/3h^2$ and, as in the SLR theory, the seven degrees of freedom u, v, w, w_x, w_S, ψ_x, and ψ_S are functions of the mid-surface coordinates X and S only. The transverse shear terms, ε_4 and ε_5, are the same as equation (24).

2.1.5 Classical Donnell Strain-Displacement Relations

In the Classical Donnell theory there are only five degrees of freedom, u, v, w, w_x, and w_S, which are dependent on X and S only. There are no ψ_i terms, which means the Classical Donnell theory assumes there are no shear rotations. The Classical Donnell theory uses kinematics similar to the Classical Von Karman flat plate kinematics with the exception of the u_2 term.

$$u_1(x,s,z) = u + zw_{,x}$$

$$u_2(x,s,z) = (1-z/R)v + zw_{,S} \qquad (29)$$

$$u_3(x,s,z) = w$$

The strain-displacement relations are the same as those used for the modified Donnell theory in the previous section. When the kinematics of equation (29) are substituted into the strain-displacement equation (25) the Classical Donnell strain-displacement relations result:

$$\varepsilon_1 = \varepsilon_1^0 + z^p \kappa_{1p}$$

$$\varepsilon_1^0 = u_{,x} + \frac{1}{2} w_{,x}^2 \qquad (30)$$

$$\kappa_{11} = w_{,xx}$$

$$\kappa_{1p}(p = 2,3,4,5,6,7) = 0$$

$$\varepsilon_2 = \varepsilon_2^0 + z^p \kappa_{2p}$$

$$\varepsilon_2^0 = v_{,s} - w / R + \frac{1}{2} w_{,s}^2 \qquad (31)$$

$$\kappa_{21} = w_{,ss}$$

$$\kappa_{2p}(p = 2,3,4,5,6,7) = 0$$

$$\varepsilon_6 = \varepsilon_6^0 + z^p \kappa_{6p}$$

$$\varepsilon_6^0 = u_{,s} + v_{,x} + w_{,x}\, w_{,s} \qquad (32)$$

$$\kappa_{61} = 2w_{,xs} + v_{,x} / R$$

$$\kappa_{6p}(p = 2,3,4,5,6,7) = 0$$

Because through-the-thickness shear is neglected, ε_4 and ε_5 are assumed to be zero for the classical case. It is interesting to note that where the Modified Donnell theory uses rotations ψ_i, the Classical Donnell theory makes use of the slope $w_{,i}$.

2.1.6 Shell Potential Energy

Potential energy is defined as the internal strain energy plus the work done by the external forces:

$$\Pi_p = U - W \tag{33}$$

where internal strain energy can be represented by the following equation [1]:

$$.U = 1/2\iint ([\overline{Q}]\{\varepsilon\})^T \{\varepsilon\} d\Omega dt \tag{34}$$

The $\overline{Q}$ term is a symmetric matrix composed of elements of transformed stiffnesses for the kth ply, and the shell middle surface is represented by Ω [17]. The internal strain energy is composed of two parts.

$$U = U_1 + U_2 \tag{35}$$

The first term, U_1, consists of the in-plane terms. The second part, U_2, is composed of the transverse shear terms. By substituting equation (17) into equation (34), a general expression can be generated that applies for all three theories:

$$.U_1 = 1/2 \int\int [\overline{Q}_{11}(\varepsilon_1^0 + z^p \kappa_{1p})^2 + \overline{Q}_{22}(\varepsilon_2^0 + z^p \kappa_{2p})^2 + 2\overline{Q}_{12}(\varepsilon_1^0 + z^p \kappa_{1p})(\varepsilon_2^0 + z^r \kappa_{2r}) + \overline{Q}_{66}(\varepsilon_6^0 + z^p \kappa_{6p})^2 + 2\overline{Q}_{16}(\varepsilon_1^0 + z^p \kappa_{1p})(\varepsilon_6^0 + z^r \kappa_{6r}) + 2\overline{Q}_{26}(\varepsilon_{21}^0 + z^p \kappa_{2p})(\varepsilon_6^0 + z^r \kappa_{6r})] dz d\Omega \tag{36}$$

$$.U_2 = 1/2 \int\int [\overline{Q}_{44}(\varepsilon_4^0 + z^2 \kappa_{42})^2 + \overline{Q}_{55}(\varepsilon_5^0 + z^2 \kappa_{52})^2 + 2\overline{Q}_{45}(\varepsilon_4^0 + z^2 \kappa_{42})(\varepsilon_5^0 + z^2 \kappa_{52})] dz d\Omega$$

where p,r = 1, 2, ... 7. Integration over the thickness of the laminate provides the strain energy as a function of the shell datum surface. A symmetric lay-up also allows elasticity arrays which are multiplied by odd powers of z to be canceled. If the strain-displacement

relations for the three theories discussed in the previous sections are considered in the general expression:

$$\{\varepsilon\} = \{\varepsilon^0\} + [\kappa]\{z\} \tag{37}$$

Then equation (36) can be manipulated into the following form [17]:

$$\begin{aligned} U_1 = 1/2 \int & \{\varepsilon^0\}^T [A] \{\varepsilon^0\} \, d\Omega \\ & + 1/2 \int 2 \{\varepsilon^0\}^T ([B] + [D] + [E] + [F] + [G] + [H] + [I]) \{\kappa\} d\Omega \\ & + 1/2 \int \{\kappa\} ([D] + [E] + [F] + [G] + [H] + [I] + [J] + [K] + [L] \\ & + [P] + [R] + [S] + [T]) \{\kappa\} \, d\Omega \end{aligned} \tag{38}$$

$$U_2 = 1/2 \int (\{\varepsilon^0\}^T [A] \{\varepsilon^0\} + 2 \{\varepsilon^0\} [D] \{\kappa\} + \{\kappa\}^T [F] \{\kappa\}) d\Omega$$

where

$$\{ [A, B, D, E, F, G, H, I, J, K, L, P, R, S, T] \} =$$

$$\int [\bar{Q}] \{1, z, z^2, z^3, z^4, z^5, z^6, z^7, z^8, z^9, z^{10}, z^{11}, z^{12}, z^{13}, z^{14}\} \, dz \tag{39}$$

2.1.7 Finite Element Solution

The equation of motion to be solved is that of static equilibrium where $\sum F = 0$. The internal strain energy can be represented as:

$$U = 1/2 \, q^T [K + N_1(q)/3 + N_2(q^2)/6] \, q \tag{40}$$

where q is defined as the column vector of nodal displacements, K is a constant stiffness matrix, N_1 is a matrix of stiffness terms that are a function of linear displacements, and N_2 is an array of stiffness terms based on quadratic displacements. The external work is:

$$W = q^T R \tag{41}$$

where R is a column vector of nodal loads. If one substitutes equations (40) and (41) into equation (33) and takes the first variation, the result is:

$$\delta\Pi_p = \delta q^T [(K + N_1 (q)/2 + N_2 (q^2)/3)\, q - R] = 0 \qquad (42)$$

$$= \delta q^T F(q) = 0$$

The first variation of the potential energy , $\delta\Pi_p = 0$, yields the static equilibrium equation. This equation is at a minimum for static equilibrium [35]. For an arbitrary and independent δq, it follows that:

$$F(q) = 0 \qquad (43)$$

This expression can be expanded using a Taylor series where higher order terms are neglected because Δq is assumed to be small. This results in the following:

$$F(q + \Delta q) = F(q) + (\partial F/\partial q)\, \Delta q + \ldots = 0$$

$$(\partial F/\partial q)\, \Delta q = -F(q) \qquad (44)$$

When matrix differentiation is applied to equation (42) for F the following results:

$$[\, K + N_1(q) + N_2(q^2)\,]\, \Delta q = -F(q) \qquad (45)$$

$$K_T \Delta q = -F(q)$$

This equation defines the tangent stiffness matrix $[K_T]$. The Modified Newton Raphson technique, incorporating a displacement control algorithm is used to solve:

$$[K_T]\, \Delta q = -\, [\, K + N_1(q)/2 + N_2(q^2)/3\,]q + R \qquad (46)$$

The Modified Newton Raphson technique is presented in [2], [15], and [17].

2.2 Finite Element Modeling

A principal part of finite element modeling is the mesh used in the analysis. Initially this research used six meshes to model the five cutouts and the solid shell. These meshes were the same used by Del Barga for the 304.8 mm x 508 mm (12" x 20") panels

except for the solid shell (see Appendix A). According to Del Barga, these meshes were all similar to the 304.8 mm x 508 mm (12" x 20") panels with 50.8 mm x 50.8 mm (2" x 2") and 101.6 m x 101.6 mm (4" x 4") cutouts used by Hatfield. The solid shell mesh used in this research was the same used for the 50.8 mm x 50.8 mm (2" x 2") cutout except no elements were removed from the stiffness matrix and the degrees of freedom within the cutout were not specified (See Figures 2 and 3). These meshes used 12.7 mm (0.5") square elements around the cutout, and transitioned to larger elements at a minimum of two inches away from the cutout. Dennis conducted convergence studies which indicated that the 12.7 mm square element was the optimal size for capturing the panel response around areas of large displacement and rotation and minimizing CPU run times. The mesh used for the 304.8 mm x 508 mm (12" x 20") panels for the solid shell, the 50.8 mm x 50.8 mm (2" x 2"), and 101.6 m x 101.6 mm (4" x 4") cutouts had a total of 1777 nodes and 560 elements. The mesh used for the 203.2 mm x 50.8 mm cutout had 1973 nodes and 624 elements. The mesh used for the 50.8 mm x 203.2 mm cutout had a total of 1829 nodes and 576 elements. Finally, the mesh used for the 127 x 127 mm (5" x 5") cutout had 2085 nodes and 660 elements.

Results obtained for the Classical Donnell theory when using the above models indicated that, in certain cases, the 12.7 mm (0.5") square elements were not entirely appropriate for representing the panel response around areas of large displacement and rotation. More specifically, the results obtained for each of the eight ply panels with cutouts indicated inappropriate modeling, as did every panel with a 127 x 127 mm (5" x 5") cutout (see section 2.2.1). Therefore, the inappropriate meshes were refined using 6.85 mm (0.25") square elements around the cutouts. The mesh used for the 304.8 mm x

Total nodes = 1777

Total elements = 560

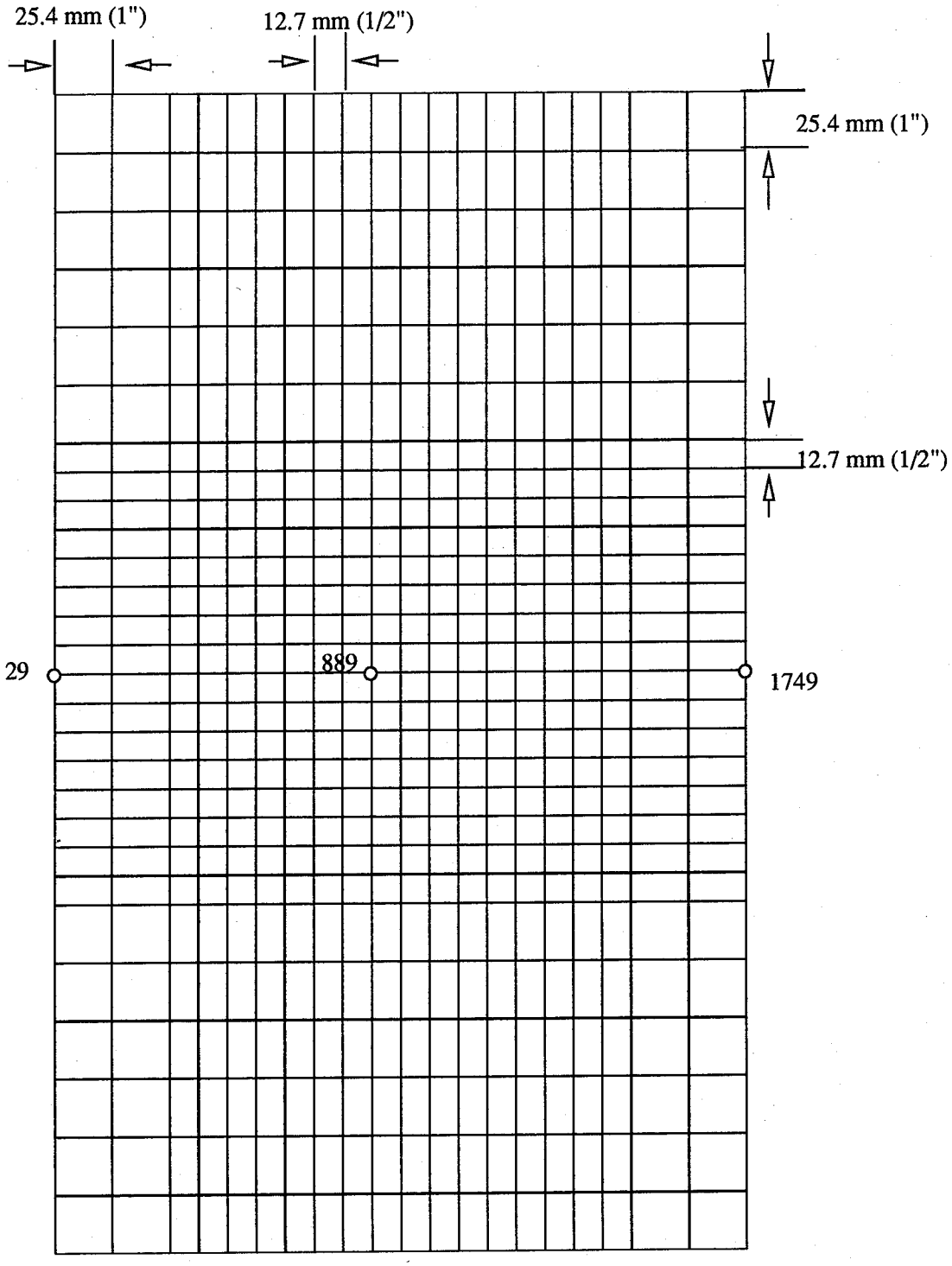

Figure 2. Finite-Element Mesh Used for 304.8 mm x 508 mm Solid (12" x 20") Panel

Total nodes = 1777

Total elements = 560

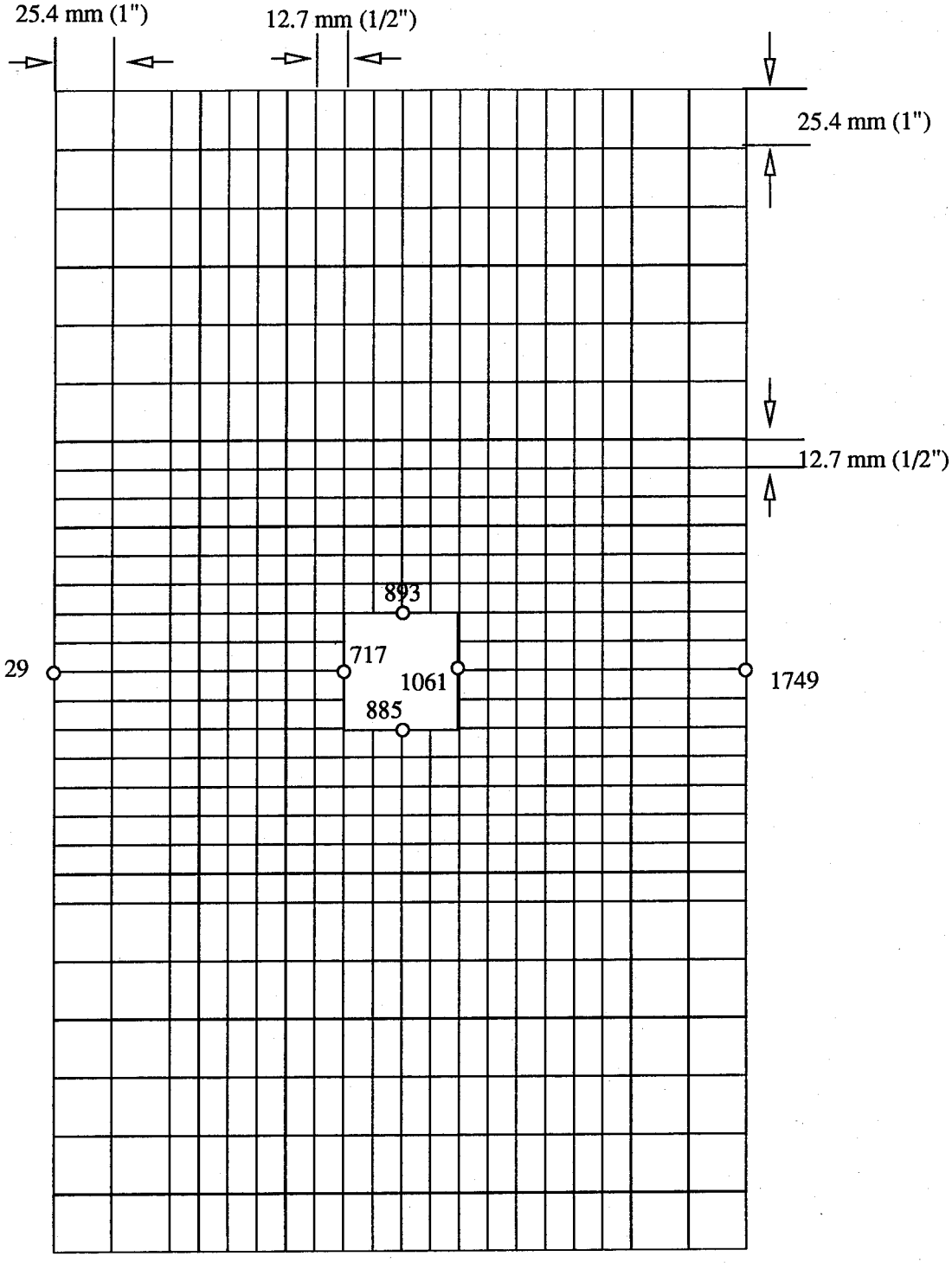

Figure 3. Finite-Element Mesh Used for 304.8 mm x 508 mm (12" x 20") Panel With 50.8 mm x 50.8 mm (2" x 2") Cutout

508 mm (12" x 20") panels for the 50.8 mm x 50.8 mm (2" x 2") cutout was refined three times to insure convergence (see Figures 4-6). The first model used the 6.85 mm (0.25") square elements only 12.7 mm (0.5") from the cutout and the second model went out 26.4 mm (1") from the cutout. The first model used 2773 nodes and 884 elements while the second required 3153 nodes and 1008 elements. The final model refined the elements along the free edge by adding a line of nodes 12.7 mm away from the free edge. This was done to reduce any possible distortion in the S direction caused by rectangular shaped elements. This model used 3301 nodes and 1080 elements.

The larger square cutouts both used the 6.85 mm square elements 26.4 mm from the respective cutouts (see Figures 7-10). The refined model for the 101.6 m x 101.6 mm (4" x 4") cutout had a total of 3985 nodes and 1280 elements while the refined mesh used for the 127 x 127 mm (5" x 5") cutout had 4913 nodes and 1584 elements. The two rectangular cutouts used the 6.85 mm square elements 26.4 mm around the corners of the cutout. This is where Del Barga identified the maximum global transverse shear strains to occur [1] and refining the mesh along the entire length of the cutout would create an excessive number of nodes and elements. The refined mesh used for the 50.8 mm x 203.2 mm cutout had a total of 3253 nodes and 1040 elements and the refined mesh used for the 203.2 mm x 50.8 mm cutout had 3397 nodes and 1088 elements.

The SHELL program uses a two dimensional 36 degree of freedom rectangular curved finite element, where the element shape functions are derived assuming a displacement field (see Figure 11). This element incorporates the through-the-thickness parabolic transverse shear distribution. The four corner nodes have seven degrees of freedom (u, v, w, $\psi_{,x}$, $\psi_{,s}$, $w_{,x}$, and $w_{,s}$). The mid-side nodes have two degrees of

Total nodes = 2773

Total elements = 884

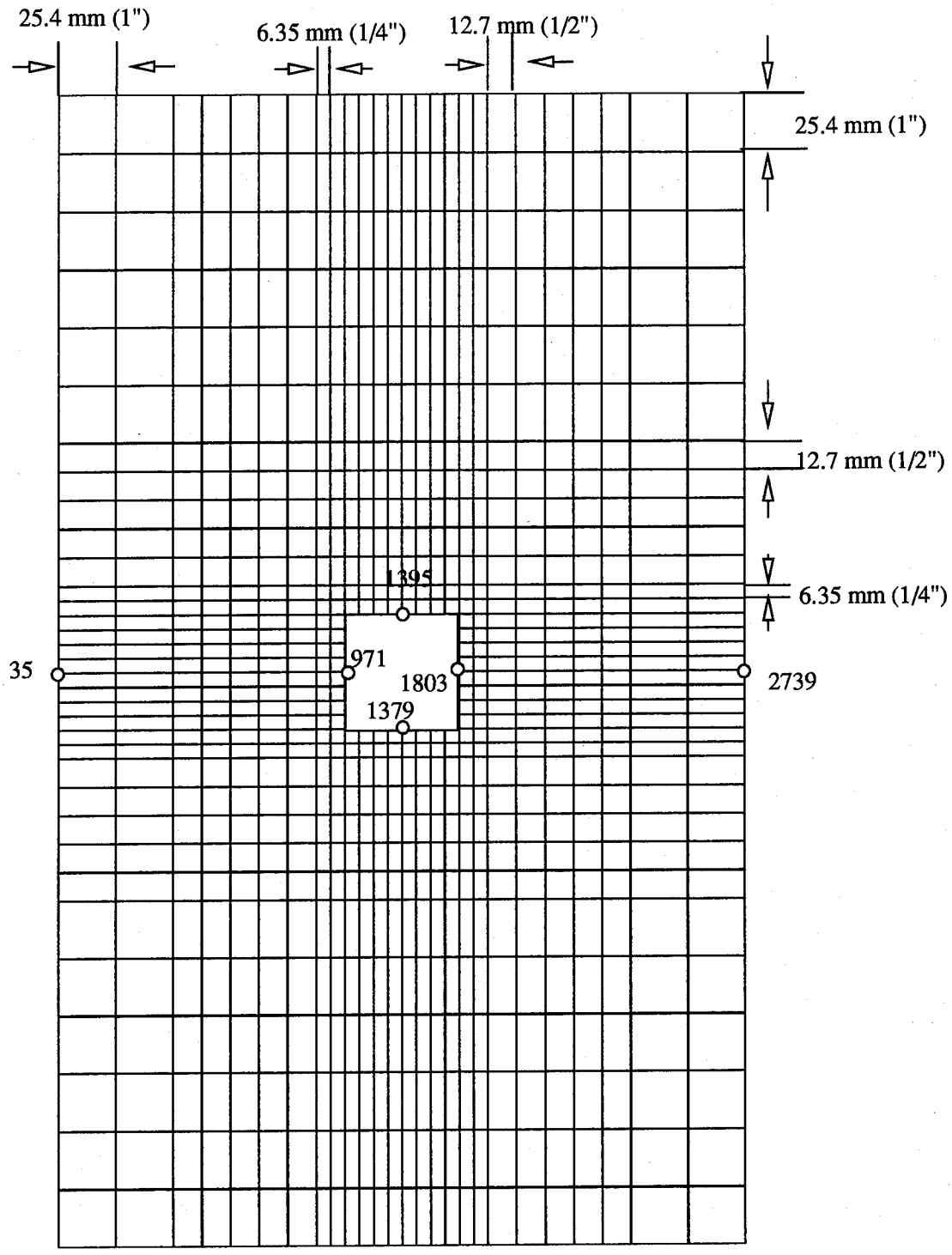

Figure 4. Finite-Element Mesh Used for 304.8 mm x 508 mm (12" x 20") Panel With 50.8 mm x 50.8 mm (2" x 2") Cutout First Refinement 12.7 mm (1/2") Around Cutout

Total nodes = 3153

Total elements = 1008

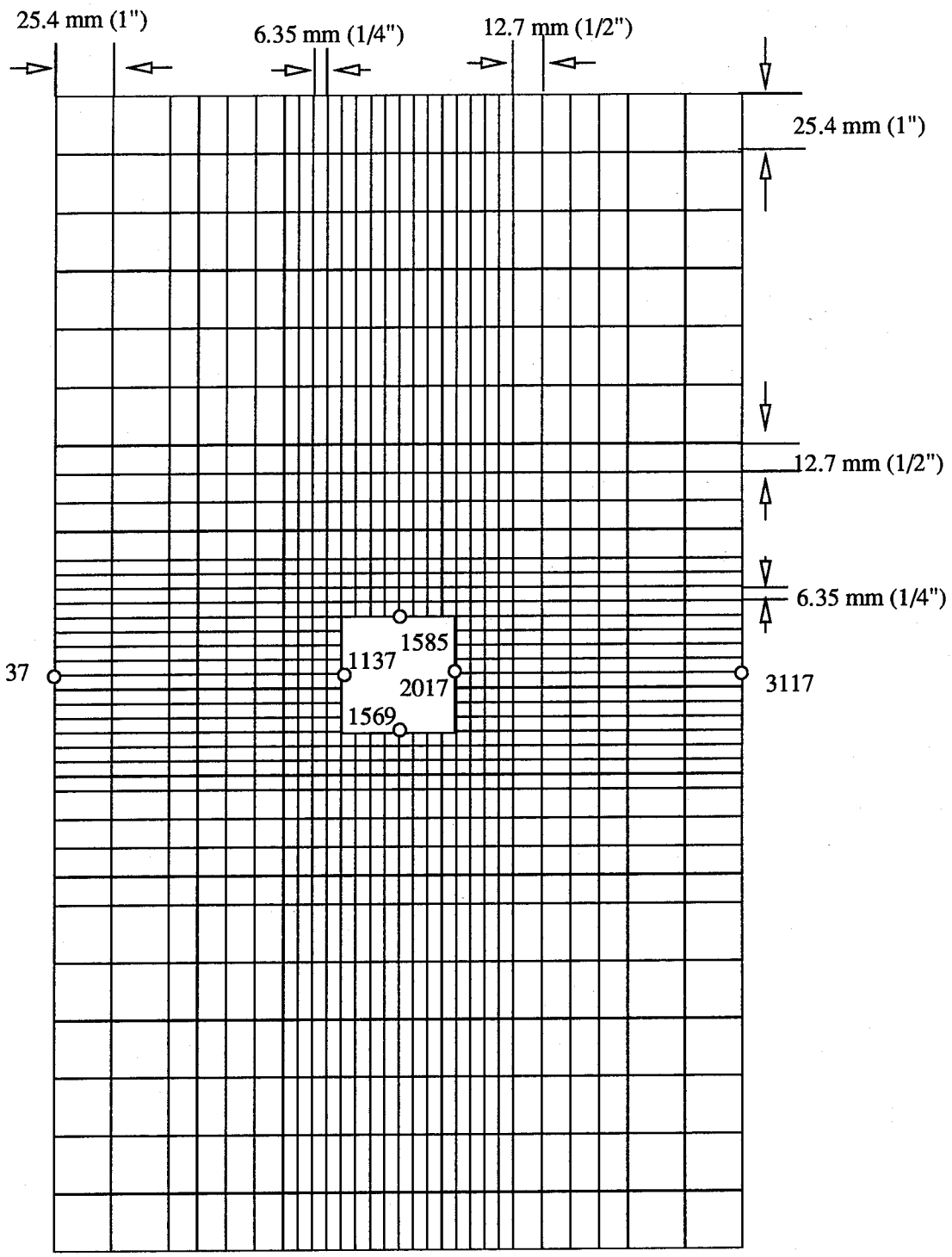

Figure 5. Finite-Element Mesh Used for 304.8 mm x 508 mm (12" x 20") Panel With 50.8 mm x 50.8 mm (2" x 2") Cutout Second Refinement 25.4 mm (1") Around Cutout

Total nodes = 3301

Total elements = 1080

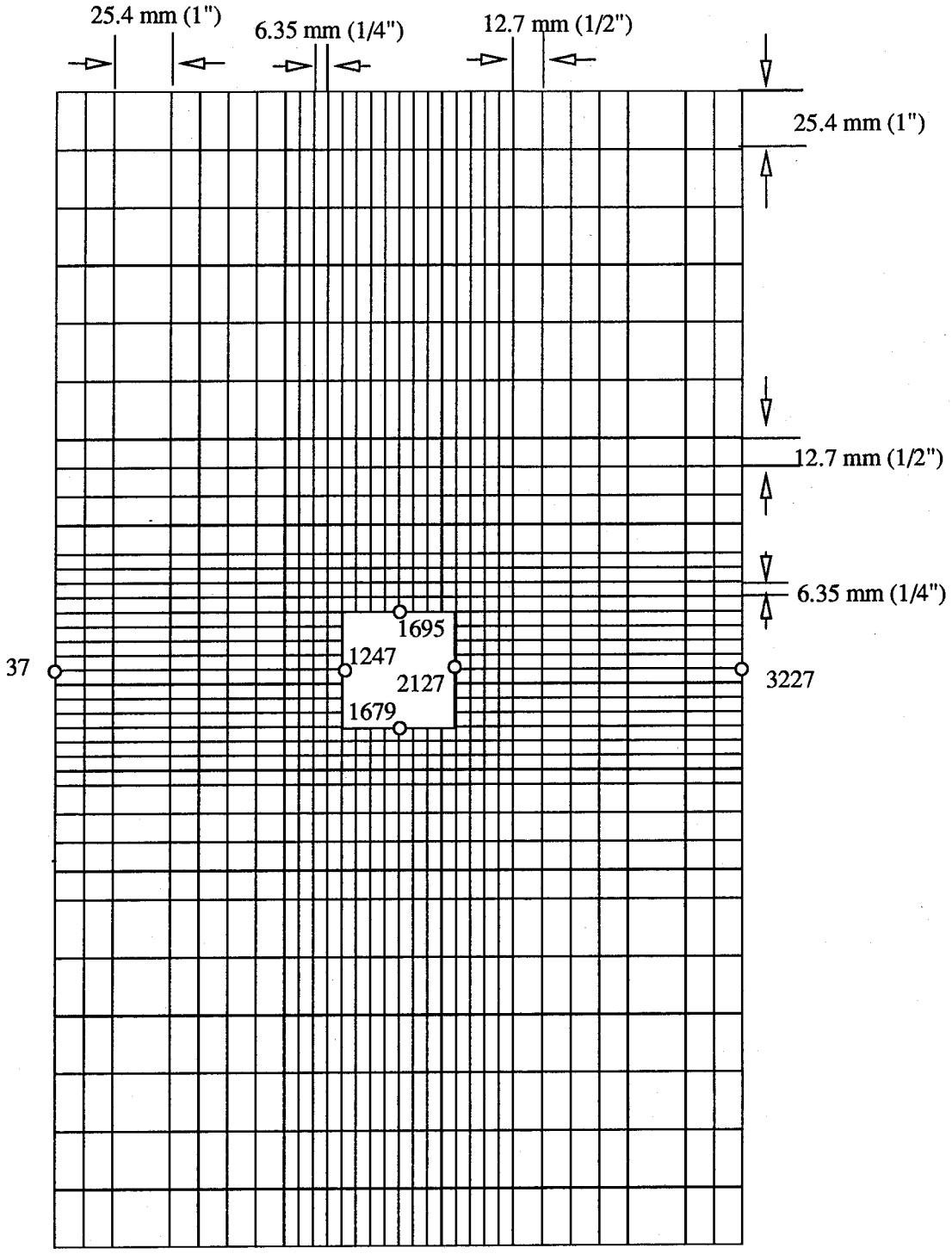

Figure 6. Finite-Element Mesh Used for 304.8 mm x 508 mm (12" x 20") Panel With 50.8 mm x 50.8 mm (2" x 2") Cutout Third Refinement 12.7 mm (1/2") From Free Edges

freedom (u and v). This element was previously used by Shimmels, Hatfield, and Del Barga in their collapse analysis of cylindrical panels with large cutouts [15,18, and 1].

The CLASSIC program uses a two dimensional 28 degrees of freedom rectangular curved finite element similar to the 36 degrees of freedom element used in SHELL, except the four corner nodes do not have the rotational degrees of freedom $\psi_{,x}$, and $\psi_{,s}$. This element does not incorporate the through-the-thickness parabolic transverse shear distribution either.

Although it is not visible in Figures 3-10, there are elements inside the cutouts. This is due to the automatic mesh generation used by both the SHELL and CLASSIC programs. The programs model the cutout by leaving out the stiffness for the elements within the cutout area [20], which is allowed because all the nodes of these elements within the cutout region are also constrained ($u = v = w = \psi_x = \psi_s = w_{,x} = w_{,s} = 0$) in the input file. This algorithm was not originally available to CLASSIC, but was added for this research.

The material properties used for the SHELL analysis are located in Table 2. The program CLASSIC used the same properties except for the shear properties, which it neglects. These material properties were deemed to be too stiff by Del Barga based on his experimental results [1]. He determined a knockdown factor of 0.9831 which was applied to all numerical loads obtained in this research. This factor was based on a linear variation in collapse load predicted by the numerical results caused by varying the material properties used by the SHELL program from those of the actual AS4/3501-6 graphite epoxy panels used for experimental data.

Total nodes = 3985

Total elements = 1280

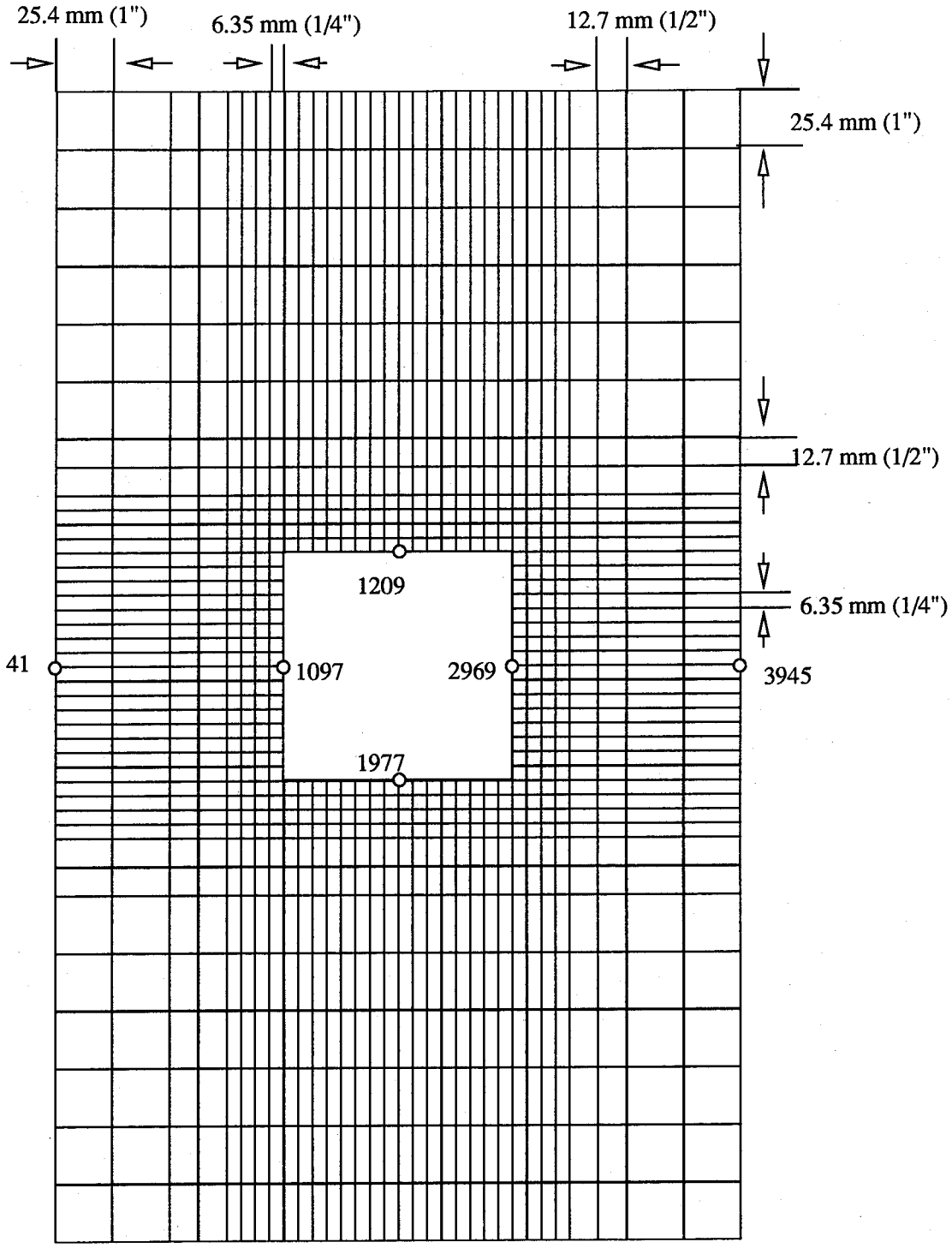

Figure 7. Finite-Element Mesh Used for 304.8 mm x 508 mm (12" x 20") Panel With 101.6 mm x 101.6 mm (4" x 4") Cutout Refined 25.4 mm (1") Around Cutout

Total nodes = 4913

Total elements = 1584

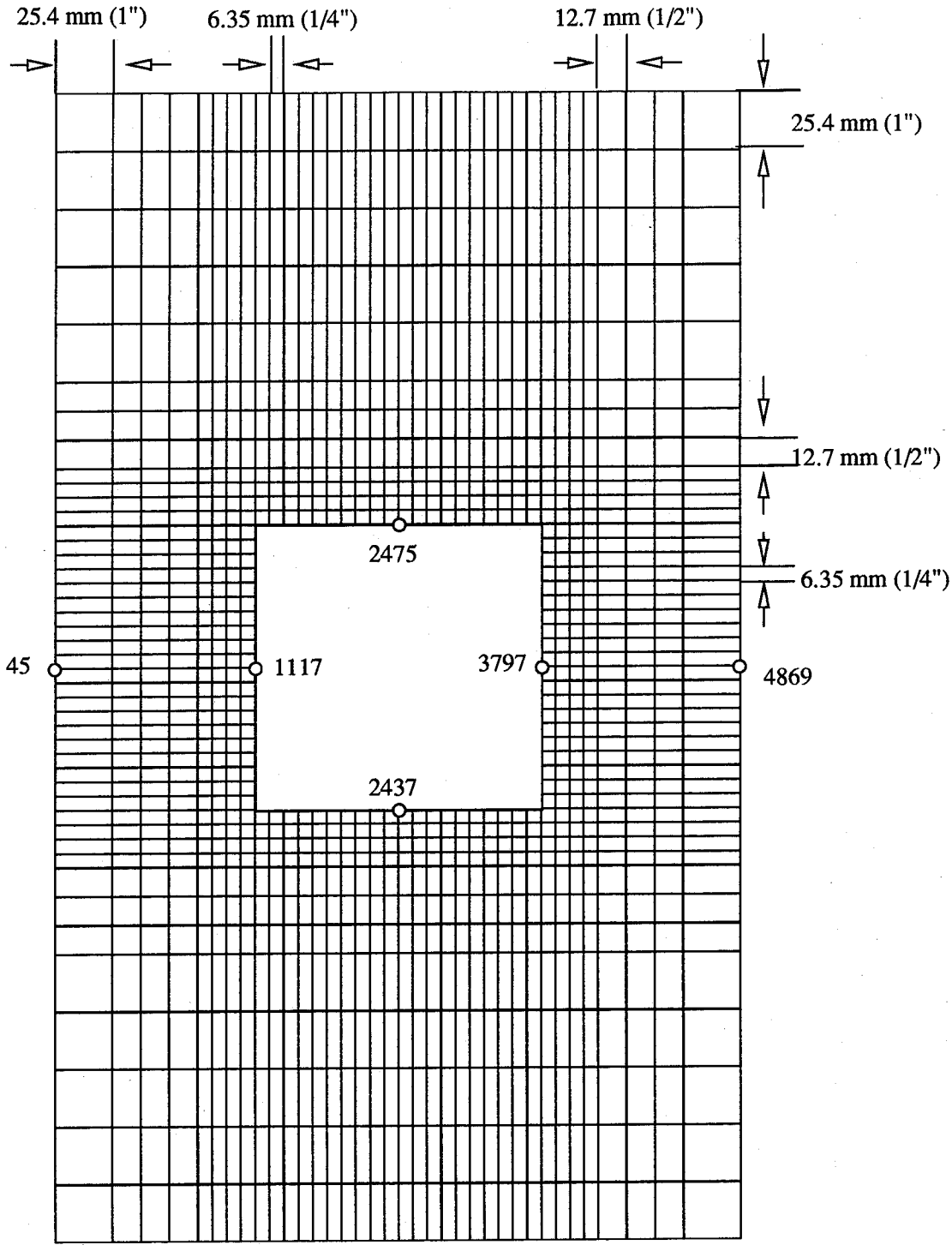

Figure 8. Finite-Element Mesh Used for 304.8 mm x 508 mm (12" x 20") Panel With 127 mm x 127 mm (5" x 5") Cutout Refined 25.4 mm (1") Around Cutout

Total nodes = 3253

Total elements = 1040

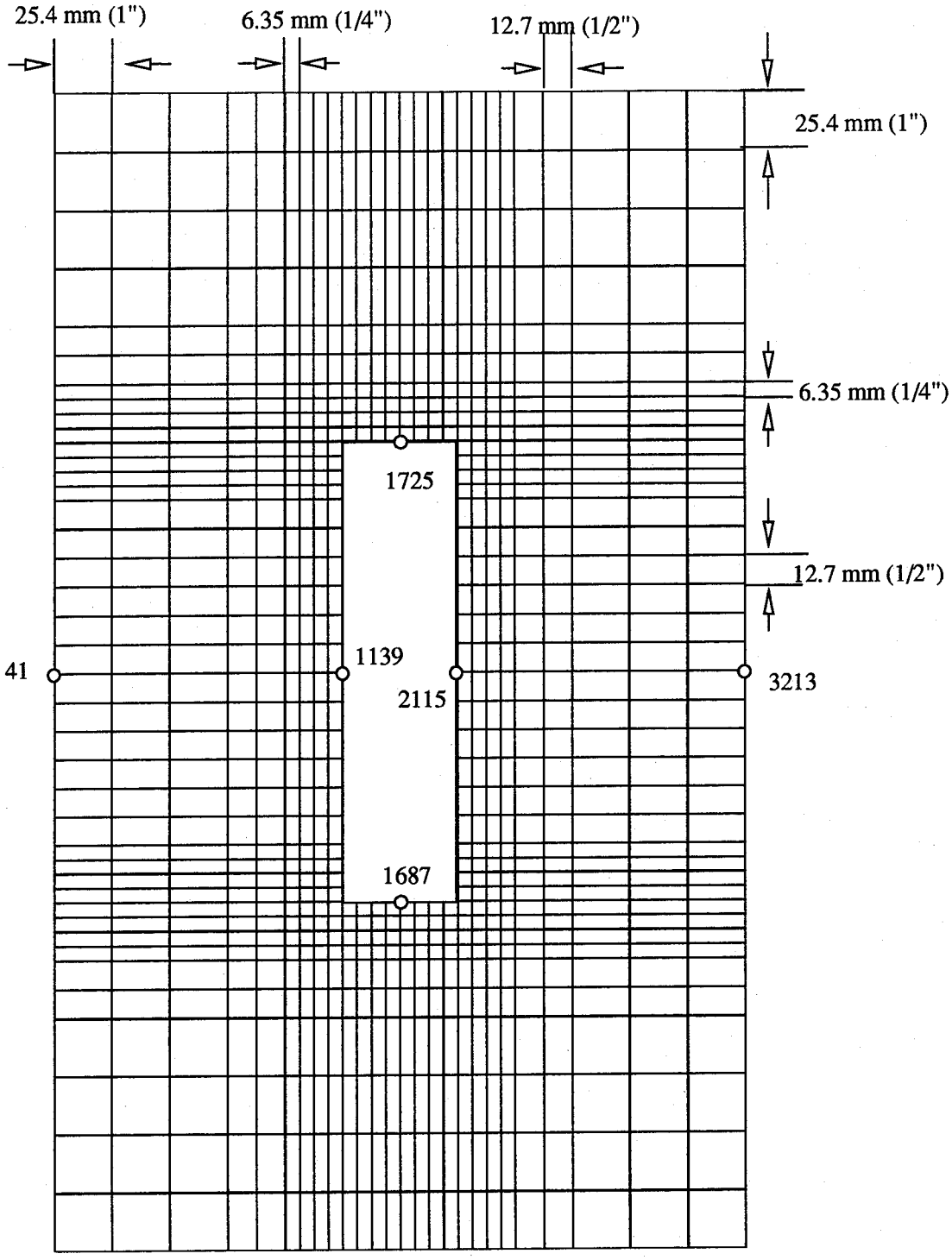

Figure 9. Finite-Element Mesh Used for 304.8 mm x 508 mm (12" x 20") Panel With 50.8 mm x 203.3 mm (2" x 8") Cutout Refined 25.4 mm (1") Around Cutout Corners

Total nodes = 3397

Total elements = 1088

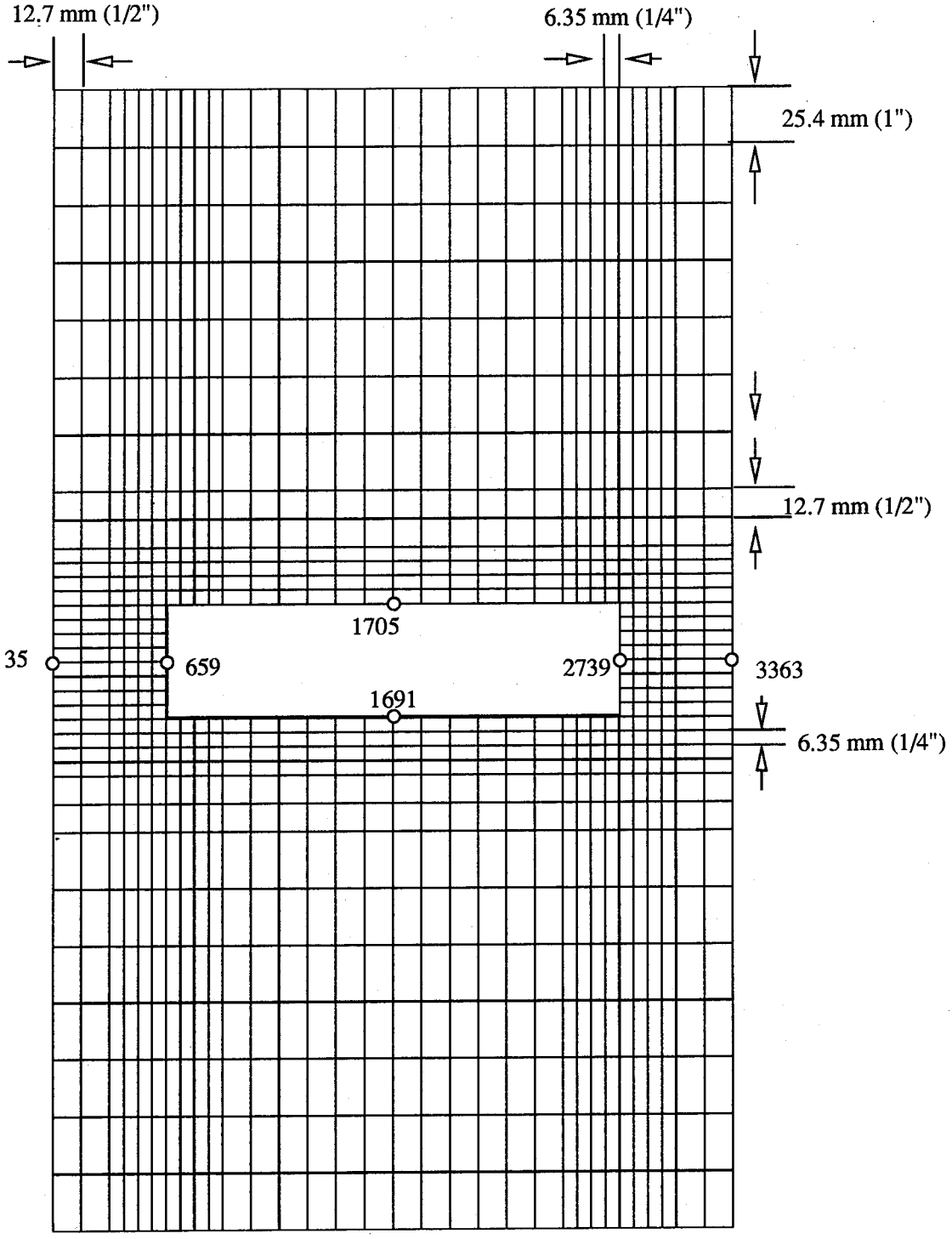

Figure 10. Finite-Element Mesh Used for 304.8 mm x 508 mm (12" x 20") Panel With 203.3 mm x 50.8 mm (8" x 2") Cutout Refined 25.4 mm (1") Around Cutout Corners

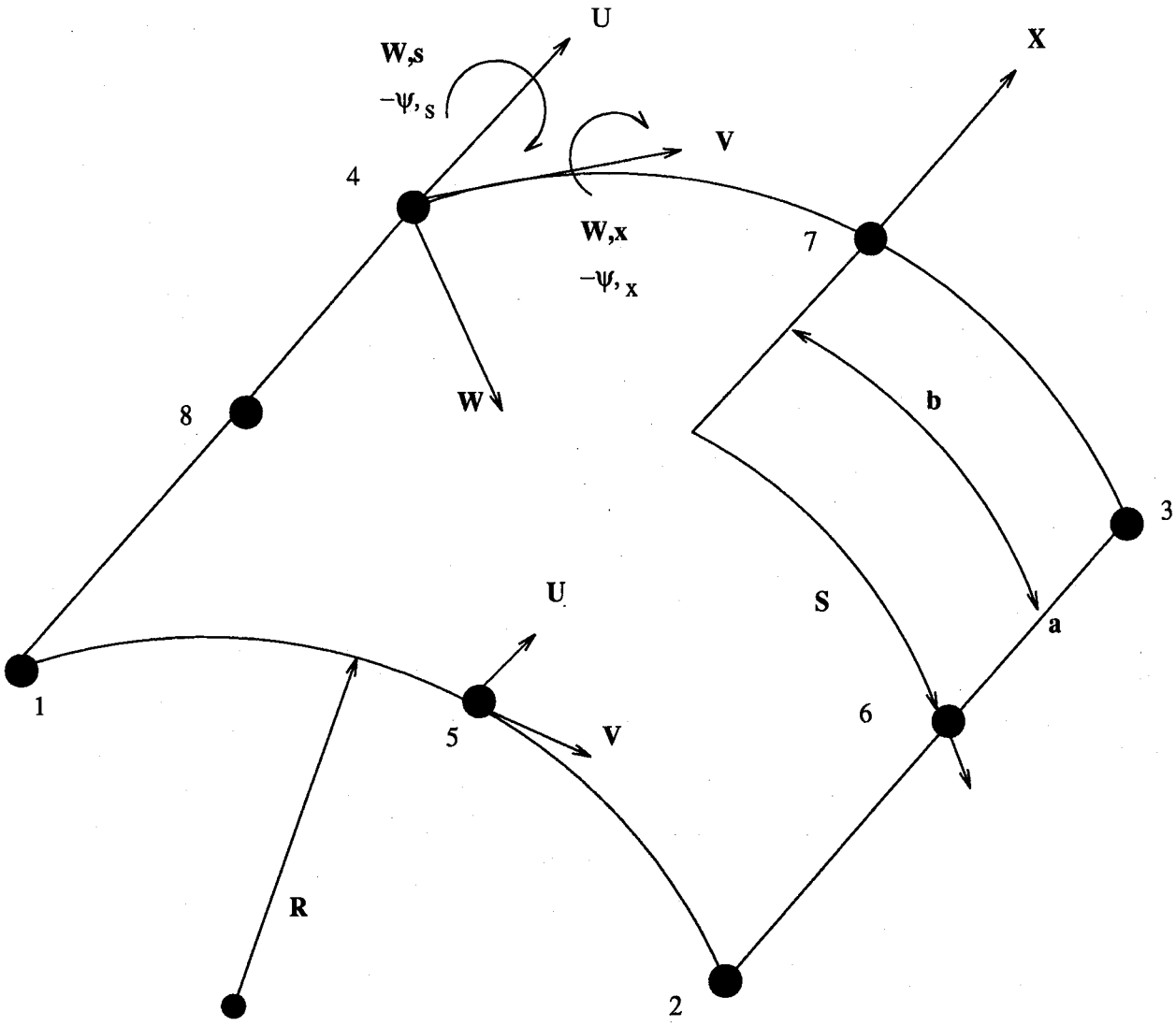

Figure 11: SHELL 36-Degree-of-Freedom Element

Table 2. Properties of AS4/3501-6 Used by SHELL [1]

Elastic Modulus Along Fibers in Compression (E_1)	135.8 GPa (19.7 Msi)
Elastic Moduli Transverse to Fibers in Compression ($E_2 = E_3$)	10.9 GPa (1.579 Msi)
Major Poisson's Ratio (ν_{12})	0.276
Elastic Moduli in Shear ($G_{12} = G_{13}$)	6.4 GPa (0.925 Msi)
Transverse Elastic Modulus in Shear (G_{23})	3.2 Gpa (0.462 Msi)

The average ply thicknesses of each panel/cutout configuration was the same used by Del Barga in his research [1]. The solid 8 and 16 ply shells used the same average thicknesses as their respective 50.8 mm x 50.8 mm (2" x 2") cutout counterparts. The 32 ply shells had the same average ply thickness as their respective 16 ply counterparts. All panels were analyzed for a radius of curvature of 304.8 mm (12"). This dimension is the radius of curvature measured to the convex outside surface of the shell. Both the SHELL and CLASSIC programs interpret the radius of curvature input to be at the mid-ply or datum surface.

All of the ply lay-ups analyzed used a symmetric quasi-isotropic lay-up of [0/45/-45/90]. All of the panel configurations and cutout combinations were analyzed using the same boundary conditions. The panel vertical edges were free, which left all seven degrees of freedom at each element's corner nodes and the two in plane degrees of freedom of each element's mid-side nodes unconstrained along the free vertical edges. The bottom horizontal edge of the panel was completely constrained, which left all seven

degrees of freedom at the element corner nodes and the two degrees of freedom at the element mid-side nodes constrained along this edge ($u = v = w = \psi_x = \psi_S = w_{,x} = w_{,S} = 0$). The panel top horizontal edge was allowed to displace axially a prescribed incremental amount in the u direction. However, the remaining degrees of freedom were all constrained. Thus, six degrees of freedom at the element corner nodes were constrained ($v = w = \psi_x = \psi_S = w_{,x} = w_{,S} = 0$) and one degree of freedom at the element mid-side nodes was constrained ($v = 0$) along the horizontal top edge of the panel.

The two programs used in this research apply a prescribed uniform axial compressive displacement at each of the top edged nodes. The programs calculate the load at each top edge node required to displace the amount prescribed. Then, the total compressive load is calculated using all of the top edge nodal loads. The prescribed initial displacement increment used in the analyses was 0.0015" for the 8 ply panels and 0.003" for the 16 and 32 ply panels.

All numerical analyses were run on SUN SPARC 20 computers. A sample input deck used for both programs is included in Appendix B.

2.2.1 Convergence Study

The finite-element models used by Del Barga were optimized for cpu run time using the SLR theory. The Classical Donnell theory had never been used on models as large as Del Barga's before this research. Therefore, a convergence study was initially performed by repeatedly refining the model used for the 8 ply 304.8 mm x 508 mm (12" x 20") panel with the 50.8 mm x 50.8 mm (2" x 2") cutout. All three theories were run

using the refined models mentioned in the previous section. The collapse loads for each run are listed in Table 3.

Table 3. Collapse Loads for 8 ply 304.8 mm x 508 mm (12" x 20") Panel With 50.8 mm x 50.8 mm (2" x 2") Cutout

Theory	SLR	Modified Donnell	Classical Donnell
Original Mesh	6930 N	6956.67 N	6765.4 N
1st Refinement	6729.8 N	6765.4 N	6676.45 N
2nd Refinement	6729 N	6738.7 N	6680.9 N
3rd Refinement	6685.34 N	6725.7 N	6725.7 N

These results indicate monotonic convergence for both the SLR and the Modified Donnell theories because their collapse loads continue to decrease with each refinement in which the last refinement is within 5% of the previous value. The Classical Donnell theory, however does not converge monotonically. The collapse load estimated by this theory first decreases then increases with no definite trend, although the variation of the results with each refinement is within 5% of the previous value. This oscillating motion indicates that the elements used in the Classical Donnell theory are incompatible for this model [38]. These elements have 28 degrees of freedom, but the shape function for w is Hermitian. By not taking into account the rotations ψ_x and ψ_S these elements lack the overall effect of making the third order shape function, which is incompatible for the w and $w_{,j}$ terms, more dominating. This characteristic was diluted in the 36 degree of freedom element with the addition of ψ_x and ψ_S. Figure 12 provides a graphical

representation of the convergence trends for the collapse loads of the three theories versus the number of elements in the mesh.

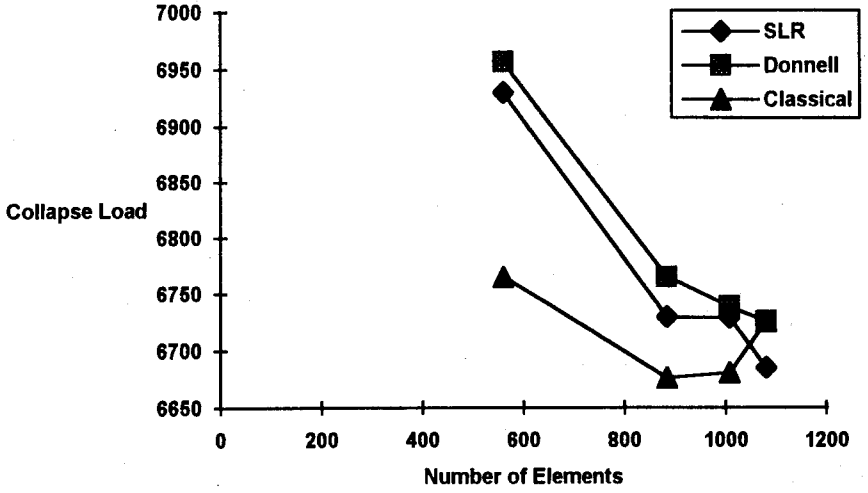

Figure 12: Collapse Load vs. Number of Elements for 8 ply 304.8 mm x 508 mm (12" x 20") Panel With 50.8 mm x 50.8 mm (2" x 2") Cutout

An additional observation that can be made from Table 3 is that the collapse load predicted by the Classical Donnell theory was lower than those predicted by both the SLR and Modified Donnell theories except for the 3rd refinement. The results prior to the 3rd refinement are not realistic considering the fact that Classical Donnell neglects both through-the-thickness shear and large rotations. This should lead to higher predicted collapse loads than the two more complex theories. This behavior was also observed in the initial results obtained for each of the cutout configurations used for the 8 ply shells and both the 16 and 32 ply shells with 127 x 127 mm (5" x 5") cutouts. These results and the results of the refined meshes are listed in Tables 4-9. The trends displayed in these tables support the observation that the results for the Classical Donnell theory are not monotonically converging. The refined results show an increase in the predicted collapse

load for the Classical Donnell theory in each of the cases involving a 127 mm x 127 mm cutout. The remaining 8 ply cases showed a decrease in the collapse load. The SLR and Modified Donnell theories, on the other hand, show a trend of decreasing predicted collapse loads with refinement in every case.

There does not appear to be a discernible trend in the convergence of any of the results for the Classical Donnell theory. However, it is interesting to note that the collapse loads in Table 3 first decrease then increase to a value closer to the two more advanced theories, and the other cases also approach values closer to the monotonically converging theories. Therefore, it is possible that instead of monotonically converging, the Classical Donnell theory is converging in an oscillating manner, where the oscillations decrease in amplitude until it is fully converged at values close to, but above, the collapse loads predicted by the other two theories.

Table 4. Collapse Loads for 8 ply 304.8 mm x 508 mm (12" x 20") Panel With 101.6 mm x 101.6 mm (4" x 4") Cutout

Theory	SLR	Modified Donnell	Classical Donnell
Original Mesh	5181.9 N	5297.6 N	5190.8 N
Refined Mesh	5052.9 N	5146.3 N	5146.3 N

Table 5. Collapse Loads for 8 ply 304.8 mm x 508 mm (12" x 20") Panel With 127 mm x 127 mm (5" x 5") Cutout

Theory	SLR	Modified Donnell	Classical Donnell
Original Mesh	3327.1 N	3402.7 N	3095.8 N
Refined Mesh	3247 N	3322.7 N	3322.7 N

Table 6. Collapse Loads for 8 ply 304.8 mm x 508 mm (12" x 20") Panel With 203.2 mm x 50.8 mm (2" x 8") Cutout

Theory	SLR	Modified Donnell	Classical Donnell
Original Mesh	5533.3 N	5608.9 N	5319.8 N
Refined Mesh	5378.8 N	5453.2 N	5453.2 N

Table 7. Collapse Loads for 8 ply 304.8 mm x 508 mm (12" x 20") Panel With 50.8 mm x 203.2 mm (8" x 2") Cutout

Theory	SLR	Modified Donnell	Classical Donnell
Original Mesh	3042.4 N	3158.1 N	3060.2 N
Refined Mesh	2557.6 N	2655.5 N	2655.5 N

Table 8. Collapse Loads for 16 ply 304.8 mm x 508 mm (12" x 20") Panel With 127 mm x 127 mm (5" x 5") Cutout

Theory	SLR	Modified Donnell	Classical Donnell
Original Mesh	15,363.4 N	15,857.1 N	15,127.6 N
Refined Mesh	15,137.4 N	15,622.2 N	15,631.0 N

Table 9. Collapse Loads for 8 ply 304.8 mm x 508 mm (12" x 20") Panel With 127 mm x 127 mm (5" x 5") Cutout

Theory	SLR	Modified Donnell	Classical Donnell
Original Mesh	75,847.3 N	78,894.2 N	78,075.7 N
Refined Mesh	75,073.3 N	78,058 N	78,058.9 N

3. Results and Discussion

3.1 Introduction

This chapter has three sections. In the first section the data obtained using the SLR theory in this research is used in conjunction with Del Barga's numerical results to expand on his study of cutout dimensionallity and panel thickness [1]. The second section concentrates primarily on the effects of through-the-thickness shear and large rotations observed in the numerical results obtained with the SLR, Modified Donnell, and Classical Donnell theories. The final section compares the numerical results of these three theories to experimental results obtained in previous research [1,18].

Throughout this section the same convention will be used to describe the panel configurations in each table. Since all of the panels are the same length, 304.8 mm x 508 mm (12" x 20"), each panel configuration can be described by just three numbers. The first number indicates the number of plies in the layup followed by the word ply. The second two numbers in the designation describe the type of cutout. For example the designation 8ply0x0 would be used for the 8 ply panel without a cutout while the 32 ply panel with a 127 mm x 127 mm (5" x 5") cutout would be indicated by the designation 32ply5x5.

3.2 Cutout Dimensionality and Panel Thickness

Del Barga performed a collapse study using the SLR theory in the SHELL program for each of the cutout sizes used in this study for 8 and 16 ply 304.8 mm x 508

mm (12" x 20") panels. For this research, solid panel configurations were included in addition to the 5 cutout sizes used by Del Barga for 8, 16, and 32 ply 304.8 mm x 508 mm (12" x 20") panels. All of the analyses used the following boundary conditions: the panels had free vertical edges, with the bottom horizontal edge completely constrained and the top horizontal edge allowed only to displace in the axial direction (u). The panels were loaded through a prescribed displacement and the applied total load along the panel top edge was output by the SHELL program for each increment. The SHELL program also included displacements and rotations for all element corner nodes for each increment.

Table 10 displays the numerically derived global collapse load and top edge displacements (u). Global is defined as pertaining to the entire panel. The results in Table 10 indicate the maximum load analytically applied to the panels just before the panels collapsed. Table 10 also shows the panel top edge displacement (u) that is associated with the global collapse load. These results coincide with Del Barga's finding that the collapse load decreases with increased cutout area and decreased panel thickness.

Figures 13-18 illustrate the effects of panel thickness on the collapse loads by cutout size for the 304.8 mm x 508 mm (12" x 20") panels. These figures support Del Barga's findings that the stiffness of the panels is increased for increasing panel thickness. In addition, these figures illustrate that the collapse load increases with increasing panel thickness.

Del Barga also investigated the effects of cutout dimensionality. Figures 19-21 demonstrate the effects of cutout size on collapse load, panel stiffness, and non-linear response of the panel. They also show that for every case, except one, the collapse load decreases with decreasing extensional width and increasing cutout area. Extensional

Table 10. Numerical Global Collapse Load and Top Edge Displacement

Panel	Collapse Load		u Displacement	
Designator	Kn	(lbs)	mm	(in)
8ply0x0	10.555	2373	.4191	.0165
8ply2x2	6.572	1478	.28575	.01125
8ply4x4	4.967	1136	.381	.015
8ply5x5	3.192	730	.28575	.01125
8ply2x8	5.378	1210	.36195	.01425
8ply8x2	2.558	575	.55245	.02175
16ply0x0	38.316	8762	.74295	.02925
16ply2x2	29.959	6851	.6477	.0255
16ply4x4	23.216	5309	.762	.03
16ply5x5	15.137	3403	.6477	.0255
16ply2x8	27.926	6386	.8763	.0345
16ply8x2	13.460	3078	.8001	.0315
32ply0x0	193.149	44168	2.1717	.0855
32ply2x2	160.075	36605	1.6383	.0645
32ply4x4	99.386	22727	1.2573	.0495
32ply5x5	75.073	16878	1.3716	.054
32ply2x8	90.705	20742	.9906	.039
32ply8x2	67.222	15372	1.6002	.063

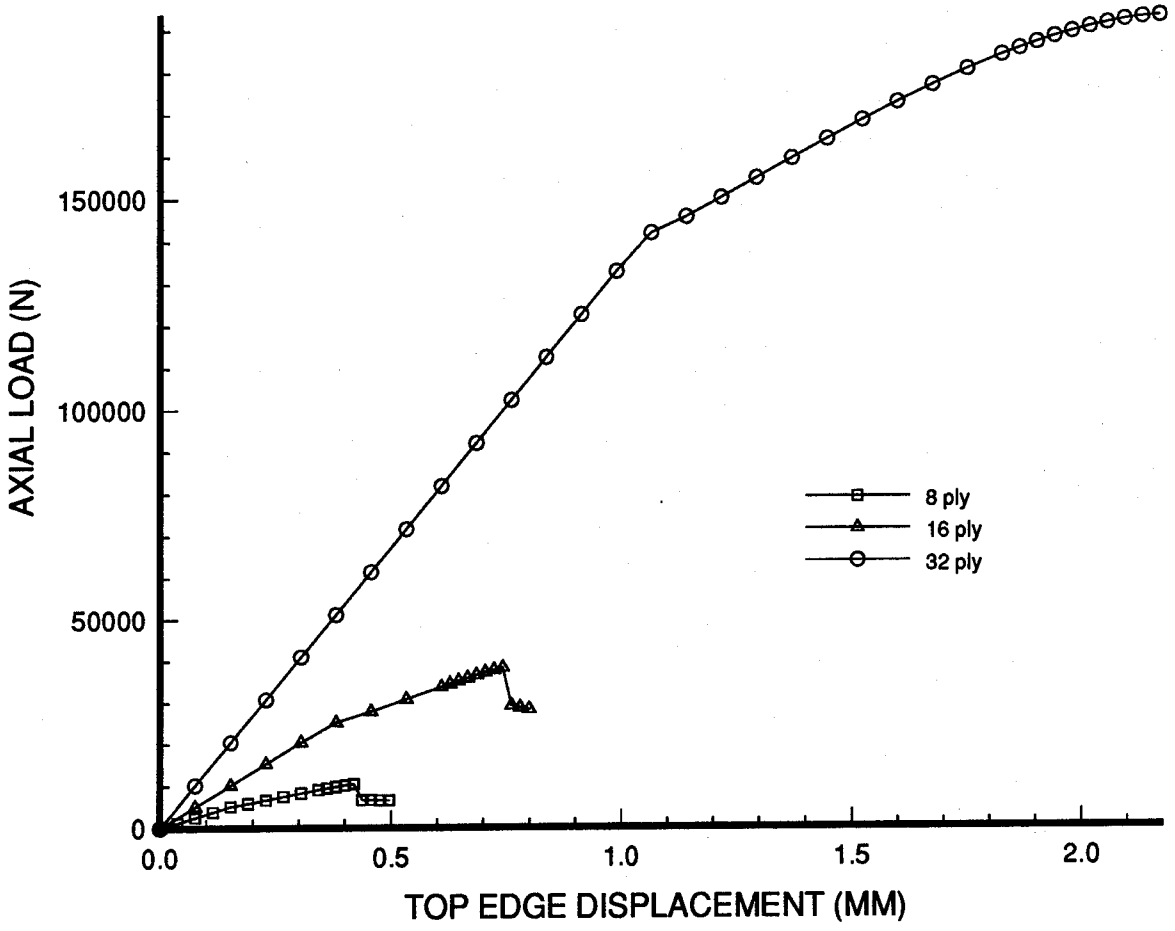

Figure 13: Effects of Thickness on a
Solid 304.8 mm x 508 mm
(12" x 20") Panel

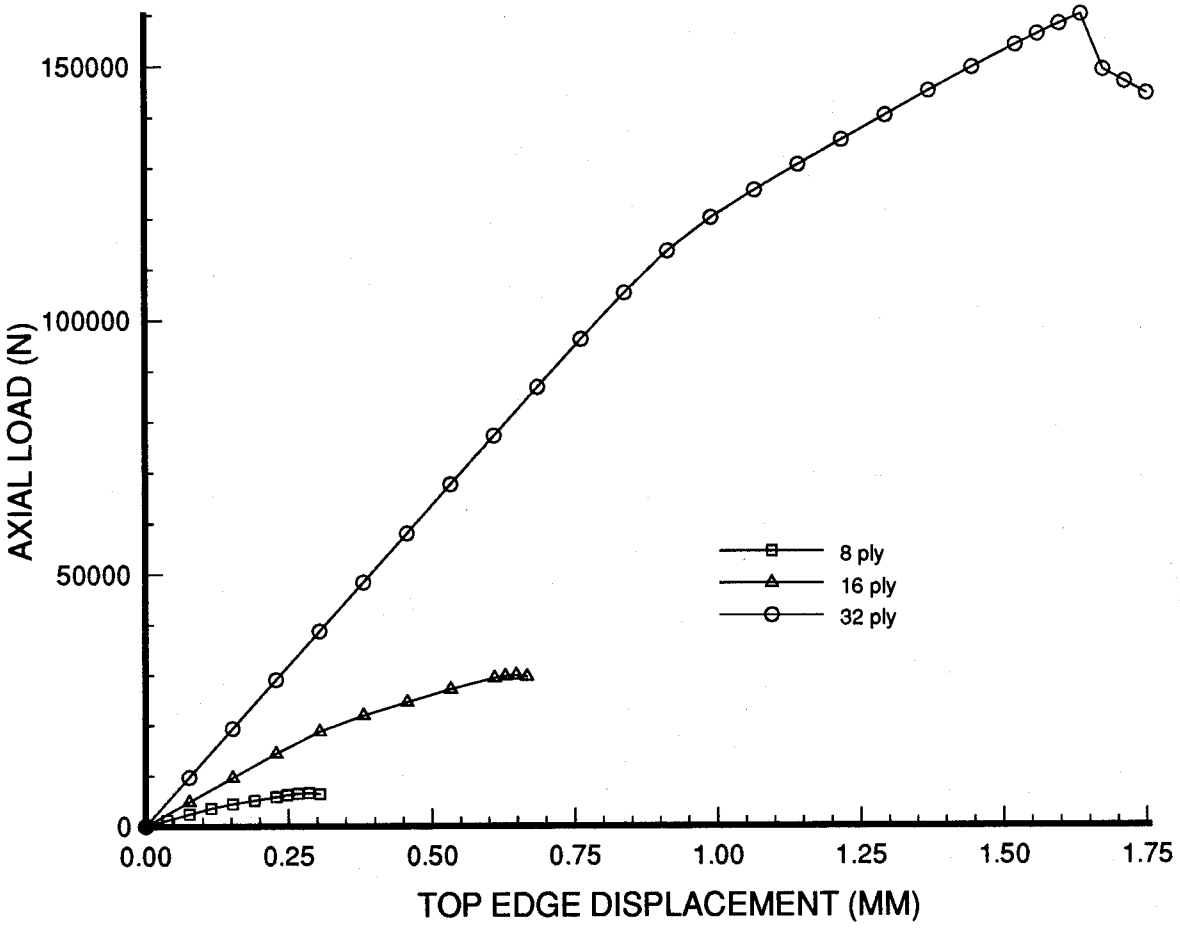

Figure 14: Effects of Thickness on a
50.8 mm x 50.8 mm (2" x 2") Cutout in a
304.8 mm x 508 mm (12" x 20") Panel

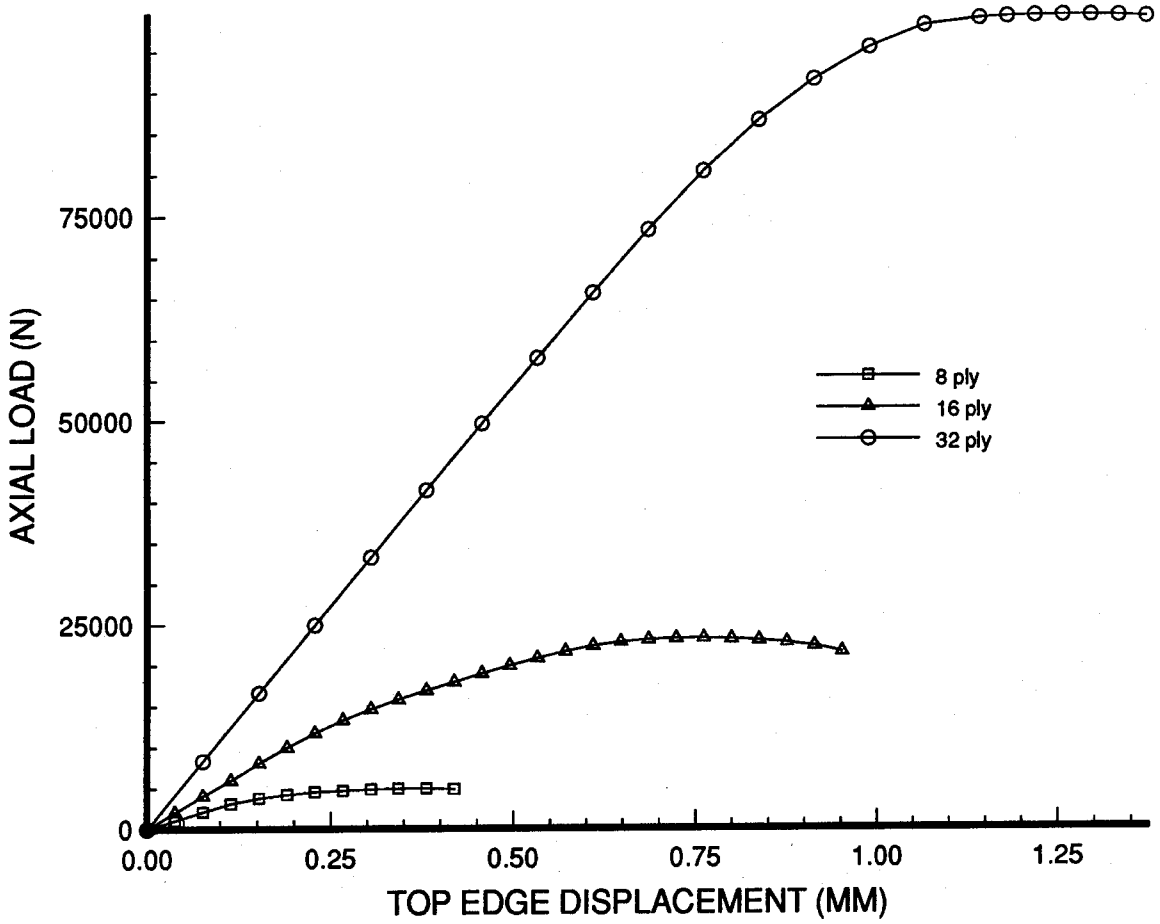

Figure 15: Effects of Thickness on a
101.6 mm x 101.6 mm (4" x 4") Cutout in a
304.8 mm x 508 mm (12" x 20") Panel

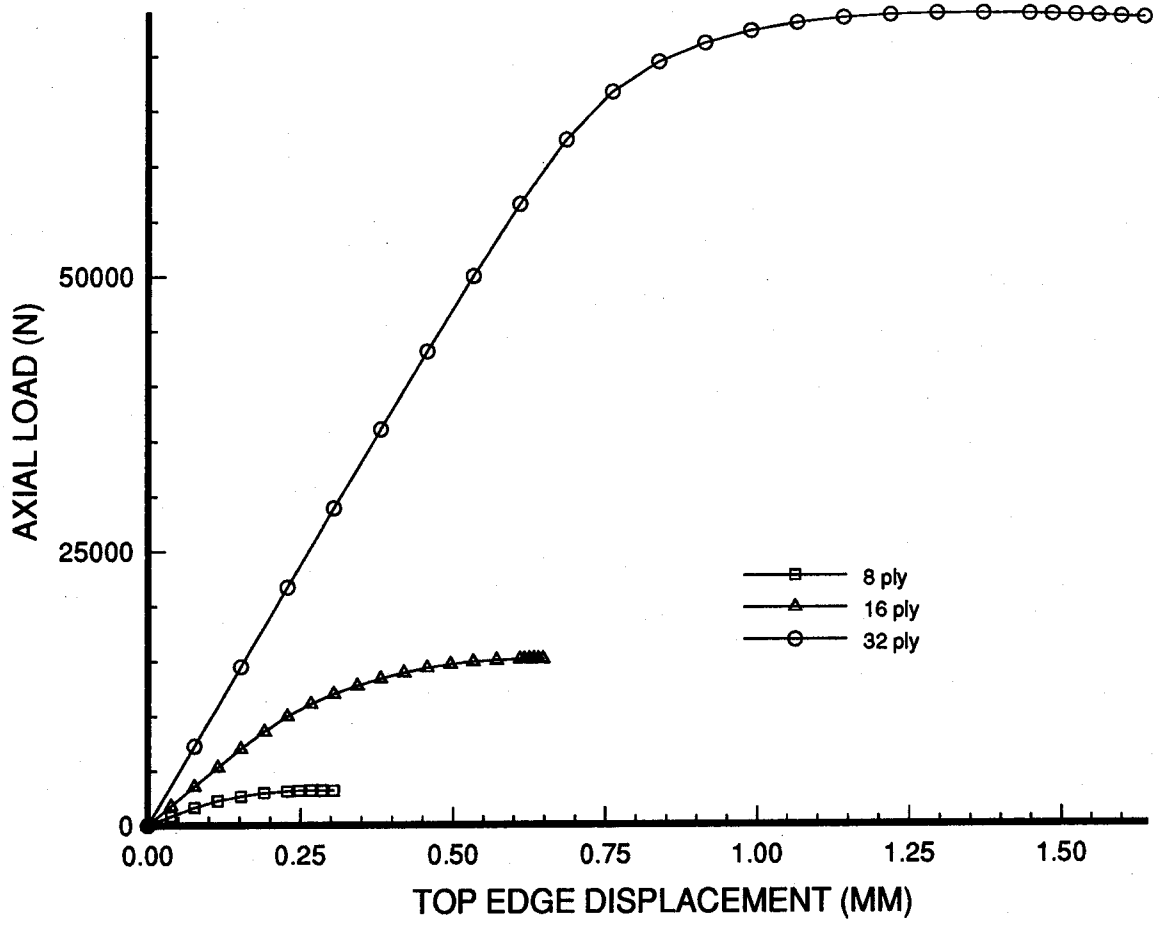

Figure 16: Effects of Thickness on a
127 mm x 127 mm (5" x 5") Cutout in a
304.8 mm x 508 mm (12" x 20") Panel

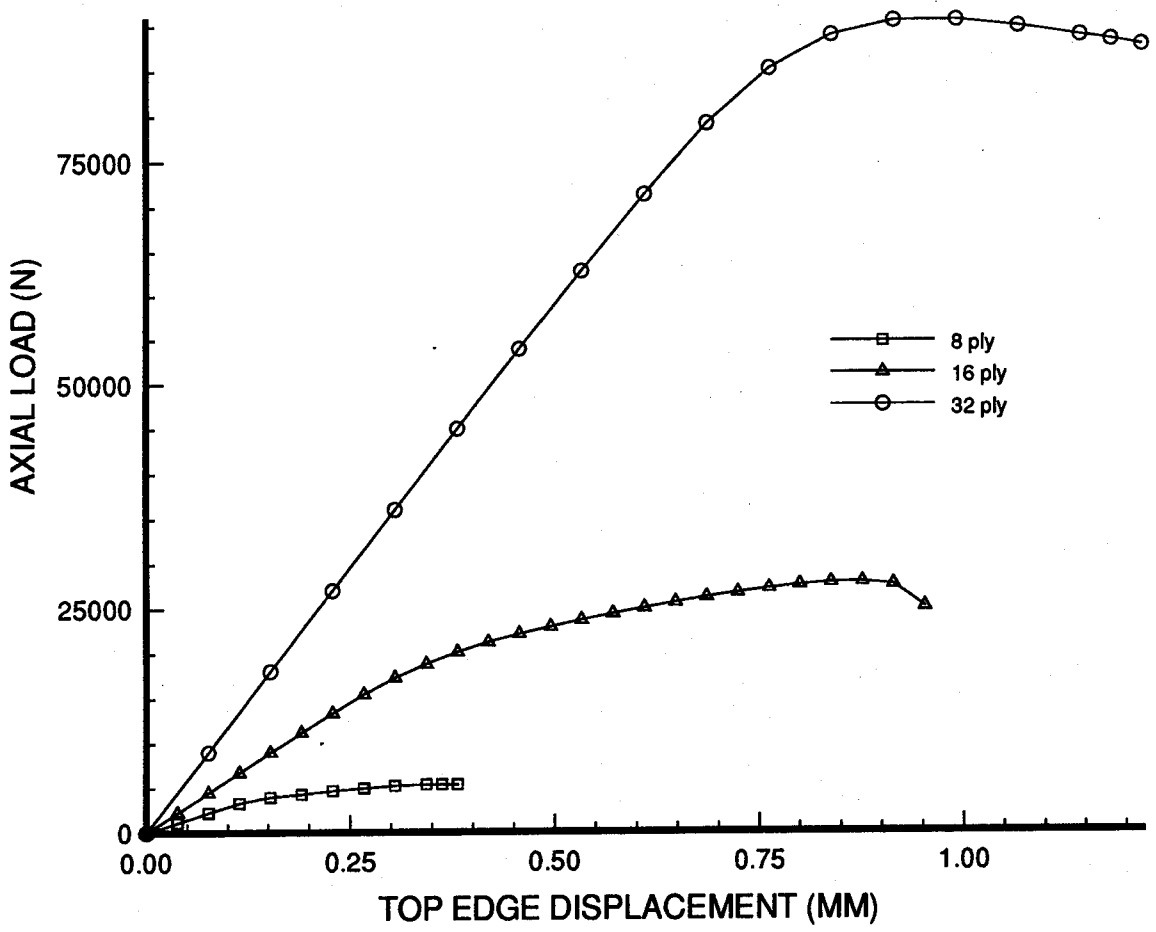

Figure 17: Effects of Thickness on a
50.8 mm x 203.2 mm (2" x 8") Cutout in a
304.8 mm x 508 mm (12" x 20") Panel

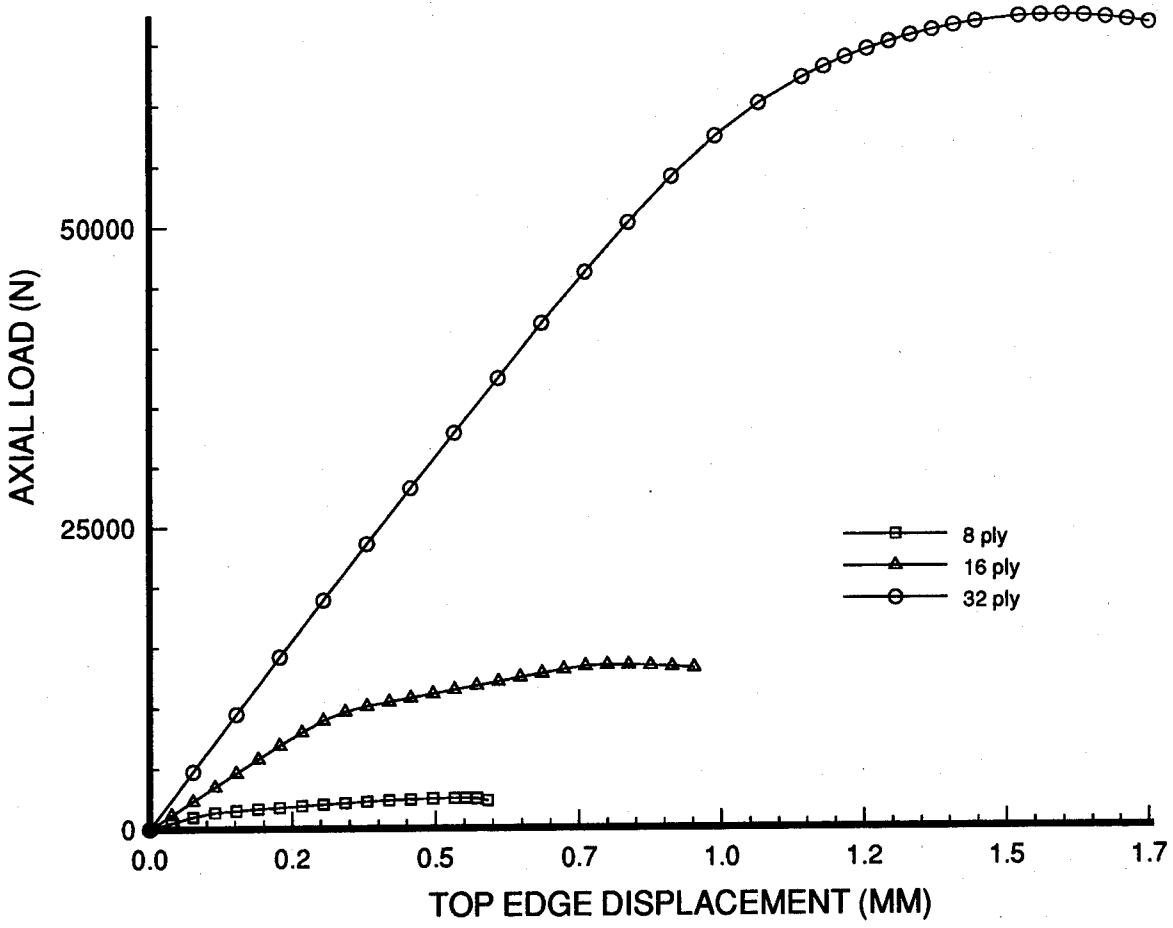

Figure 18: Effects of Thickness on a
203.2 mm x 50.8 mm (8" x 2") Cutout in a
304.8 mm x 508 mm (12" x 20") Panel

width is defined as the distance from the free edge of the cutout to the free edge of the panel. For example, a panel with 127 mm x 127 mm cutout has an extensional width of 88.9 mm (3.5"). This is fairly simple to calculate. The formula is simply to take the difference in the width of the panel and the width of the cutout and divide by two since the cutouts are symmetric. Thus, for this example half the difference in the width of the panel, 304.8 mm (12"), and the width of the cutout, 127 mm (5"), is 88.9 mm (3.5"). A solid panel has an extensional width equal to half the width of the panel, 152.4 mm (6") and in every case has the stiffest response and the greatest collapse load.

The effects of extensional width are more apparent when comparing collapse loads of panels with equivalent cutout area. The exception is for the 32 ply panel configuration with a 50.8 mm x 203.2 mm cutout, which collapsed at a lower load than the 101.6 mm x 101.6 mm cutout (see Figure 21). This mirrors Del Barga's results, where his exception was noticed for 24 ply panels. He made the assertion that this can be attributed to the amount of transverse shear and bending motion each of these panels experienced [1]. This assertion is supported by the results pertaining to through-the-thickness shear discussed later in this section.

Figures 19-21 also show that the load versus displacement curves become more non-linear as the cutout area increases and the extensional width decreases. This indicates a greater distribution of bending is occurring for the larger cutouts and cutouts with small extensional widths[1]. Also, the slopes of the load versus displacement curves decrease for increasing cutout area and decreasing extensional width. Thus, stiffness increases with decreasing cutout area and increasing extensional width.

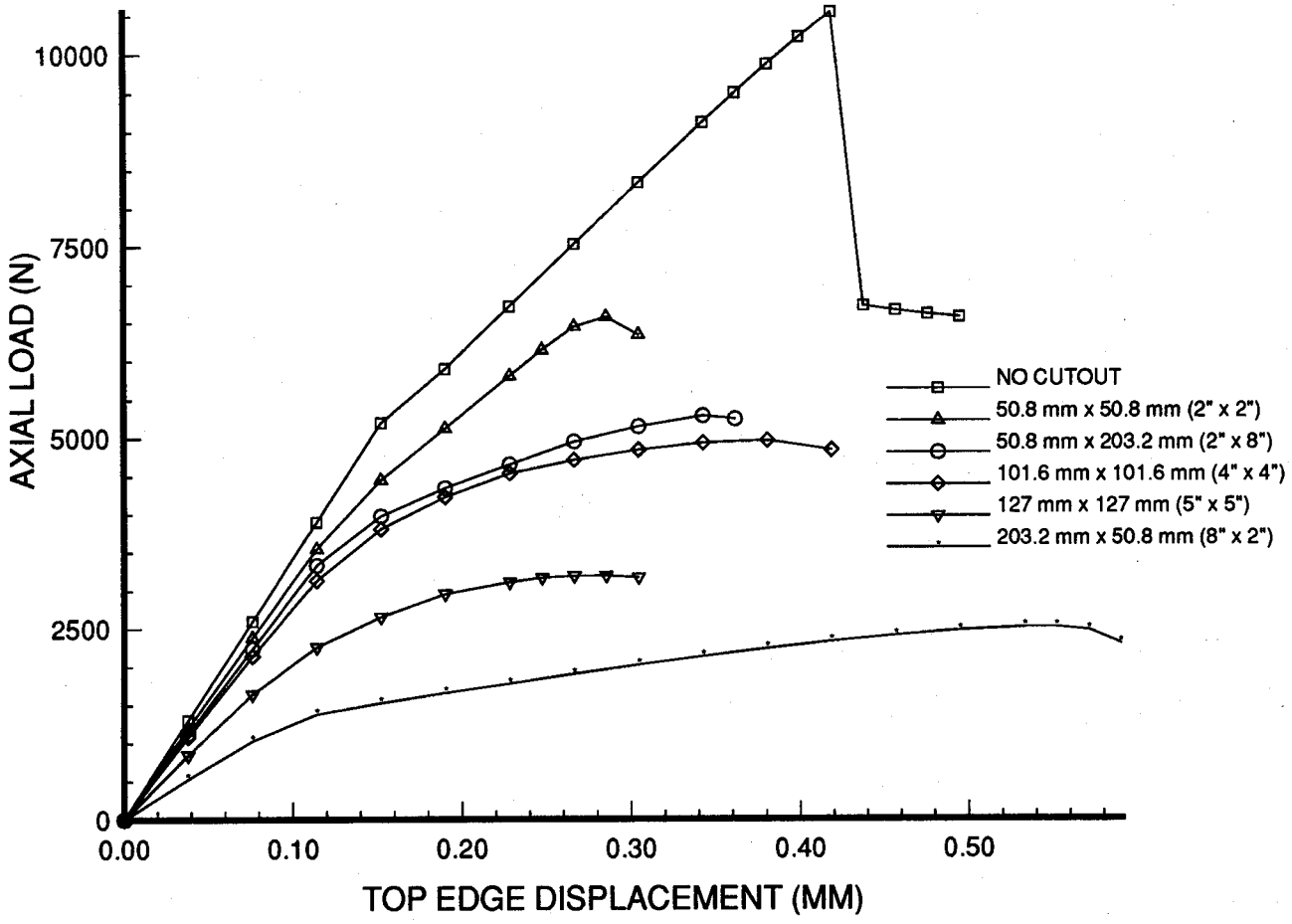

Figure 19: The Effects of Varying Cutout Size
On the Load vs. Displacement Curve for a
304.8 mm x 508 mm (12" x 20") Panel
[0/45/-45/90]s

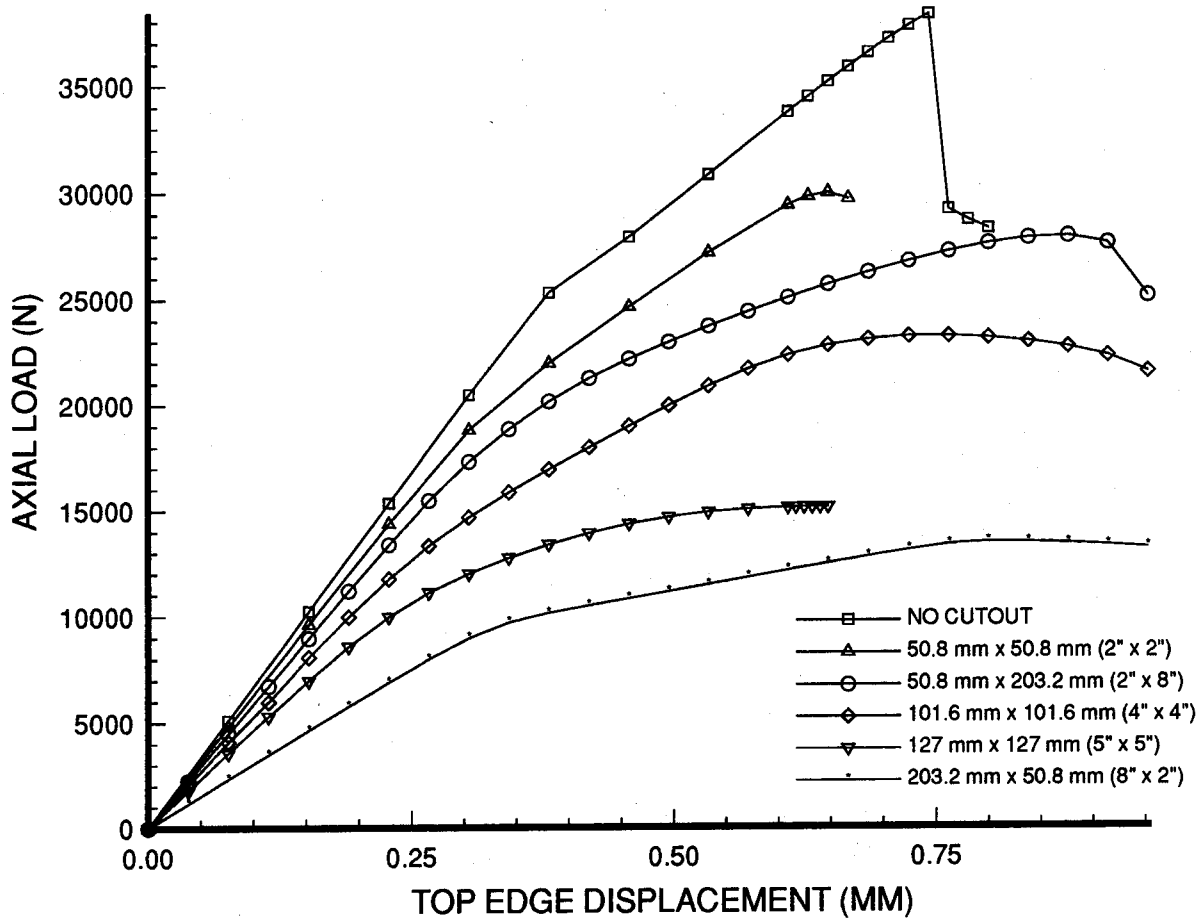

Figure 20: The Effects of Varying Cutout Size
On the Load vs. Displacement Curve for a
304.8 mm x 508 mm (12" x 20") Panel
[0/45/-45/90]2s

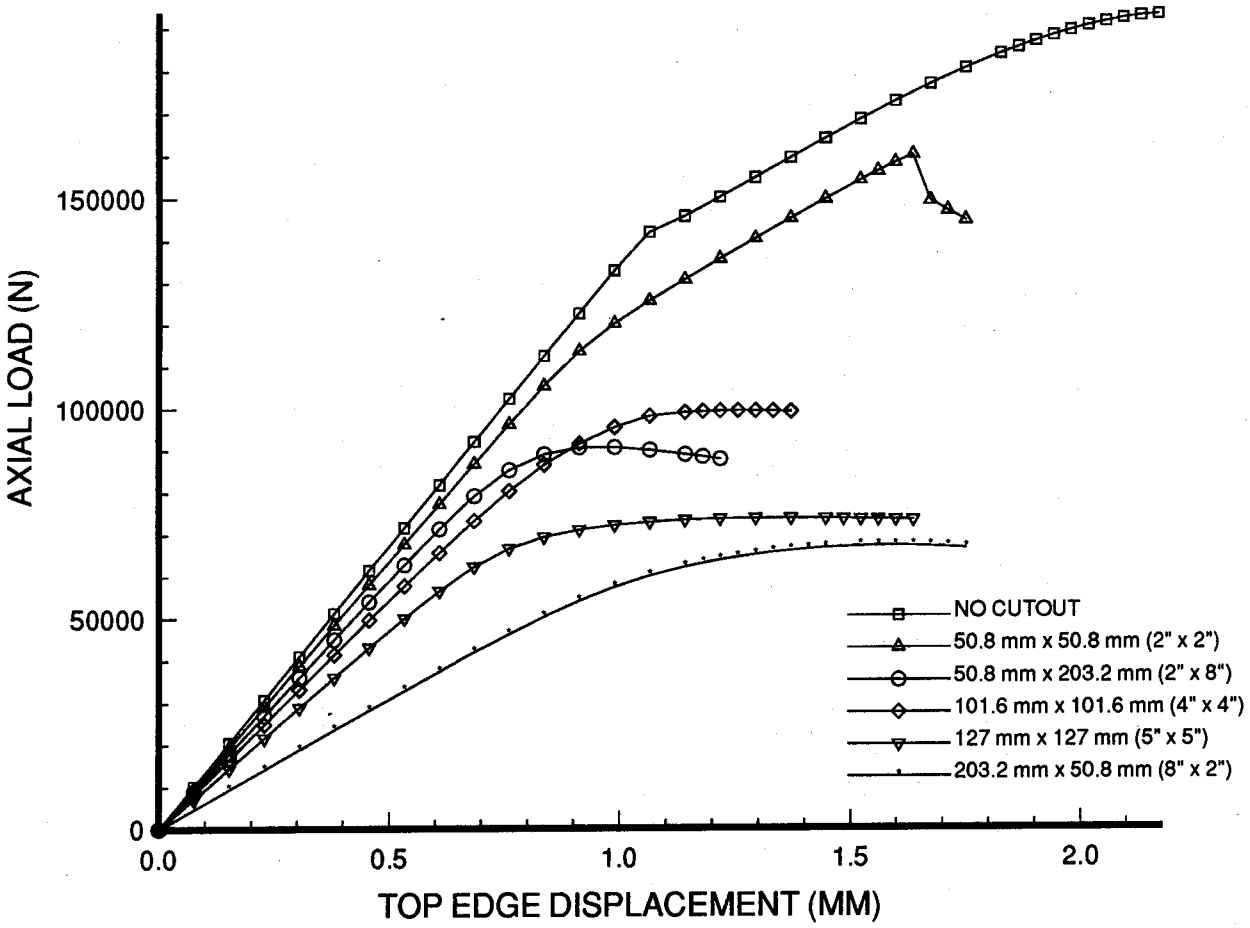

Figure 21: The Effects of Varying Cutout Size
On the Load vs. Displacement Curve for a
304.8 mm x 508 mm (12" x 20") Panel
[0/45/-45/90]4s

Table 11 documents the magnitudes of the maximum radial displacements (w) observed in each panel configuration. This table helps to verify that a nonlinear theory is required for panels with large cutouts undergoing axial compression. The radial displacements range from 2-5 times the panel thickness in the 32 ply cases, 5-7 times the panel thickness in the 16 ply cases, and 8-11 times the panel thickness in the 8 ply cases.

Each panel configuration experienced the maximum radial displacement along the free vertical edge of the panel. This maximum occurred on or near the horizontal centerline of the panel. The distribution of the radial displacements tended to increase in magnitude along the horizontal centerline as the vertical edge of the cutout was approached. All the panels exhibited exact symmetry of radial displacements along the horizontal and vertical centerlines of the panel. However, the remaining radial displacements displayed asymmetry about the horizontal and vertical centerlines of the panel. The values for radial displacements were equivalent in magnitude and direction at diagonals to each other. This asymmetry is caused by the presence of the +45 and -45 degree oriented plies which affect the bending stiffness terms D_{16} and D_{26}. These terms affect the in-plane twisting moment (M_{xy}) [1]. Three dimensional orthographic plots for each of the panels investigated in this research are located with their respective load displacement curve plots in the next section and Appendix C. The displacements have been scaled by a factor of five in these figures for plotting purposes.

One advantage of the SHELL program is its ability to handle large rotations more completely with the coupling of u, v, and w into the rotation. Another attribute is that it incorporates a parabolic transverse shear strain distribution through the thickness of the panel. Table 12 documents the global maximum bending rotations (ψ_S) and the global

Table 11. Global Numerical Radial Displacements (w)

Panel	Maximum | w |		w/h
Designator	mm	(in)	Ratio
8ply0x0	9.7165	.38254	9.56
8ply2x2	7.6057	.29944	7.486
8ply4x4	10.419	.4102	10.255
8ply5x5	8.4932	.33438	8.36
8ply2x8	8.9819	.35362	8.84
8ply8x2	11.186	.4404	11.01
16ply0x0	11.1333	.43832	5.48
16ply2x2	10.3099	.4059	5.07
16ply4x4	11.5524	.45482	5.685
16ply5x5	10.485	.4128	5.16
16ply2x8	13.2674	.52234	6.53
16ply8x2	10.6497	.41928	5.24
32ply0x0	19.3375	.76132	4.76
32ply2x2	14.077	.55422	3.46
32ply4x4	9.6317	.3792	2.37
32ply5x5	12.3063	.4845	3.03
32ply2x8	9.06526	.3569	2.23
32ply8x2	9.6215	.3788	2.3675

maximum shear strains. The transverse shear strains are defined as:

$$\varepsilon_4 = | \psi_S | - | w_{,S} | \qquad (1)$$

$$\varepsilon_5 = | \psi_x | - | w_{,x} |$$

The maximum bending rotations occurred at or near the same location as the global maximum radial displacement for most of the panels, which was the horizontal centerline of the panel along the panel free vertical edge. In cases where the maximum global bending rotation did not coincide with the maximum global radial displacement, it instead coincided with the maximum local radial displacement [1]. Del Barga defined local as being along the cutout edges.

Just as the radial displacements along the panels' free vertical edges for all the panels increased as the horizontal centerline of the panel was approached, so did the bending rotations. Also, the bending rotations were symmetric along the panels' horizontal and vertical centerlines. However, for the rest of the panel, equivalent magnitudes of bending rotations occurred at diagonals to each other.

In general, the maximum global transverse shear strains occurred at the cutout corners for panels with cutouts and near the center of the panel (the intersection of horizontal and vertical centerlines) for solid panels. Equivalent magnitudes of transverse shear strains occurred at diagonals to each other. For more specifics on the exact locations of the maximum transverse shear strains, see Del Barga [1].

It is interesting to note that for the eight ply panels the transverse shear strain was greater for a rectangular cutout versus a square cutout with equivalent cutout area. The opposite appears true as the panel thickness is increased. One example is where the 32 ply panels had a larger transverse shear strain with a square cutout than a rectangular cutout

Table 12. Global Maximum Bending Rotations and Transverse Shear Strain

Panel Designator	Global ψ_s (deg.)	Global $\lvert\varepsilon_4\rvert$	Global $\lvert\varepsilon_5\rvert$
8ply0x0	9.2	.001130	.000669
8ply2x2	7.5	.001190	.001313
8ply4x4	9.2	.000503	.001303
8ply5x5	7.8	.001347	.000964
8ply2x8	9.8	.000824	.000869
8ply8x2	10.2	.002230	.001146
16ply0x0	9.1	.000610	.000412
16ply2x2	8.1	.001130	.002322
16ply4x4	8.2	.002333	.001558
16ply5x5	7.6	.002357	.001565
16ply2x8	13.0	.001324	.003420
16ply8x2	8.9	.001970	.001707
32ply0x0	13.1	.000038	.000852
32ply2x2	9.9	.000432	.002041
32ply4x4	5.9	.007007	.006587
32ply5x5	7.3	.006804	.004704
32ply2x8	5.0	.002974	.001316
32ply8x2	3.6	.004594	.001394

with the same cutout area. This helps to explain the exception mentioned earlier that was similar to Del Barga's 24 ply case where the collapse load of the panel with a 101.6 mm x 101.6 mm cutout exceeded the collapse load of the equally thick panel with a 50.8 mm x203.2 mm cutout (see Figure 21). Del Barga explained this occurrence by considering the transverse shear strain (ε_5) along the vertical edge of each cutout. He found that since the magnitudes of the transverse shear strain (ε_5) were greater for the panel with a 101.6 mm x 101.6 mm cutout than the panel with a 50.8 mm x 203.2 mm cutout (see Table 12), the panel with a 101.6 mm x 101.6 mm cutout is absorbing the majority of the axial compressive energy through the distribution taken up by transverse shear strain. This causes bending to decrease and the panel to increase in apparent flexural rigidity. Thus, it collapses at a higher load than the panel with a 50.8 x 203.2 mm cutout even though its extensional width is less. Note, this is more obvious if one observes the two load versus axial displacement curves shown in Figure 21. The two curves relating to the geometries concerned intersect at about 90 KN or 0.9 mm. The 101.6 x 101.6 mm cutout configuration reacts in a stiffer axial fashion from that point until collapse.

The area of significant (>0.001) shear strain is compared for the two panels in Figures 22 and 23. It is obvious that the areas of significant shear strains are much greater in the 32 ply panel with a 101.6 mm x 101.6 mm cutout than the 32 ply panel with a 50.8 mm x 203.2 mm cutout for both ε_4 and ε_5. Del Barga's findings are affirmed by Figure 23. The entire area between the vertical free edge of the cutout and the vertical free edge of the panel experiences significant shear strain ε_5 for the panel with a 101.6 mm x 101.6 mm cutout whereas the panel with a 50.8 mm x 203.2 mm cutout experiences practically no

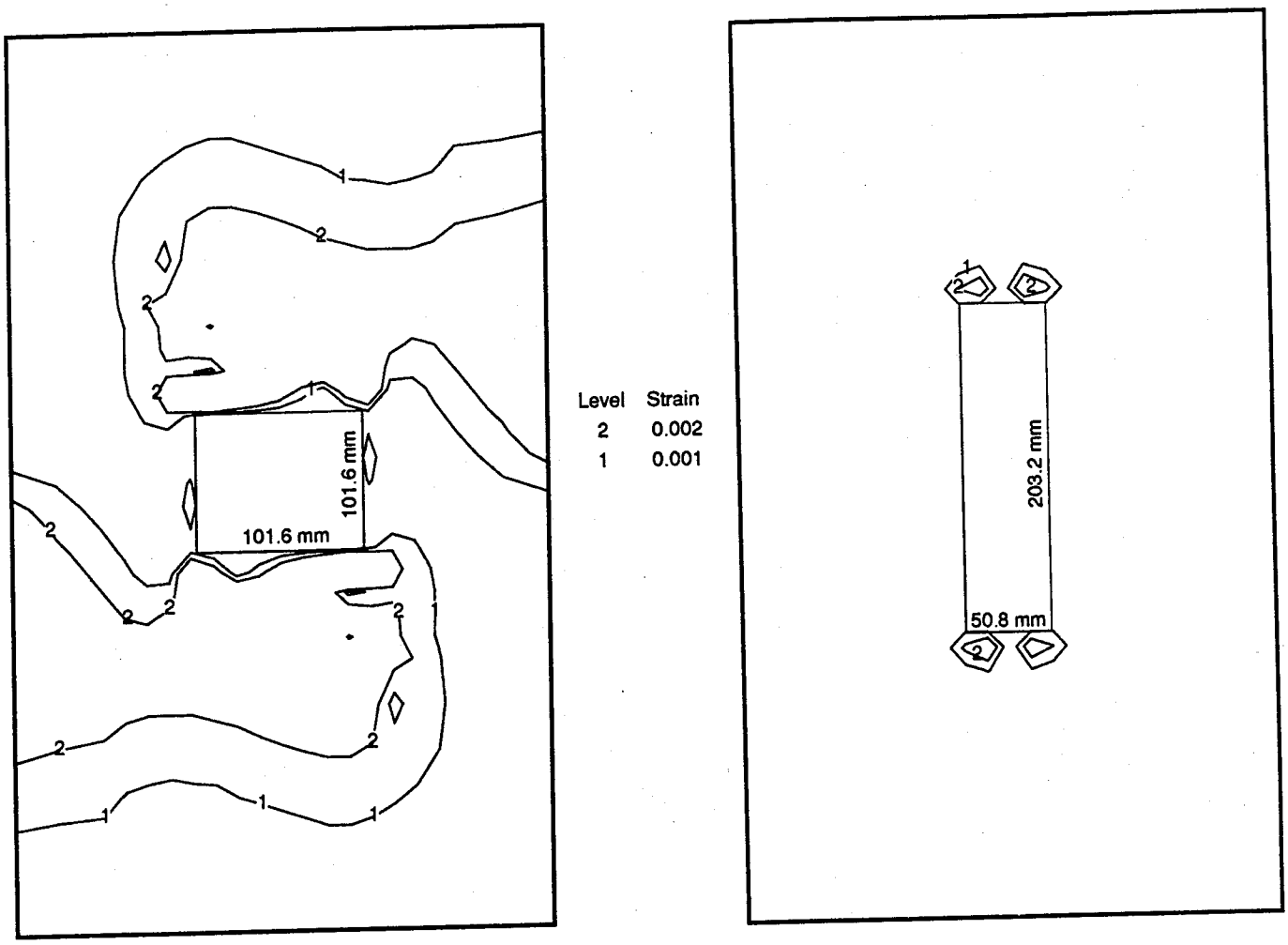

Figure 22: Contours of Transverse Shear Strain ε_4 for
101.6 mm x 101.6 mm (4" x 4") Cutout and
50.8 mm x 203.2 mm (2" x 8") Cutout,
304.8 mm x 508 mm (12" x 20") Panel,
[0/45/-45/90]4s

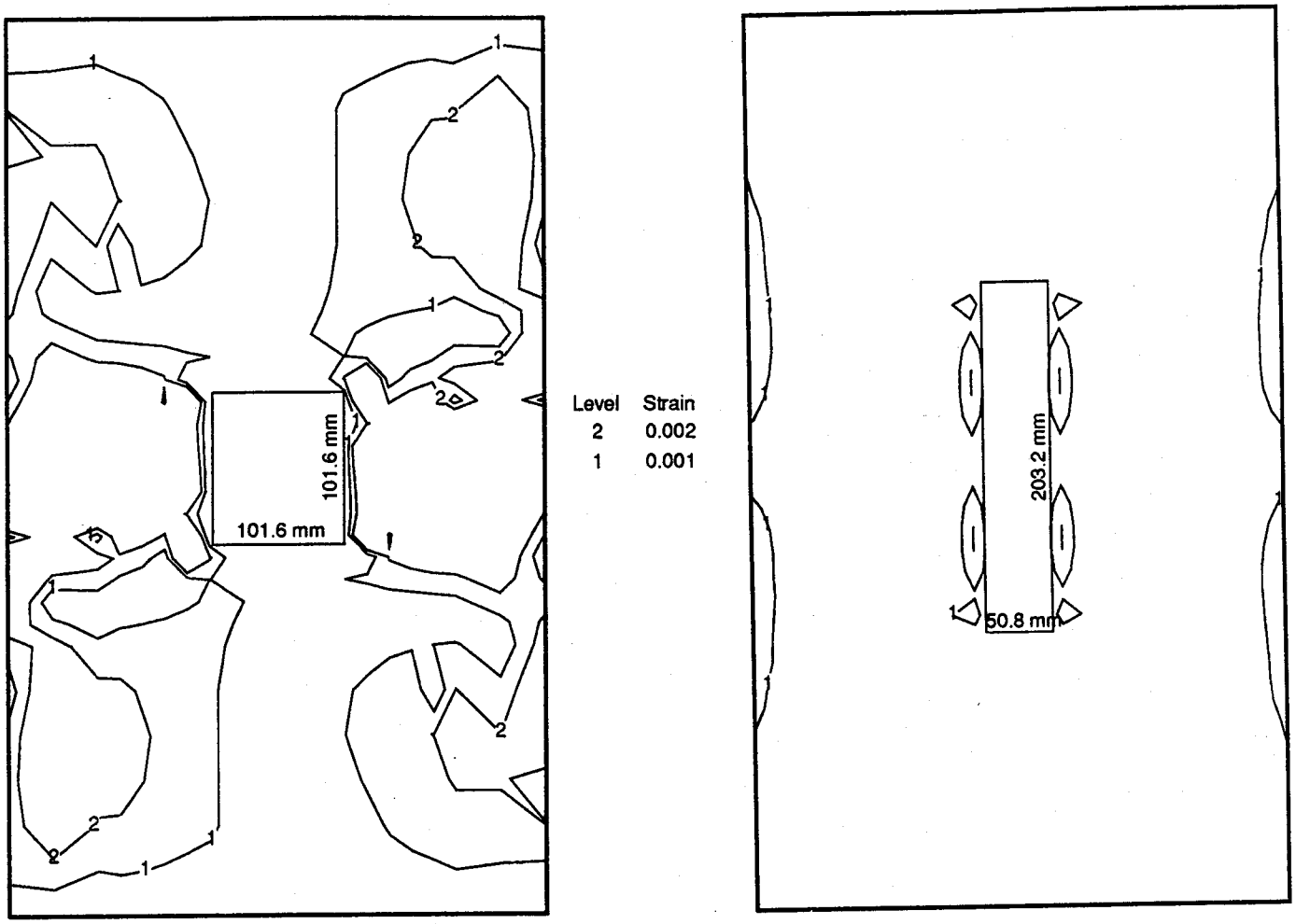

Figure 23: Contours of Transverse Shear Strain ε_5 for
101.6 mm x 101.6 mm (4" x 4") Cutout and
50.8 mm x 203.2 mm (2" x 8") Cutout,
304.8 mm x 508 mm (12" x 20") Panel
[0/45/-45/90]4s

shear strain in this area. Therefore, the 32 ply panel with a 101.6 mm x 101.6 mm cutout is absorbing more axial compressive energy through transverse shear strain while the 32 ply panel with a 50.8 mm by 203.2mm cutout is absorbing most of the axial compressive energy through bending which causes it to collapse at a lower load.

3.3 Through-the-Thickness Shear and Large Rotations

In this section, the effects of through-the-thickness shear and large rotations are examined by comparing the collapse analysis performed on each of the panel configurations used in this research by the SLR, Modified Donnell, and Classical Donnell theories. Since Classical Donnell is the most basic of the three theories, it is useful to normalize the collapse loads predicted by the three theories to the collapse load predicted by Classic, since it should always be the highest. This way it can be noticed where the three theories diverge. This has been done for each of the cutout configurations used in this study (six total), plotting the normalized collapse load for each theory versus the ratio of the radius of curvature to thickness of the panel (R/h). By noticing where Modified Donnell differs in its prediction of the collapse load from that predicted by Classical Donnell, it can be determined at what radius-to-thickness ratio through-the-thickness shear becomes important in cylindrical composite panels, and what effect cutouts have on through-the-thickness shear. Also, by observing where SLR differs from Modified Donnell it can be determined when large rotations become a factor in the solution.

Figures 24 and 25 represent the normalized collapse loads predicted by the three theories at various radius of curvature to thickness ratios for both solid panels and panels

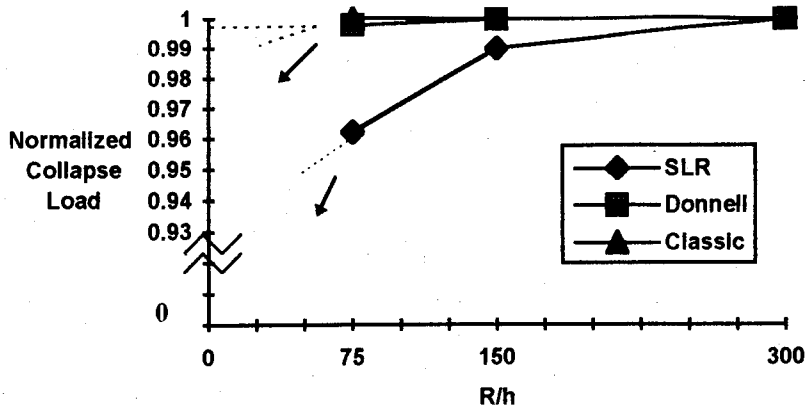

Figure 24: Normalized Load versus R/h for Solid
304.8 mm x 508 mm (12" x 20") Panel

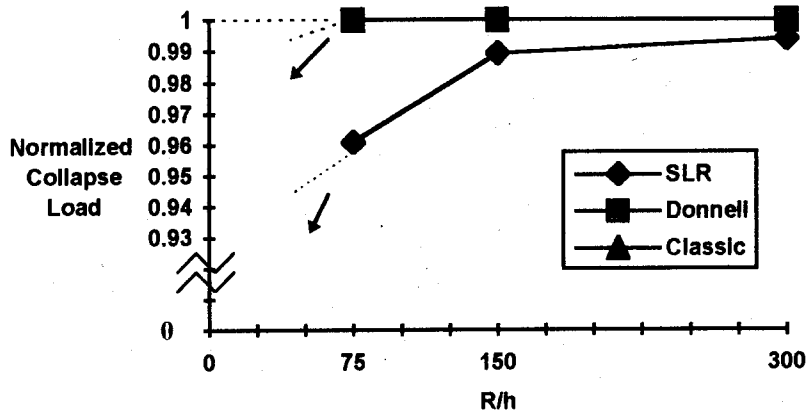

Figure 25: Normalized Load versus R/h for a
50.8 mm x 50.8 mm (2" x 2") Cutout in a
304.8 mm x 508 mm (12" x 20") Panel

with a 50.8 mm x 50.8 mm cutout respectively. Both figures show very little difference in the collapse loads predicted by the Modified Donnell and Classical Donnell theories even for the 32 ply shells. However, the SLR theory predicts a moderately lower collapse load (4%) than either of the Donnell theories in both figures for the 32 ply cases. This indicates that there are large rotations or displacements occurring at or near collapse which do not effect the collapse load as greatly when Modified Donnell and Classical Donnell theories

are used. The dotted lines have been added to show how the curves would tend to follow as thickness increases and the ratio R/h decreases.

The actual predicted collapse loads are plotted in Figures 26 and 27 for the solid 32 ply panel and 32 ply panel with a 50.8 mm x 50.8 mm cutout respectively. These figures also show the deformed panel at collapse and at 50% collapse load. Both panels appear to have undergone large radial displacements along their free edges at collapse, which would also imply large rotation. This is verified by Tables 11 and 12. Therefore, this situation requires a high order nonlinear theory like SLR which can account for large rotations and displacements. It is interesting to note that there is relatively little radial displacement occurring at the 50% collapse point, which makes sense because this occurs in the linear portion of the load versus displacement curve.

As the cutout size increases, through-the-thickness shear and large rotations begin to play a greater role. Figures 28 and 29 document the slight, but detectable, divergence of predicted collapse loads using SLR theory from the results predicted by the Classical Donnell and Modified Donnell theories for 8, 16, and 32 ply shells with 101.6 mm x 101.6 mm (4" x 4") and 127 mm x 127 mm cutouts. They also indicate a difference in the results predicted by Modified Donnell and Classical Donnell for both the 16 and 32 ply shells. These differences are generally fairly small (< 3%), except for the predicted collapse loads for the 32 ply cases by the SLR theory. However, the effects of through-the-thickness shear and large rotations are definitely more observable than for the solid panels and panels with the smaller 50.8 mm x 50.8 mm cutouts. With the exception of the free edges, the rotations and shear strains along the cutout edge are generally larger than

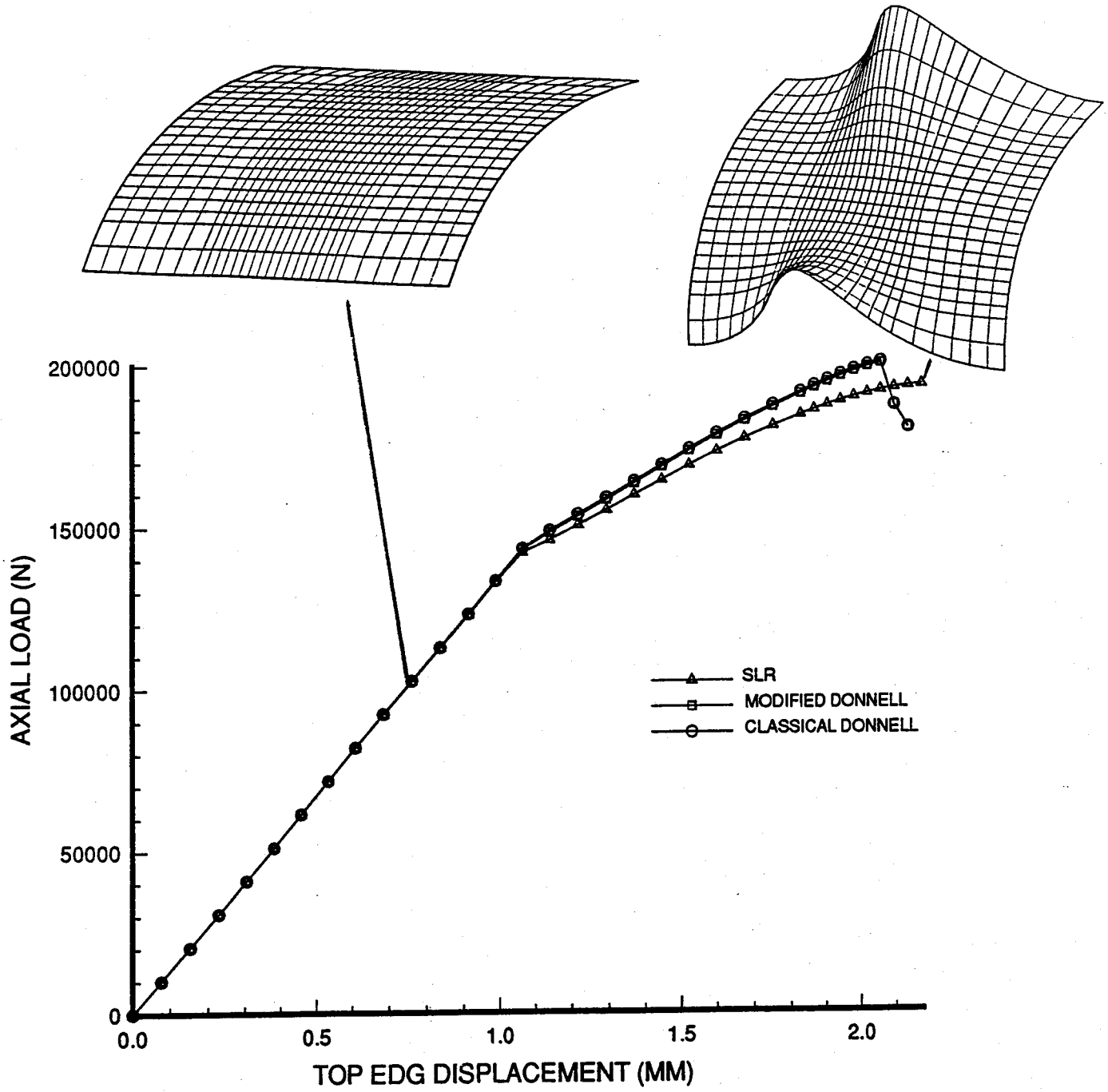

Figure 26: Load vs. Top Edge Displacement, Comparing SLR, Modified Donnell, and Classical Donnell, for a Solid 304.8 mm x 508 mm (12" x 20") Panel [0/45/-45/90]4s

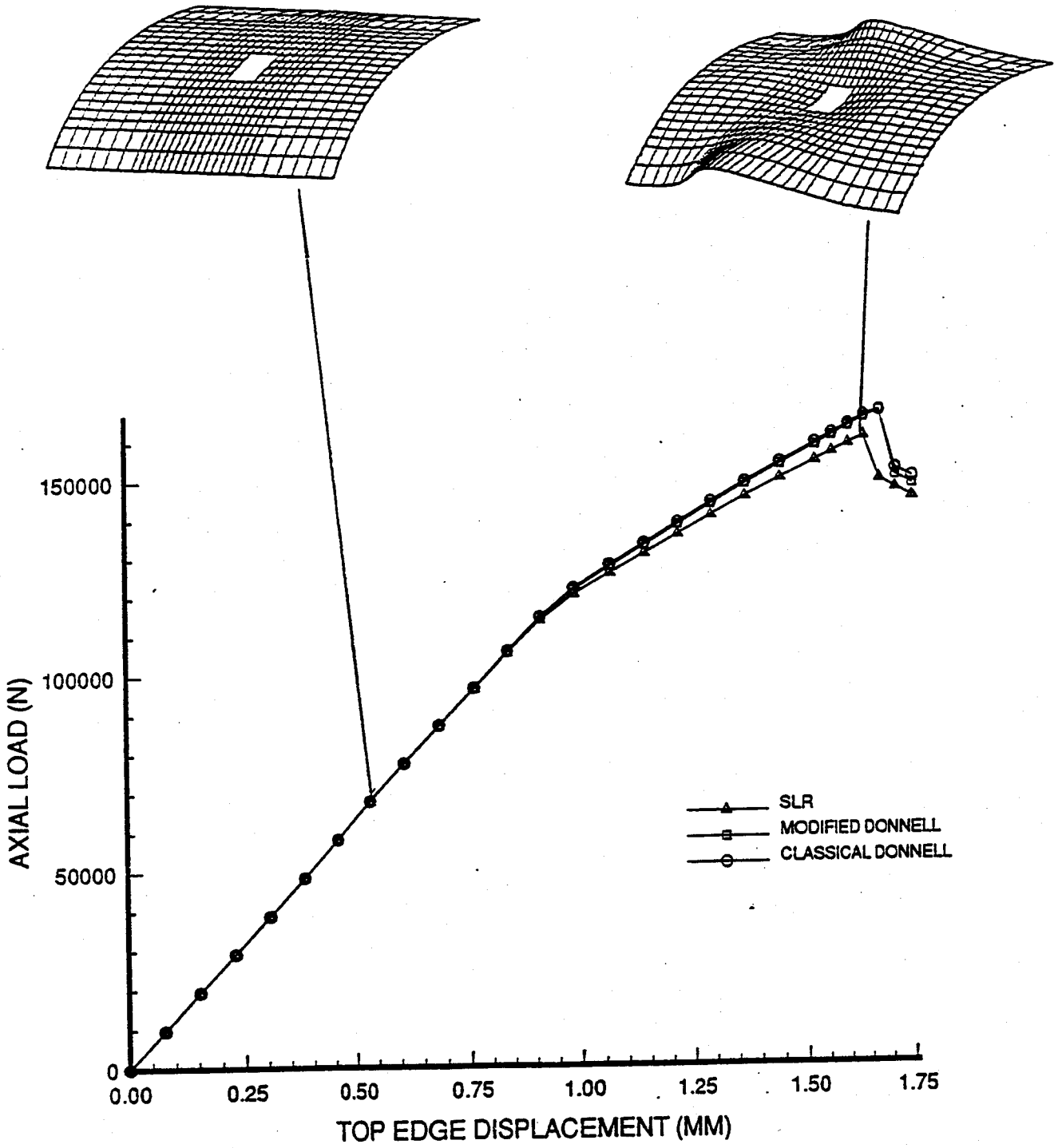

Figure 27: Load vs. Top Edge Displacement, Comparing SLR, Modified Donnell, and Classical Donnell, 50.8 mm x 50.8 mm (2" x 2") Cutout, 304.8 mm x 508 mm (12" x 20") Panel [0/45/-45/90]4s

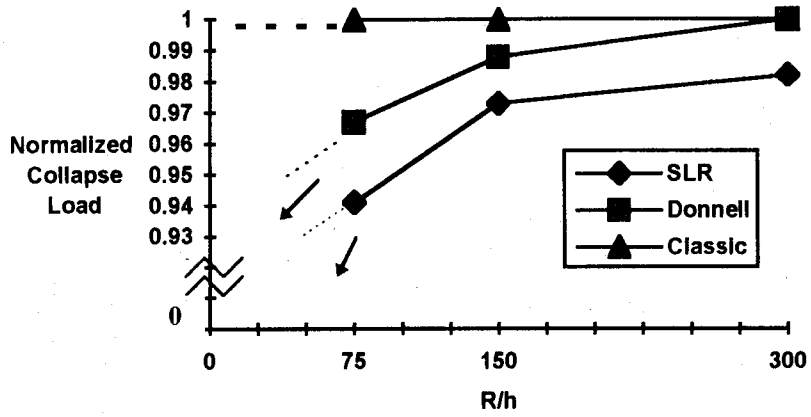

Figure 28: Normalized Load versus R/h for a
101.6 mm x 101.6 mm (4" x 4") Cutout in a
304.8 mm x 508 mm (12" x 20")

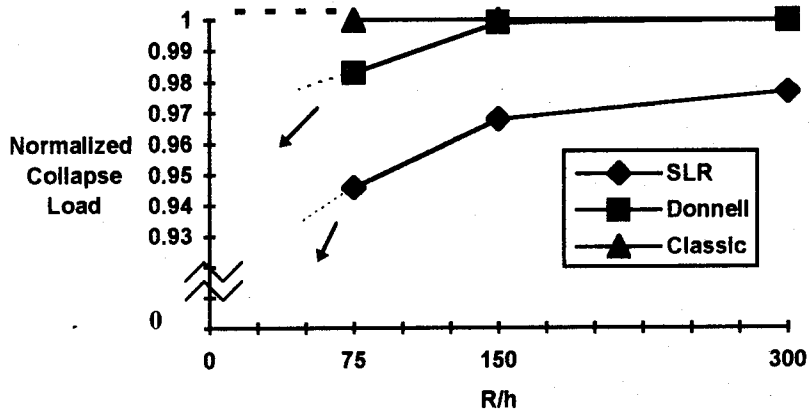

Figure 29: Normalized Load versus R/h for a
127 mm x 127 mm (5" x 5") Cutout in a
304.8 mm x 508 mm (12" x 20") Panel

what is measured throughout the rest of the panel, especially at the cutout corners. By increasing the size of the cutout, the region where these large shear strains and rotations occur inside the panel is increased. Thus, these effects are more noticeable for larger cutouts. The actual collapse loads predicted by each theory for the 32 ply panels with

101.6 mm x 101.6 mm and 127 x 127 mm cutout configurations are displayed in Figures 30 and 31 respectively. These figures represent the cases for each cutout configuration with the most noticeable differences in the load vs. displacement curves predicted by the three theories.

The rectangular cutout configurations provide interesting results concerning patterns of how the results obtained from the SLR and Modified Donnell theories diverge from the results acquired from the Classical Donnell theory with decreasing R/h ratio. The normalized collapse loads for both the 50.8 mm x 203.2 mm and 203.2 mm x 50.8 mm cutouts are presented in Figures 32 and 33. Both of these figures exhibit divergence in the results obtained from the Classical Donnell and SLR theories even for the thin 8 ply shells. This indicates that large rotations are taking place for these cutout configurations. The figures both indicate that the results for Classical Donnell and Modified Donnell differ only for the 32 ply cases. This shows that through-the-thickness shear becomes important for these cutout configurations as thickness increases. For these particular cases it becomes important at an R/h of 75. However, the curves plotted for the SLR and Modified Donnell theories show a tendency of converging as R/h decreases. This trend can be observed in both Figures 32 and 33, although it is most apparent in Figure 33. This is a result of through-the-thickness shear becoming increasingly important with increasing thickness. The effects of large rotations on the other hand are not as dependent on thickness, but rather seem to be more a function of cutout area.

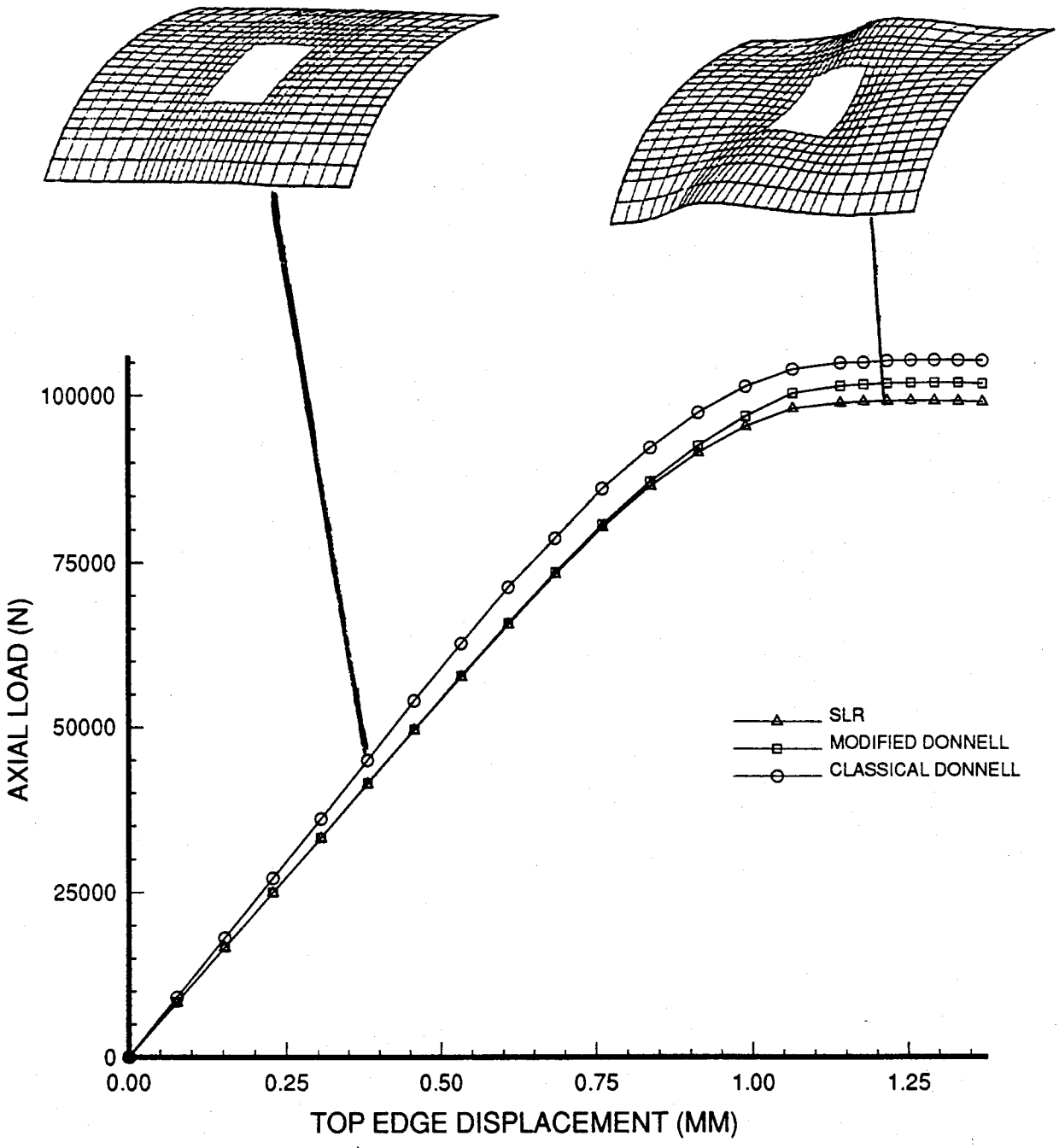

Figure 30: Load vs. Top Edge Displacement, Comparing SLR, Modified Donnell, and Classical Donnell, 101.6 mm x 101.6 mm (4" x 4") Cutout, 304.8 mm x 508 mm (12" x 20") Panel [0/45/-45/90]4s

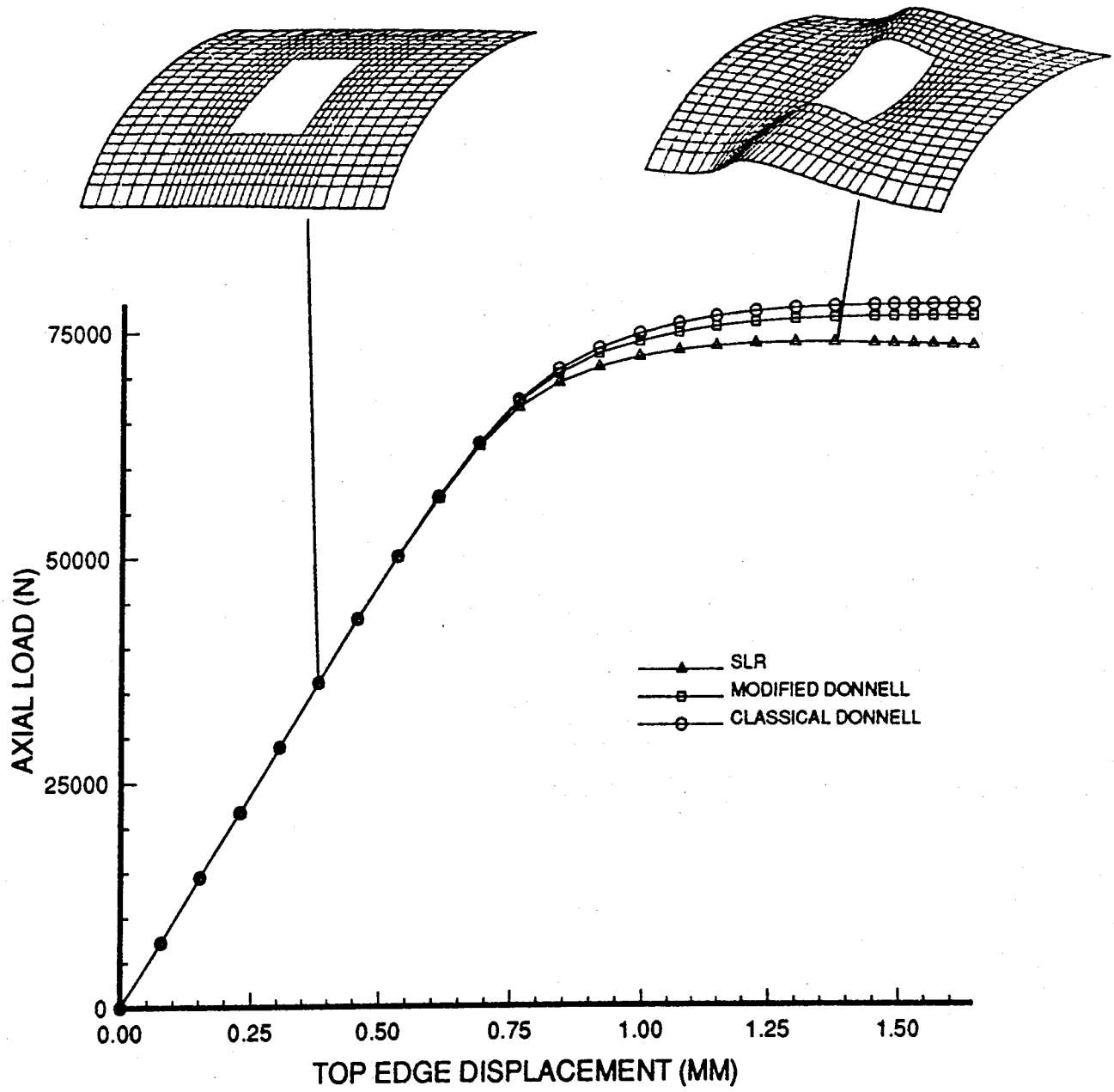

Figure 31: Load vs. Top Edge Displacement, Comparing SLR, Modified Donnell, and Classical Donnell, 127 mm x 127 mm (5" x 5") Cutout, 304.8 mm x 508 mm (12" x 20") Panel [0/45/-45/90]4s

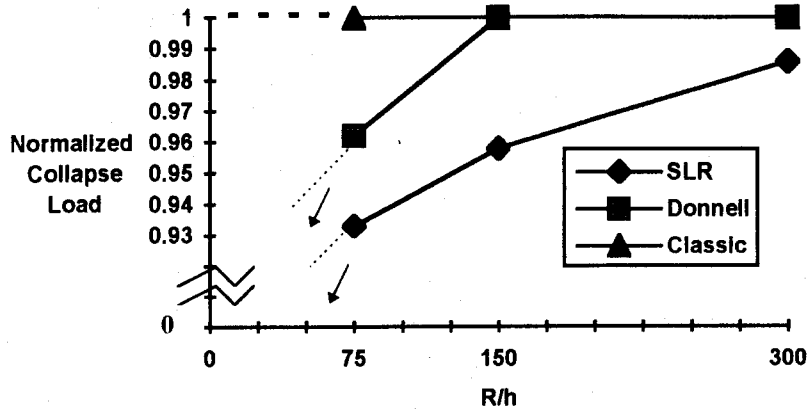

Figure 32: Normalized Load versus R/h for a
50.8 mm x 203.2 mm (2" x 8") Cutout in a
304.8 mm x 508 mm (12" x 20") Panel

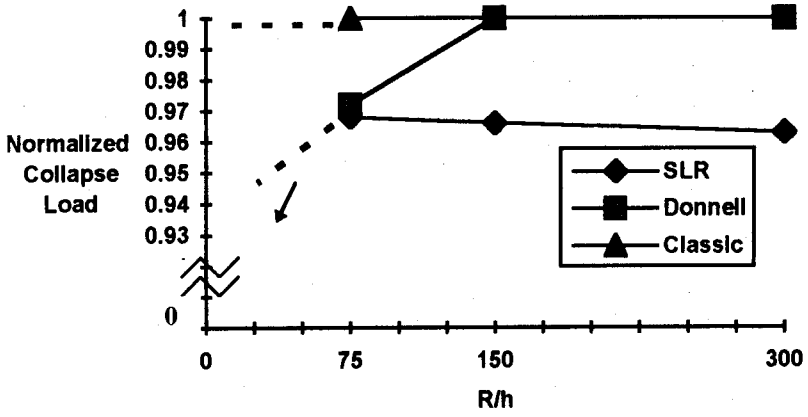

Figure 33: Normalized Load versus R/h for a
203.2 mm x 50.8 mm (8" x 2") Cutout in a
304.8 mm x 508 mm (12" x 20") Panel

Figures 34 and 35 document the actual load vs. displacement curves predicted by each of the three theories for the 32 ply panels with a 50.8 mm x 203.2 mm cutout and 203.2 mm x 50.8 mm cutout respectively. The three dimensional orthographic plot for the 32 ply panel with a 203.2 mm x 50.8 mm cutout at collapse in Figure 34 is unique among

all of the three dimensional plots created for the collapsed shells in this research. It is unique because it is the only shell to collapse facing concave in instead of concave out. That is, the radial displacements along the free edges for this case are in the positive w direction instead of the negative w direction. This inverted shape for the shell is similar in shape to the shells that would snap through in Palazotto and Dennis [17]. However, in Palazotto and Dennis's case, the load was applied in the transverse direction and the load displacement curves in Figure 35 do not display any evidence of snapping through. Figure 33 indicates that large rotations are important for the thinner panels with the 203.2 mm x 50.8 mm cutout while through-the- thickness shear is not. However, both Figures 33 and 35 indicate that through-the-thickness shear is important for the 32 ply panel while large rotations are not. This would mean that less bending is occurring because more of the axial compressive energy is going into through-the-thickness shear. The bending rotation (ψ_S) recorded in table 12 for this case is only 3.6 degrees, which is much lower than for the thinner panels with a 203.2 mm x 50.8 mm cutout and lower than the other 32 ply panels with different cutouts. Thus, it is likely that the through-the-thickness shear caused variations in the radial displacements along the free edge which led to the shape of the collapsed shell displayed in Figure 35.

It is important to note that the three dimensional orthographic plot for the 32 ply panel with a 101.6 mm x 101.6 mm cutout at collapse in figure 30 displays asymmetry in the radial displacements about the horizontal and vertical center lines. The maximum radial displacements along the free edges appear to occur just below the horizontal centerline on the left side of the panel (near side) and just above the horizontal centerline on the right side (far side). This also happens to be close to where large concentrations of

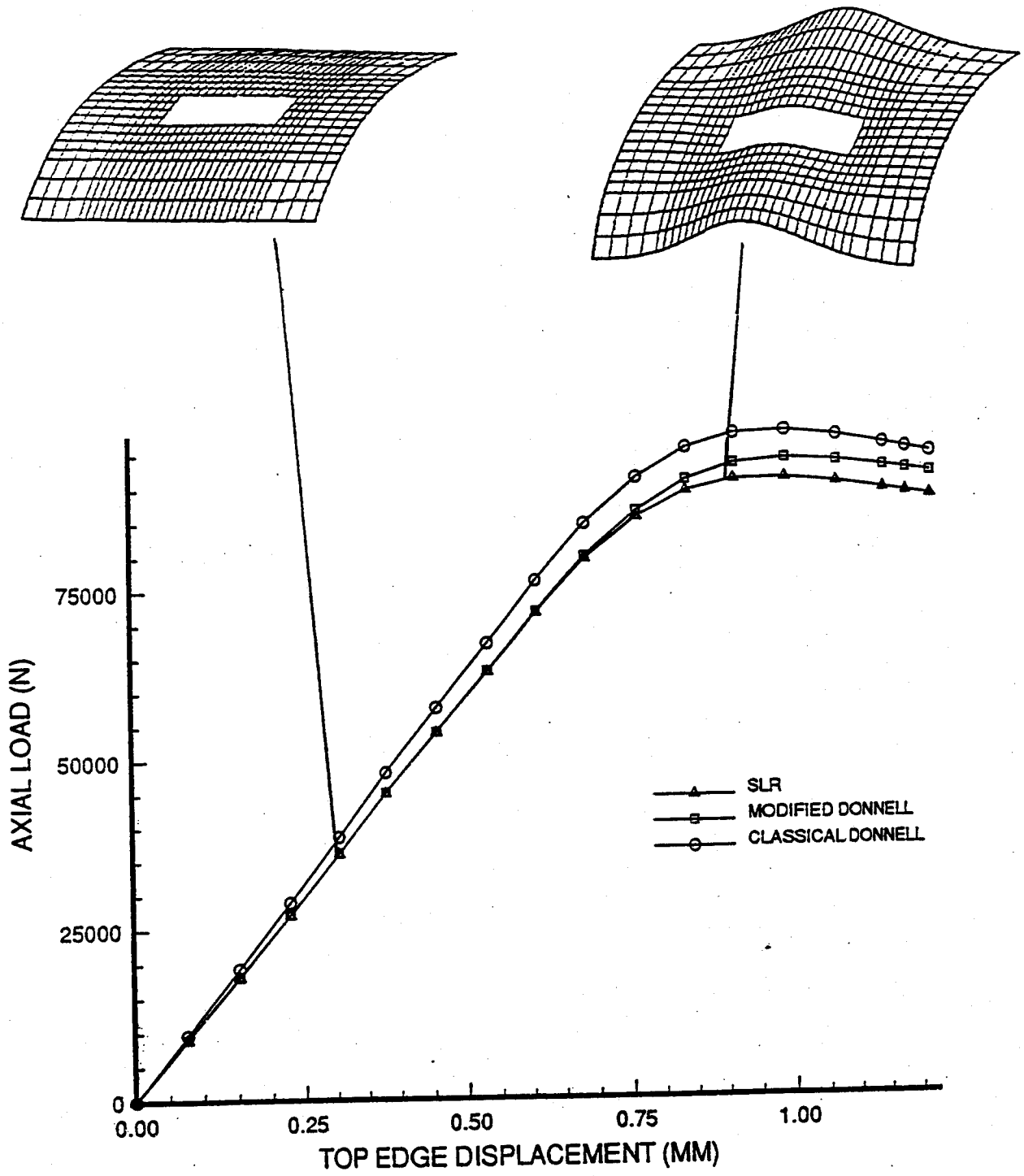

Figure 34: Load vs. Top Edge Displacement, Comparing SLR, Modified Donnell, and Classical Donnell, 50.8 mm x 203.2 mm (2" x 8") Cutout, 304.8 mm x 508 mm (12" x 20") Panel [0/45/-45/90]4s

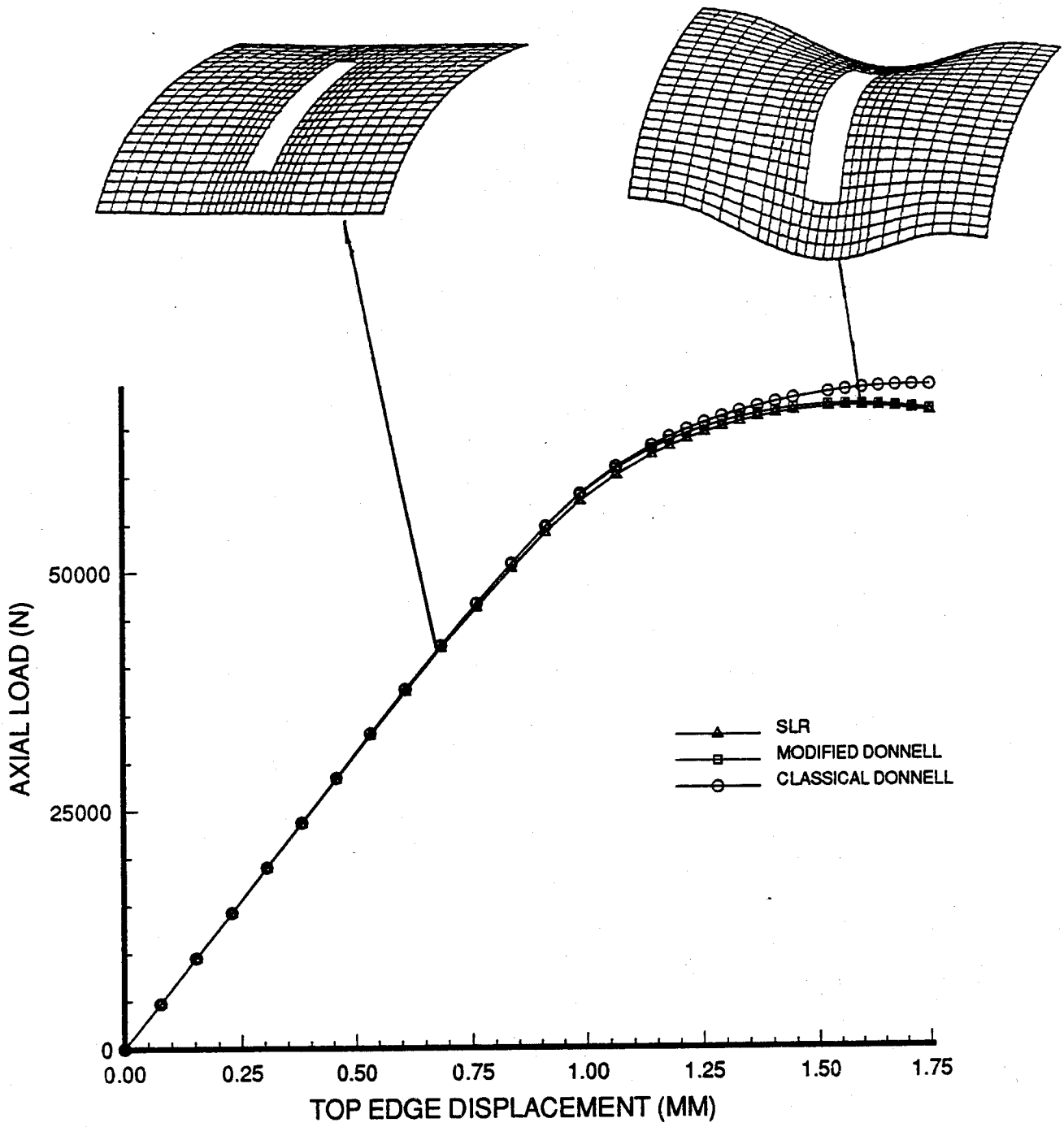

Figure 35: Load vs. Top Edge Displacement, Comparing SLR, Modified Donnell, and Classical Donnell, 203.2 mm x 50.8 mm (8" x 2") Cutout, 304.8 mm x 508 mm (12" x 20") Panel [0/45/-45/90]4s

the shear strain ε_4 are occurring in figure 22 for the same panel. As was discussed in section 3.2, the 32 panel with a 50.8 mm x 203.2 mm cutout does not experience as much transverse shear strain and thus experiences more bending. The three dimensional orthographic plot in Figure 34 of the panel at collapse shows that the radial displacement along the free edges is symmetric about the horizontal centerline with a maximum radial displacement occurring at the horizontal centerline. These observations show the results of increased bending in the 32 ply panel with a 50.8 mm x 203.2 mm cutout and of large shear strains occurring in the 32 ply panel with a 101.6 mm x 101.6 mm cutout which supports the findings in section 3.2 for these two cases.

Considering all of the cases presented in the two past sections of this chapter, some conclusions can be drawn concerning cutout size, and how it relates to large rotations and through-the-thickness shear. For panels with no cutouts or small cutouts, like a 50.8 mm x 50.8 mm cutout (< 3% total panel area), large rotations are not important to the solution for thin panels, but do become important for the 32 ply panels. Also, through-the-thickness was not found to be a factor for any of the panels used in this study with small or no cutouts. For large cutouts, large rotations are a factor for thin panels, but become less important for the 32 ply panels. The opposite is true for through-the-thickness shear. It was not important for thin panels with large cutouts, but had a noticeable effect for each of the 32 ply panels with large cutouts.

The results compiled so far also have some implications on the relationships between extensional width and through-the-thickness shear. In this research it was found that through-the-thickness shear comes into play only for the 32 ply panels with large

cutouts. The observations made for each of the three 32 ply cases with equivalent cutout area all indicate that when through-the-thickness shear comes into play less, bending occurs for cutouts with less extensional width. This is because more axial compressive energy is absorbed into transverse shear.

3.4 Evaluating the Different Shell Theories

The objective of this section is to compare the accuracy of the three theories in predicting the responses of the panels undergoing axial compression. Experimental results obtained from Del Barga [1] and Hatfield [18] were used to compare the accuracy of the three theories for each of the cutout configurations used in this study for both 8 and 16 ply panels. No experimental results were available for the 32 ply panels. The experimental results for the solid 8 and 16 ply panels were compiled by Hatfield. The rest of the experimental results were from Del Barga's work. Table 13 documents the experimental collapse loads and top edged displacements of all the panels compared in this section.

This section is broken down into three main parts. First, observations are made about how the experimental results compared to the numerical results for specific cases. Then the percent differences are compared using the three theories' numerically predicted results to those of the experimental results for each of the cutout configurations for 8 and 16 ply panels. These results are documented in Table 14. Finally, the rotations predicted by each theory are compared for the cases identified in the previous section where large rotations were determined to be important. This data has been presented in Table 15.

Table 13. Experimental Global Collapse Load and Top Edge Displacement

Panel	Collapse Load		u Displacement	
Designator	Kn	(lbs)	mm	(in)
8ply0x0	6.490	1459	.5334	.021
8ply2x2	5.525	1242	.94	.037
8ply4x4	3.473	781	.66	.026
8ply5x5	3.073	691	.64	.025
8ply2x8	3.938	885	.36195	.01425
8ply8x2	1.050	236	.24	.00945
16ply0x0	37.199	8383	1.7526	.069
16ply2x2	28.257	6353	1.2	.0472
16ply4x4	21.979	4941	1.2	.0472
16ply5x5	14.545	3270	.6477	.0255
16ply2x8	27.028	6076	.9144	.036
16ply8x2	7.846	1763	1.2	.0472

Several important observations can be made when comparing the experimental results to the numerical results for the solid 8 ply panel, the 8 ply panel with a 50.8 mm x 50.8 mm cutout, and the 16 ply panel with a 50.8 mm x 50.8 mm cutout which are found in Figures 36, 37, and 38 respectively. The experimental collapse loads are more than 38% lower than the numerical collapse load for the solid 8 ply panel (the exact percent error for each theory is listed in table 14). This is a relatively large amount of error, considering that the differences in the numerical collapse loads and the experimental results for the 8 ply panel with a 50.8 mm x 50.8 mm cutout and the solid 16 ply panel are only 16% and 4% respectively. The reason the numerical results more closely predict the collapse for the 8 ply panel with a cutout than the solid 8 ply panel is because the small cutout is similar to an imperfection in the panel. The solid panel has naturally occurring imperfections in the radius of curvature, geometry, and material, and caused by manufacture. These imperfections are not taken into account by the numerical analysis. Adding the cutout to the finite element model is similar to adding a large imperfection into the panel. Thus, the numerical results are much closer to the experimental results for the small cutout case than for the solid panel.

Another type of imperfection caused by the manufacture of the panels was a tendency for the 8 ply panels to curl following curing. This decreased the radius of curvature of the panel in its relaxed state. Uncurling the 8 ply panels when clamping it to the 304.8 mm (12") curvature loading fixture caused the center of the panel to flatten out slightly [1]. This caused the radius of curvature of the panel to be greater at the center which led to a lower collapse load. This uncurling was not a problem for the 16 ply

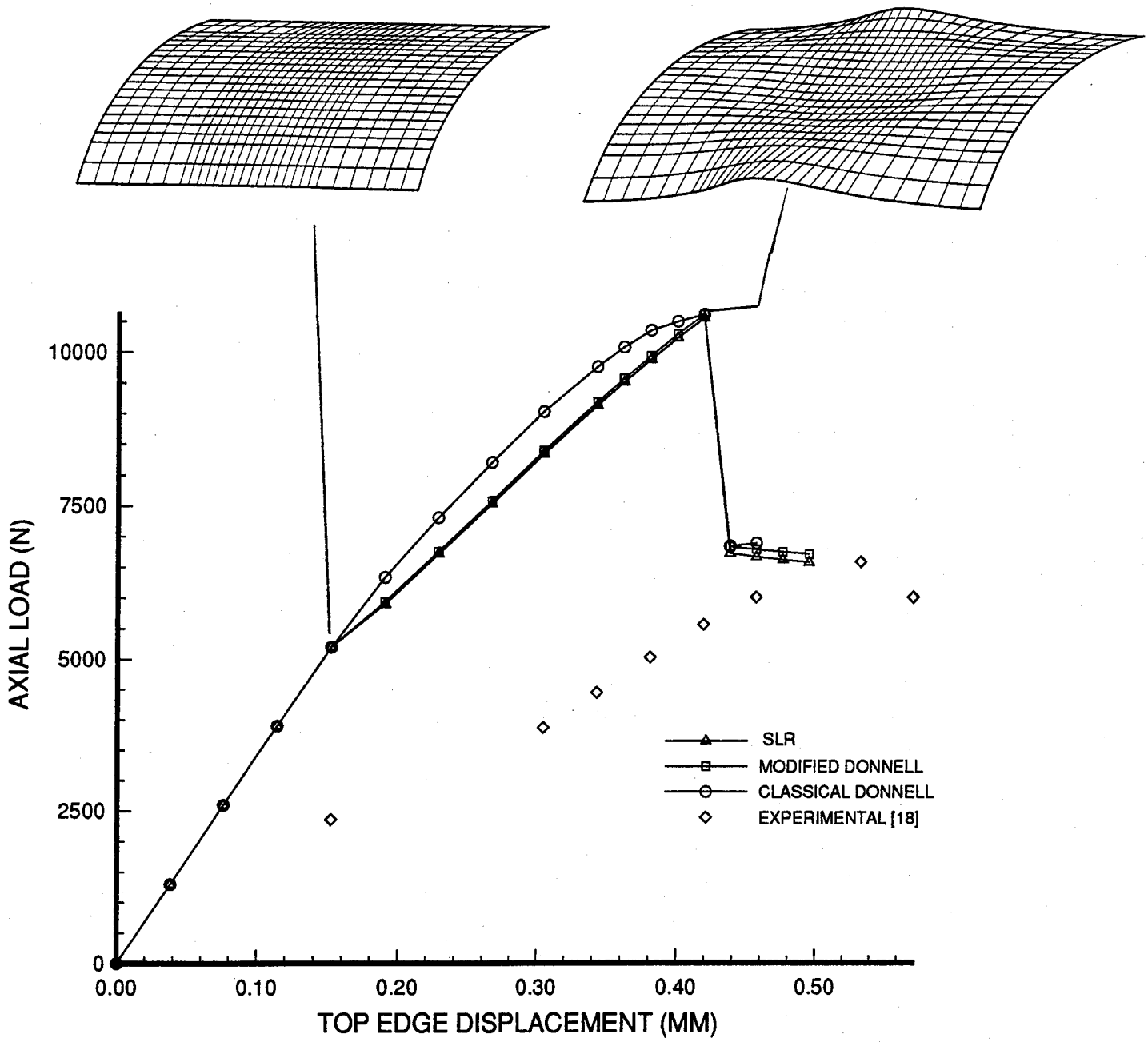

Figure 36: Load vs. Top Edge Displacement, Comparing Experimental to SLR, Modified Donnell, and Classical Donnell, Solid 304.8 mm x 508 mm (12" x 20") Panel [0/45/-45/90]s

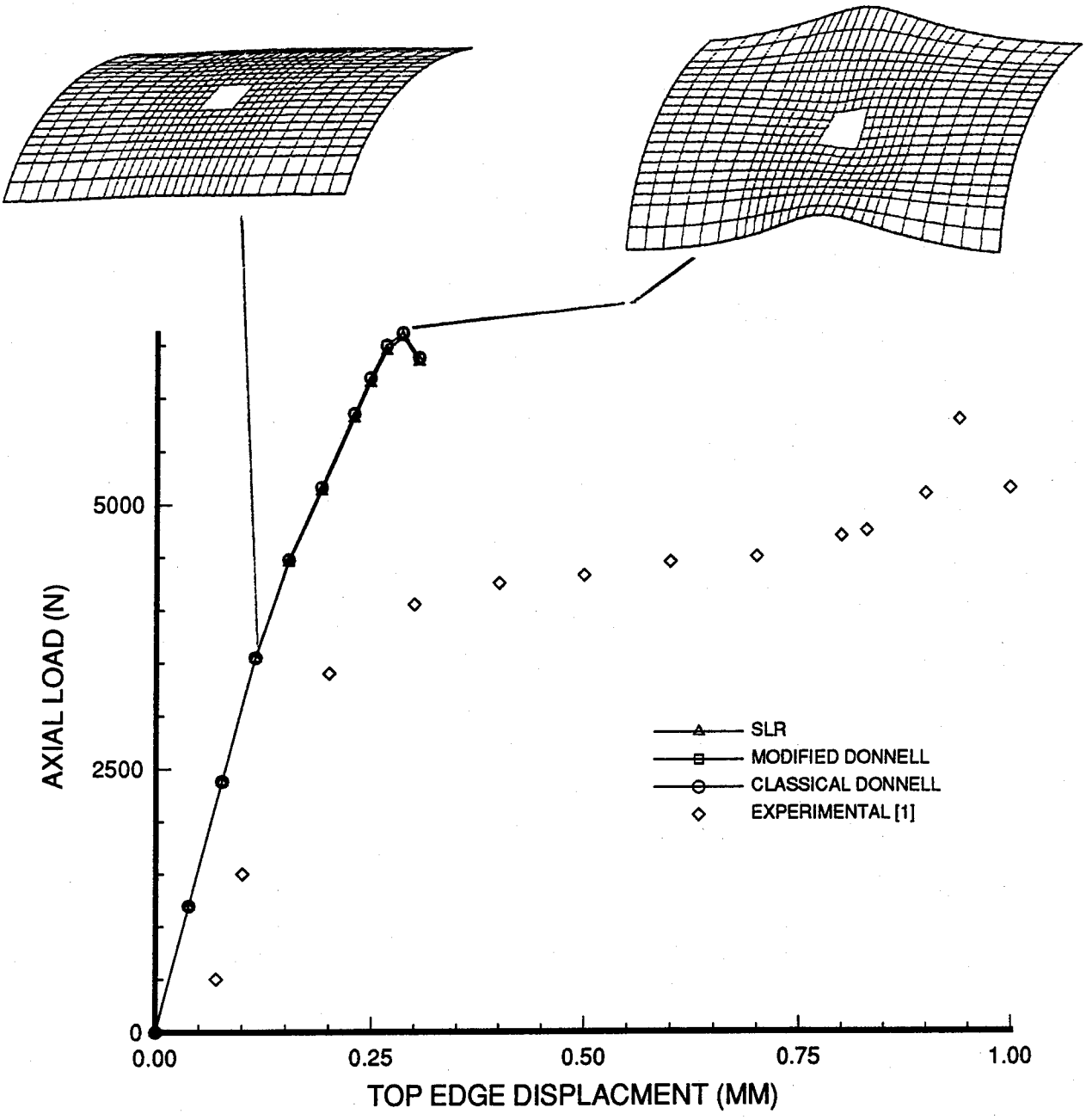

Figure 37: Load vs. Top Edge Displacement, Comparing Experimental to SLR, Modified Donnell, and Classical Donnell, 50.8 mm x 50.8 mm (2" x 2") Cutout, 304.8 mm x 508 mm (12" x 20") Panel [0/45/-45/90]s

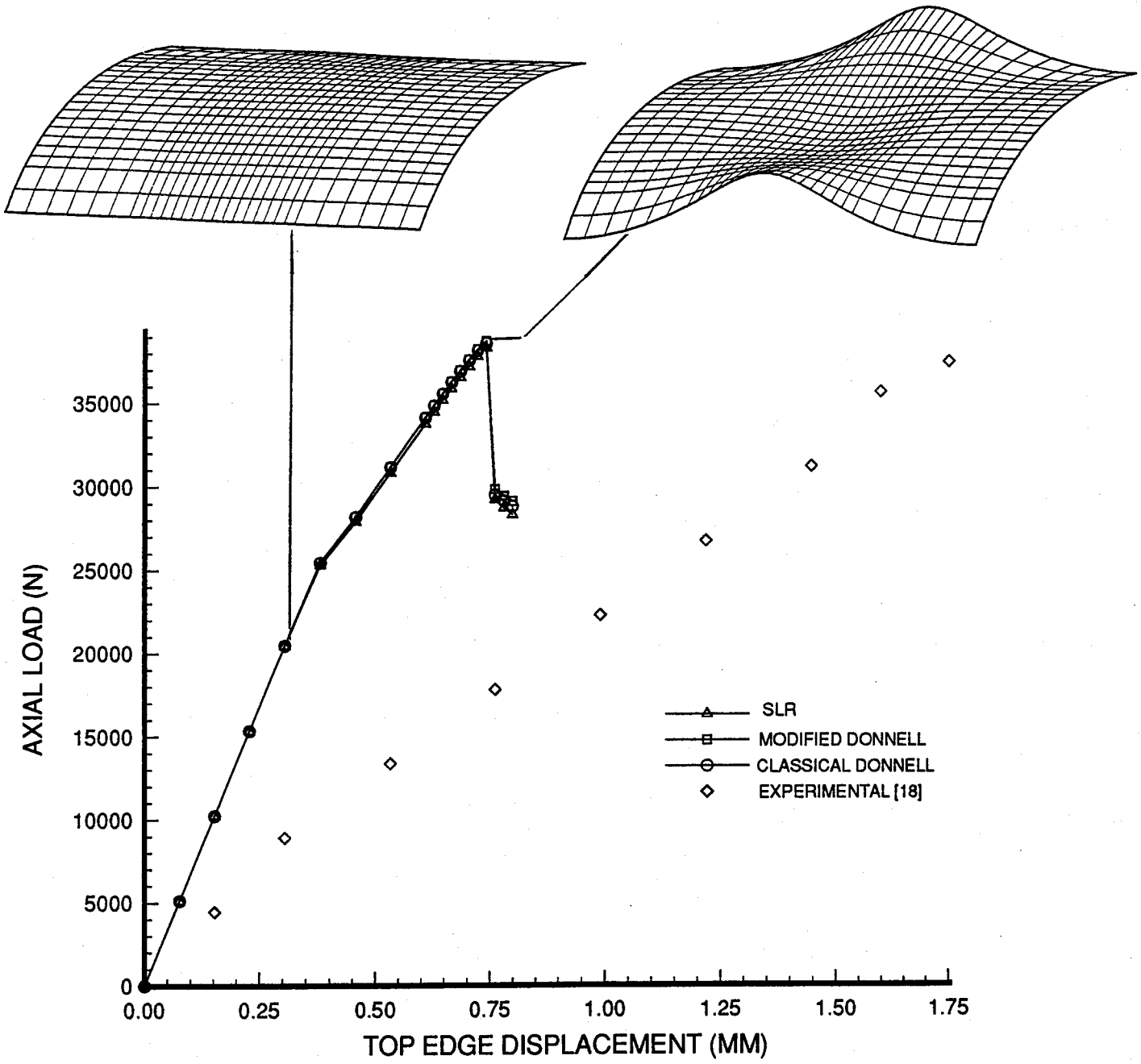

Figure 38: Load vs. Top Edge Displacement, Comparing Experimental to SLR, Modified Donnell, and Classical Donnell, Solid 304.8 mm x 508 mm (12" x 20") Panel [0/45/-45/90]2s

panels due to an increase in thickness. Thus, the numerical results for the solid 16 ply panel were much closer to the experimental results than for the solid 8 ply panel.

Table 14 documents two trends in the percent errors determined for the numerical results. The first trend is that for the 8 ply panels the percent error decreases for increasing cutout area. The panels with the 101.6 mm x 101.6 mm cutout and 50.8 mm x 202.3 mm cutout both have percent errors ranging from 25-32% while the 8 ply panel with a larger 127 mm x 127 mm cutout only experiences about 3-6 % error. The reason for this is that, as the cutout area increases, the effects due to material imperfections decrease. The load versus displacement curves for these cases comparing the numerical results to the experimental results are located in Appendix C. The only reason the percent error recorded for the numerical results obtained for the 8 ply panel with the smaller 50.8 mm x 50.8 mm cutout is not greater than those recorded in the larger cutouts is because of the additional refinements performed on this particular case for the convergence study. The second trend that is noticeable in Table 14 is that the experimental results more closely predict the collapse loads for the 16 ply panels with large cutouts than they do for the 8 ply panel with the same cutout size. This is because the thickness reduces the effects of the curling following curing that lead to flattening at the center of the panels. The load versus displacement curves for the 16 ply panels with cutouts are located in Appendix C (except for the 203.2 mm x 50.8 mm cutout).

The last observation that was noted between the numerical and experimental results occurs with the 8 and 16 ply panels with 203.2 mm x 50.8 mm cutouts. The load versus displacement curves predicted by each of the three shell theories are plotted along

Table 14. Percent Differences Between Experimental Collapse Loads and Numerical Collapse Loads for SLR, Modified Donnell and Classical Donnell

Panel	Percent Difference With Experimental Collapse Loads		
Designation	SLR	Modified Donnell	Classical Donnell
8ply0x0	38.52%	38.85%	38.85%
8ply2x2	15.94%	16.44%	16.44%
8ply4x4	30.01%	31.36%	31.36%
8ply5x5	3.74%	5.93%	5.93%
8ply2x8	24.7%	25.73%	25.73%
8ply8x2	58.95%	59.78%	59.78%
16ply0x0	2.92%	3.89%	3.89%
16ply2x2	5.68%	6.69%	6.69%
16ply4x4	5.33%	6.82%	7.90%
16ply5x5	3.92%	6.90%	6.95%
16ply2x8	3.22%	7.25%	7.25%
16ply8x2	41.71%	43.67%	43.67%

with the experimental results for the 8 ply panel in Figure 39 and for the 16 ply panel in Figure 40. The numerical results for both of these cases differed from the experimental results by roughly 59% for the 8 ply case and about 43% for the 16 ply case. According to Del Barga [1], this large difference could be due to slight curvature imperfections of the panel. The long circumferential length of these cutouts combined with the small panel extensional widths make these cases more susceptible to curvature imperfections when compared to other cutout dimensions. Any variation in radius of curvature near the cutout in the area between the vertical cutout edge and the panel vertical edge could initiate the collapse of the panel earlier than predicted. It is important to note that the three dimensional orthographic plots of the collapsed panels all closely resemble the actual collapsed panels used for the experimental results. Comparisons between the orthographic plots and photographs of the experimental panels are found in Del Barga's thesis [1].

The second part of this section concentrates on determining when it is most appropriate to apply each of the three shell theories. Table 14 provides a useful tool to determine when the more advanced theories provide a significant advantage in predicting actual collapse loads for the cases where experimental results where available. For the 32 ply cases it is still useful to consider the results presented in the previous section where the load versus displacement curves and collapse loads have been documented for each cutout configuration using all three shell theories. There appears to very little to gain by using the computationally intensive SLR theory for the 8 ply cases. The most noticeable improvement in percent difference occurs for the 8 ply panel with a 127 mm x 127 mm cutout where the SLR theory has a 2.19% advantage over the Donnell theories. Since the Classical Donnell theory costs very little in CPU computing power compared to the other

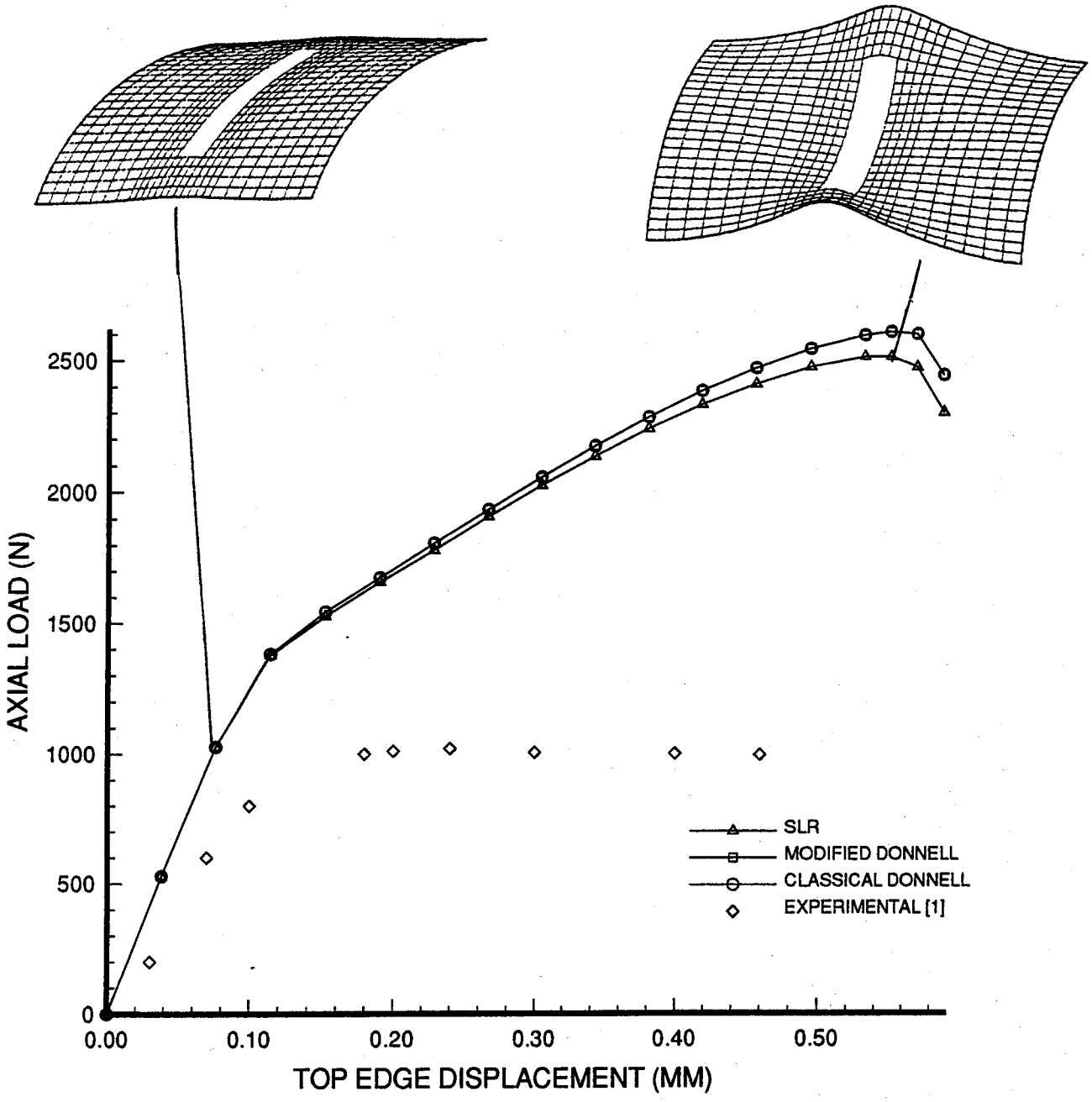

Figure 39: Load vs. Top Edge Displacement, Comparing Experimental to SLR, Modified Donnell, and Classical Donnell, 203.2 mm x 50.8 mm (8" x 2") Cutout, 304.8 mm x 508 mm (12" x 20") Panel [0/45/-45/90]s

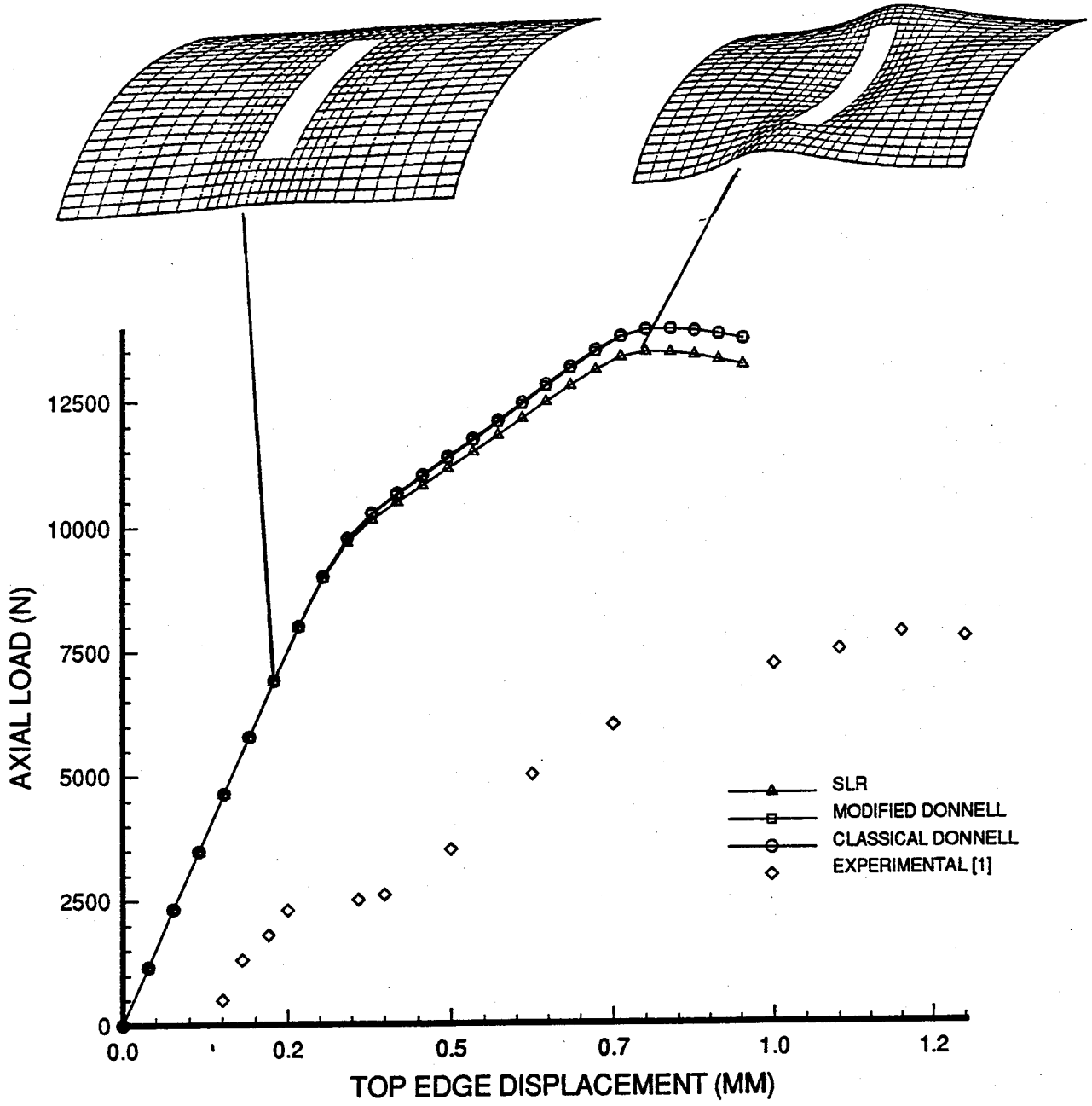

Figure 40: Load vs. Top Edge Displacement, Comparing Experimental to SLR, Modified Donnell, and Classical Donnell, 203.2 mm x 50.8 mm (8" x 2") Cutout, 304.8 mm x 508 mm (12" x 20") Panel [0/45/-45/90]2s

theories and still produces similar results, it would appear to be the logical choice for thin panels. However, because of its convergence characteristics, it requires a much more refined mesh than the Modified Donnell theory. Therefore, the Modified Donnell is the most efficient choice. The equations used in this theory are greatly simplified compared to those used in the SLR theory (See Section 2.1.4 and 2.1.5).

The Modified Donnell theory is not the best choice for the 16 ply panels. The Modified Donnell theory has less than a 2% advantage over the Classical Donnell theory in each 16 ply case represented in Table 14. The Classical Donnell theory results for the 16 ply panels were obtained without any mesh refinement, except for the 16 ply panel with a 127 mm x 127 mm cutout. Therefore, the Classical Donnell theory is the most efficient theory to use for most of the 16 ply panels. The two exceptions to this rule are the 16 ply panels with a 127 mm x 127 mm cutout and a 50.8 mm x 203.2 mm cutout. The SLR theory predicts collapse loads that are 3.5% and 4.03% closer to the experimental collapse loads than the collapse loads predicted by the Modified Donnell theory for the two respective panel configurations. Thus, the SLR theory is the best for these two cases.

Although no experimental data was available for the 32 ply panels to relate with, it is still possible to compare the results obtained for the three shell theories with these panels. As was discussed in the previous section, the large rotations which occur in the solid 32 ply panel and the 32 ply panel with a 50.8 mm x 50.8 mm cutout make SLR the most accurate theory for these two cases. The collapse loads predicted by the SLR theory were nearly 4% lower than the Donnell theories for both cases. For the rest of the 32 ply cases, through-the-thickness shear became important which made the Modified Donnell

theory more accurate than the Classical Donnell theory. However, the SLR theory predicted collapse loads that are 3% lower than those predicted by the Modified Donnell theory for the 32 ply panels with a 101.6 mm x 101.6 mm cutout, with a 127 mm x 127 mm cutout, and with a 50.8 mm x 203.2 mm cutout. The only cutout configuration for a 32 ply panel where the predicted collapse load for the SLR theory was not noticeably lower than the predicted collapse load of the Modified Donnell theory was the 203.2 mm x 50.8 mm cutout. Because of the relatively small rotations occurring in this panel, the Modified Donnell theory is the most efficient choice.

The last part of this section concerns the rotations predicted by the three theories in the cases noted where SLR predicted noticeably lower collapse loads. Table 15 lists the eight cases where this was the case. Table 15 also includes a comparison in the rotations measured in the 32 ply panel with a 203.2 mm x 50.8 mm cutout as a comparison case, because it experienced relatively small rotations and the SLR theory predicted a collapse load almost identical to that predicted by the Modified Donnell theory. The values listed in Table 15 were not always recorded at collapse. This is because the three theories did not always collapse at the same increment of u displacement, which made comparing maximum rotations difficult. Therefore, a point prior to collapse was picked where the load versus displacement curve generated using the SLR theory was diverged from the curves produced by the Donnell theories. Also, since the Classical Donnell theory does not measure the rotation ψ_S, the slope $w_{,S}$ was used. This is the same value which the Classical Donnell theory uses in place of the rotational terms in the strain displacement relations listed in sections 2.1.5 and 2.1.6.

In seven out of the nine case documented in Table 15, the rotations measured by each theory decreased with decreasing complexity. That is, the rotations measured using the SLR theory were the greatest, followed by the Modified Donnell theory. The approximations using $w_{,S}$ for the Classical Donnell theory were usually between 5-10% lower than the rotations predicted by the SLR theory. This would correlate to the fact that these panels are experiencing large rotations for which the SLR theory is best equipped to deal with. Therefore, the larger values it predicts are closer to the actual values. The two cases where the SLR theory does not predict larger rotations are for the 8 and 32 ply panels with a 203.2 mm x 50.8 mm cutout. The rotations recorded for 32 ply panel with a 203.2 mm x 50.8 mm cutout increase with decreasing complexity. Thus, the SLR theory predicts smaller rotations than the Donnell theories, which is correct. As was established in the previous section, this panel does not experience large rotations. However, the eight ply panel with a 202.3 mm x 50.8 mm cutout does experience moderately large rotations. The reason that SLR predicts a lower collapse load for this is because the displacements are greater in the U-V plane for this case according to SLR. Even though the rotations recorded using the SLR theory are not as large as they were for the Modified Donnell theory, the coupling of the u and v displacements which occurs in the strain-displacement relations in section 2.1.4 causes the SLR theory to predict a lower collapse load for this case.

Table 15. Comparison of Predicted Rotations for the SLR, Modified Donnell, and Classical Donnell Theories

Panel	u	Bending Rotation ψ_S (deg)		$w_{,s}$ (deg)
Designation	Displacement	SLR	Modified Donnell	Classical Donnell
8ply8x2	.021	9.35	9.44	9.36
16ply2x8	.036	11.84	11.50	10.93
16ply8x2	.033	9.04	8.77	8.65
32ply0x0	.072	11.31	10.97	10.63
32ply2x2	.06	9.15	8.86	8.61
32ply4x4	.042	5.16	4.99	4.78
32ply5x5	.054	7.31	7.19	7.04
32ply2x8	.039	4.96	4.79	4.64
32ply8x2	.063	3.60	3.73	3.98

4. Conclusions

The following conclusions can be made relative to this research:

1. The 28 degree of freedom element used in the Classical Donnell theory is incompatible because the corner nodes lack the rotational degrees of freedom ψ_x and ψ_S. This leads to softening in the panels for some cases, so that the predicted collapse loads are lower than for the SLR and Modified Donnell theories using the coarser meshes established by Del Barga. Refinements in the meshes indicated nonmonotonic convergence for the Classical Donnell theory. The predicted collapse loads for refined meshes using the Classical Donnell theory also more closely matched those obtained with the Modified Donnell theory. Therefore, at the penalty of refining the mesh, more confidence was obtained in the results using the Classical Donnell Theory.

2. The numerical panel response indicated that the maximum radial displacements occurred along the free panel vertical edge at or near the horizontal centerline. The radial displacements were asymmetric about the horizontal and vertical centerlines. That is, equivalent magnitudes and directions of radial displacements occurred at diagonals to each other. This was due to the +45 and -45 degree plies which affect the bending stiffness terms D_{16} and D_{26}. These terms affect the in-plane twisting moment M_{xy}. The magnitudes of the radial displacements ranged from 2-11 times the panel thickness. These large displacements indicate a need for a nonlinear theory like SLR.

3. The collapse load and stiffness of a panel increased with increased panel thickness. The collapse load and stiffness decreased with increased cutout area for panels with the same thickness. Also, the load versus displacement curves became more non-linear as the cutout areas increased and the extensional widths decreased.

4. In the case of panels with equivalent cutout areas, the collapse load and stiffness tended to decrease with a reduction in the panel extensional width. However, when through-the-thickness shear became important, the panels with a cutout configuration absorbing the majority of axial compressive energy through shear collapsed at a higher load than panels with equivalent cutout areas. This was confirmed by comparing the areas experiencing large transverse strains (>0.001 rad) in panels with equivalent cutouts. The panel with a greater area experiencing large transverse shear strains did not experience as much bending. Instead the panel displayed an uneven pattern of radial displacements near this region of large transverse shear. This increased the flexural rigidity and caused the panel to collapse at a higher load. The panel with a smaller region experiencing large transverse shear displayed an even pattern of radial displacements along the length of the panel and thus absorbed most of its energy through bending. This decreased the flexural rigidity and caused the panel to collapse at a lower load.

5. Large rotations do not play an important role in solid panels or panels with small cutouts for thin panels. As the panel thickness increases and R/h decreases to 75, rotations begin to become important as noticed by the moderately lower collapse loads

predicted by the SLR theory for these cases compared to the collapse loads predicted by the Modified Donnell theory. The opposite is true for panels with large cutouts. Rotations generally dominated the responses for the 8 and 16 ply panels with large cutouts as was noticed in the differences in the responses predicted by the SLR and Modified Donnell theories. However, for the 32 ply panels the effects of transverse shear became more important and the differences between the responses predicted by the SLR and Modified Donnell theories became smaller.

6. Through-the-thickness shear was not found to be a factor for any of the panels considered in this research with small or no cutouts. It also was not important for thin panels with large cutouts, but did have a noticeable effect for each of the 32 ply panels with large cutouts. The most noticeable effects of through-the-thickness shear were for the 32 ply panels with cutouts of equivalent areas.

7. Increased thickness and the presence of a cutout both decreased the effects of material and geometric imperfections in the panels used to obtain experimental results. This was noticed in the decrease in the percent error recorded in the numerical results for thicker solid panels and panels with cutouts versus solid panels.

8. As the cutout area became larger, the effects of material and geometric imperfections became less significant. This was noticed in the decreasing difference in experimental and numerical results with increasing cutout area. However, as the

circumferential length of the cutout increased, the more susceptible these panels became to slight imperfections in radius of curvature along the circumferential length of the cutout. Imperfections in the radius of curvature combined with the small extensional length of these panels may have resulted in the greater difference in the numerical and experimental results recorded for these panels.

9. In an evaluation of computational requirements versus accuracy, the Modified Donnell theory was determined to be the best choice of theories for predicting the responses of 8 ply panels. The Classical Donnell theory was determined to be more efficient for most of the 16 ply panels except a few cases where the SLR theory showed moderate improvements in accuracy. The SLR theory was the theory of choice for all of the 32 ply panels except one where the rotations were minimal. In that case, the Modified Donnell was the clear winner over Classical Donnell because of the importance of through-the-thickness shear in the 32 ply panels with large cutouts.

Bibliography

1. Del Barga, John C. The Effect of Cutout Dimensionallity on the Collapse Characteristics of Clyindrical Composite Shells of Varying Thickness. MS thesis, AFIT/GAE/ENY/93D-11. School of Engineering, Air Force Institute of Technology (AETC), Wright-Patterson AFB OH, December 1993 (AD-A273796).

2. Dennis, Scott T. Large Displacement and Rotational Formulation for Laminated Cylindrical Shells Including Parabolic Transverse Shear. PhD dissertation. School of Engineering, Air Force Institute of Technology (AETC), Wright-Patterson AFB OH, May 1988 (AD-A194871).

3. Becker, Marvin L. Analytical/Experimental Investigation of the Instability of Composite Cylindrical Panels. MS thesis, AFIT/GAE/AA/79D-3. School of Engineering, Air Force Institute of Technology (AETC), Wright-Patterson AFB OH, December 1979 (AD-A079850).

4. Becker, M.L., A. N. Palazotto, and N. S. Khot. "Instability of Composite Panels," Journal of Aircraft, 18: No. 9, 739-743 (September 1981).

5. Harper, James G. Buckling Analysis of Laminated Composite Circular Cylindrical Shells. MS thesis, AFIT/GAE/AA/78D-8. School of Engineering, Air Force Institute of Technology (AETC), Wright-Patterson AFB OH, December 1978 (AD-A081905).

6. Egan, Gregory S. Nonlinear Finite Element Analysis of a General Composite Shell. MS thesis, AFIT/GAE/AA/88D-12. School of Engineering, Air Force Institute of Technology (AETC), Wright-Patterson AFB OH, December 1988 (AD-A202572).

7. Almroth, B. O. and Frank Brogan. "Buckling of Cylinders with Cutouts," AIAA Journal, 8: No. 2, 236-240 (February 1970).

8. Almroth, B. O. and Frank Brogan. "Bifurcation Buckling as an Approximation of the Collapse Load for General Shells," AIAA Journal, 10: No. 4, 463-467 (April 1972).

9. Almroth, B. O. and A. M. C. Holmes. "Buckling of Shells with Cutouts, Experiment and Analysis," International Journal of Solids & Structures, 8: No. 8, 1057-1071 (August 1972).

10. Soebel, L. H., T. Weller, and B.L. Agarwal. "Buckling of Cylindrical Panels Under Axial Compression," Composites & Structures, 6: 29-35 (1976).

11. Arbocz, J. and Hol J.M.A.M. "Shell Stability Analysis in a Computer Aided Engineering (CAE) Environment," AIAA Paper No. 93-1333.

12. Janisse, T. C. and A. N. Palazotto. "Collapse Analysis of Cylindrical Composite Panels with Cutouts," Journal of Aircraft, 21: No. 9, 731-733 (September 1984).

13. Tisler, Thomas W. Collapse Analysis of Cylindrical Composite Panels with Large Cutouts Under Axial Load. MS thesis, AFIT/GAE/AA/86D-18. School of Engineering, Air Force Institute of Technology (AETC), Wright-Patterson AFB OH, December 1982 (AD-A124739).

14. Tisler, Thomas W., and A. N. Palazotto. "Considerations of Cutouts in Composite Cylindrical Panels," Computers & Structures, 29: No. 6, 1101-1110 (1987).

15. Schimmels, Scott A. Investigation of Collapse Characteristics of Cylindrical Composite Panels With Large Cutouts. MS thesis, AFIT/GAE/ENY/89D-33. School of Engineering, Air Force Institute of Technology (AETC), Wright-Patterson AFB OH, December 1989 (AD-A216378).

16. Schimmels, Scott A. and Anthony Palazotto. "Collapse Characteristics of Cylindrical Composite Panels Under Axial Loads," AIAA Journal, 30: No. 5, 1447-1449 (May 1992).

17. Palazotto, Anthony N. and Scott T. Dennis. Nonlinear Analysis of Shell Structures. Washington DC: American Institute of Aeronautics and Astronautics, Inc., 1992.

18. Hatfield, James C. Effect of Thickness and Ply Layup on the Collapse Characteristics of Cylindrical Composite Shells with Large Cutouts. MS thesis, AFIT/GAE/ENY/92D-20. School of Engineering, Air Force Institute of Technology (AETC), Wright-Patterson AFB OH, December 1992 (AD-A258909).

19. Bushnell, David. Computerized Buckling Analysis of Shells. the Netherlands: Martinus Nijhoff Publishers, 1985.

20. Palazotto, Anthony N. and Scott Dennis. "Static Response of a Cylindrical Composite Panel with Cutouts Using a Geometrically Nonlinear Theory," AIAA Journal, 28: No. 6, 1082-1088 (June 1990).

21. Sridharan, Srinivasan, and Madjid Zeggane. "Postbuckling Response of Stiffened Composite Cylindrical Shells," AIAA Journal, 30: No. 12, 2897-2905 (December 1992).

22. Bert, Charles W., and Philip H. Francis. "Composite Material Mechanics: Structural Mechanics," AIAA Journal, 12: No. 9, 1173-1181 (September 1974).

23. Reddy, J. N. "Exact Solutions of Moderately Thick Laminated Shells," Journal of Engineering Mechanics, 110: No. 5, 794-809 (May 1984).

24. Reddy, J. N., and K. Chandrashekhara. "Nonlinear Analysis of Laminated Shells Including Transverse Shear Strains," AIAA Journal, 23: No. 3, 440-441 (March 1985).

25. Reddy, J.N., and C. F. Liu. "A Higher-Order Shear Deformation Theory of Laminated Elastic Shells," International Journal of Engineering Science, 23: No. 3, 319-33 (March 1985).

26. Stein, Manuel. "Nonlinear Theory for Plates and Shells Including the Effects of Transverse Shearing," AIAA Journal, 24: No. 9, 1537-1544 (September 1986).

27. Pagano, N. J. "Influence of Shear Coupling in Cylindrical Bending of Anisotropic Laminates," Journal of Composite Materials, 4: 330-343 (July 1970).

28. Pagano, N. J. "Exact Solutions for Composite Laminates in Cylindrical Bending," Journal of composite Materials, 3: 398-411 (July 1969).

29. Dorninger, Konrad. "A Nonlinear Layered Shell Finite Element with Improved Transverse Shear Behavior," Composites Engineering, 1: No. 4, 211-224 (1991).

30. Ren, J. G. "Exact Solutions for Laminated Cylindrical Shells in Cylindrical Bending," Composites Science and Technology, 29: 169-187 (1987).

31. Linnemen, P. E. Vibration and Buckling Characteristics of Composite Cylindrical Panels Incorporating the Effects of a Higer Order Shear Theory. MS thesis, AFIT/GA/AA/88D-6. School of Engineering, Air Force Institute of Technology (AETC), Wright-Patterson AFB OH, December 1988.

32. Linnemen, P. E., and Anthony N. Palazotto. "Vibration and Buckling Characteristics of Composite Cylindrical Panels Incorporating the Effects of a Higher Order Shear Theory," International Journal of Solids and Structures, 28: No. 3, 341-361 (1991).

33. Tighe, Kathleen V. The Use of a Higher Order Kinematic Relationship on the Analysis of Cylindrical Composite Panels. MS thesis, AFIT/GA/AA/91D-17. School of Engineering, Air Force Institute of Technology (AETC), Wright-Patterson AFB OH, December 1991.

34. Tighe, Kathleen V. and Anthony N. Palazotto. "Higher Order Cylindrical Panel Relationships Considering General Ply Layups," Composite Structures 27: 225-242 (1994).

35. Smith, Randy A. and A. N. Palazotto. "Comparison of Eight Variations of a Higher-Order Theory for Cylindrical Shells," AIAA Journal 31: No. 6, 1125-1132 (June 1993).

36. Jones, Robert M. Mechanics of Composite Materials. New York: Hemisphere Publishing Corporation, 1975.

37. Saada, Adel S. Elasticity Theory and Applications. Malabar, FL: Krieger Publishing Company, Inc., 1989.

38. Cook, Robert D. and others. Concepts and Applications of Finite Element Analysis. New York: John Wiley and Sons, 1989.

APPENDIX A

ADDITIONAL FINITE ELEMENT MODELS

Total nodes = 1777

Total elements = 560

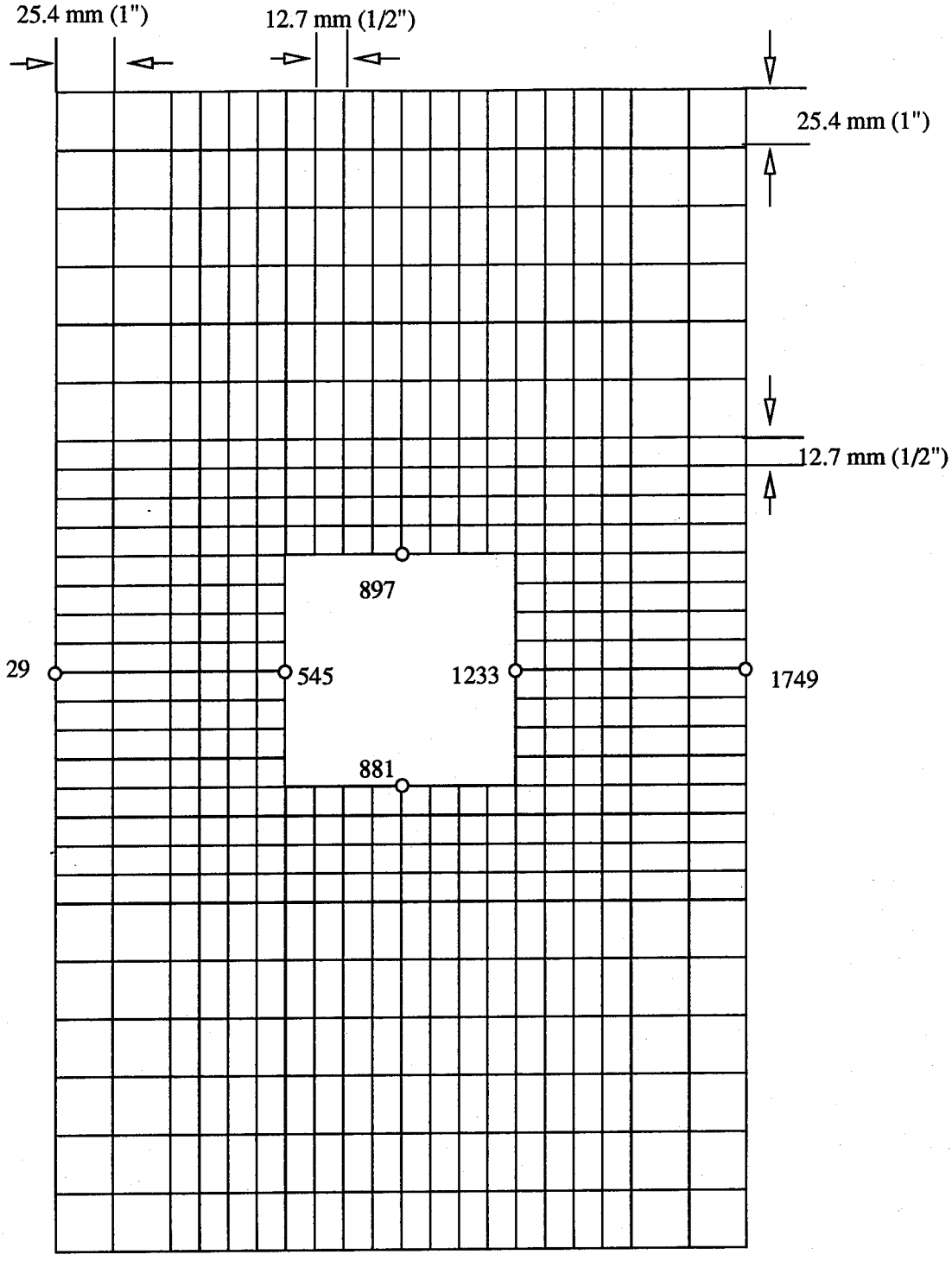

Figure 41. Finite-Element Mesh Used for 304.8 mm x 508 mm (12" x 20") Panel With 101.6 mm x 101.6 mm (4" x 4") Cutout

Total nodes = 2085

Total elements = 660

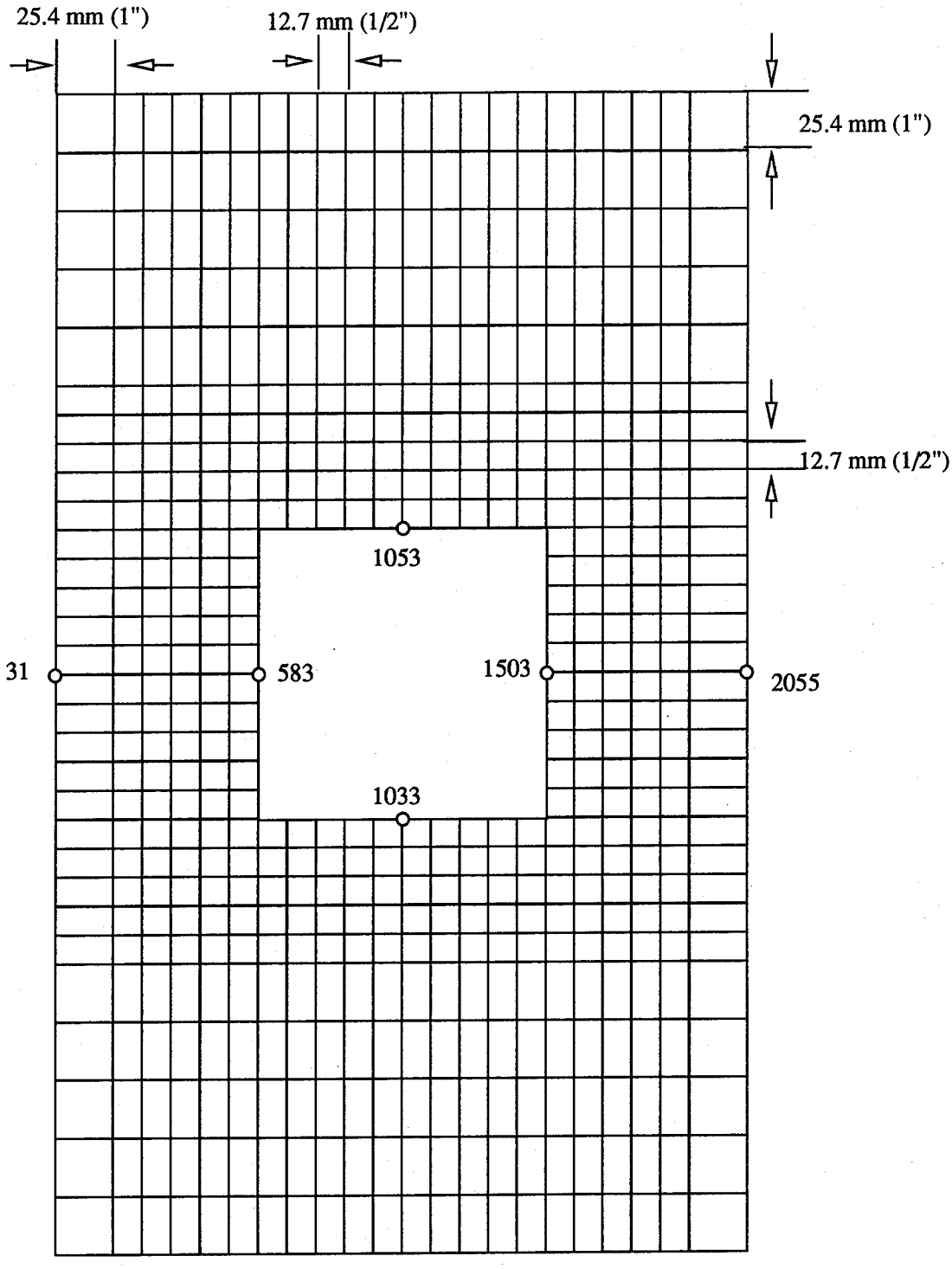

Figure 42. Finite-Element Mesh Used for 304.8 mm x 508 mm (12" x 20") Panel With 127 mm x 127 mm (5" x 5") Cutout

Total nodes = 1829

Total elements = 576

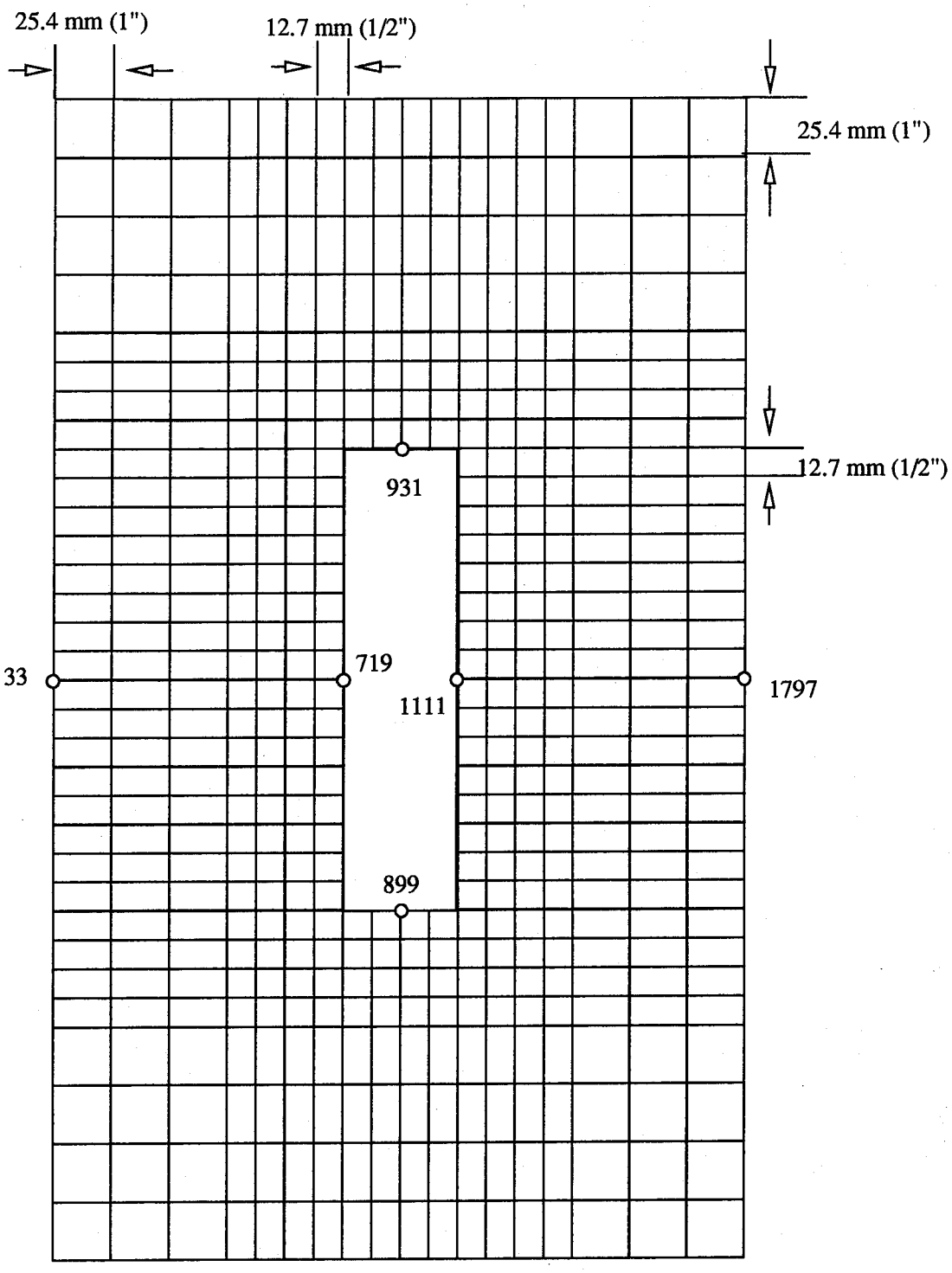

Figure 43. Finite-Element Mesh Used for 304.8 mm x 508 mm (12" x 20") Panel With 50.8 mm x 203.3 mm (2" x 8") Cutout

Total nodes = 1973

Total elements = 624

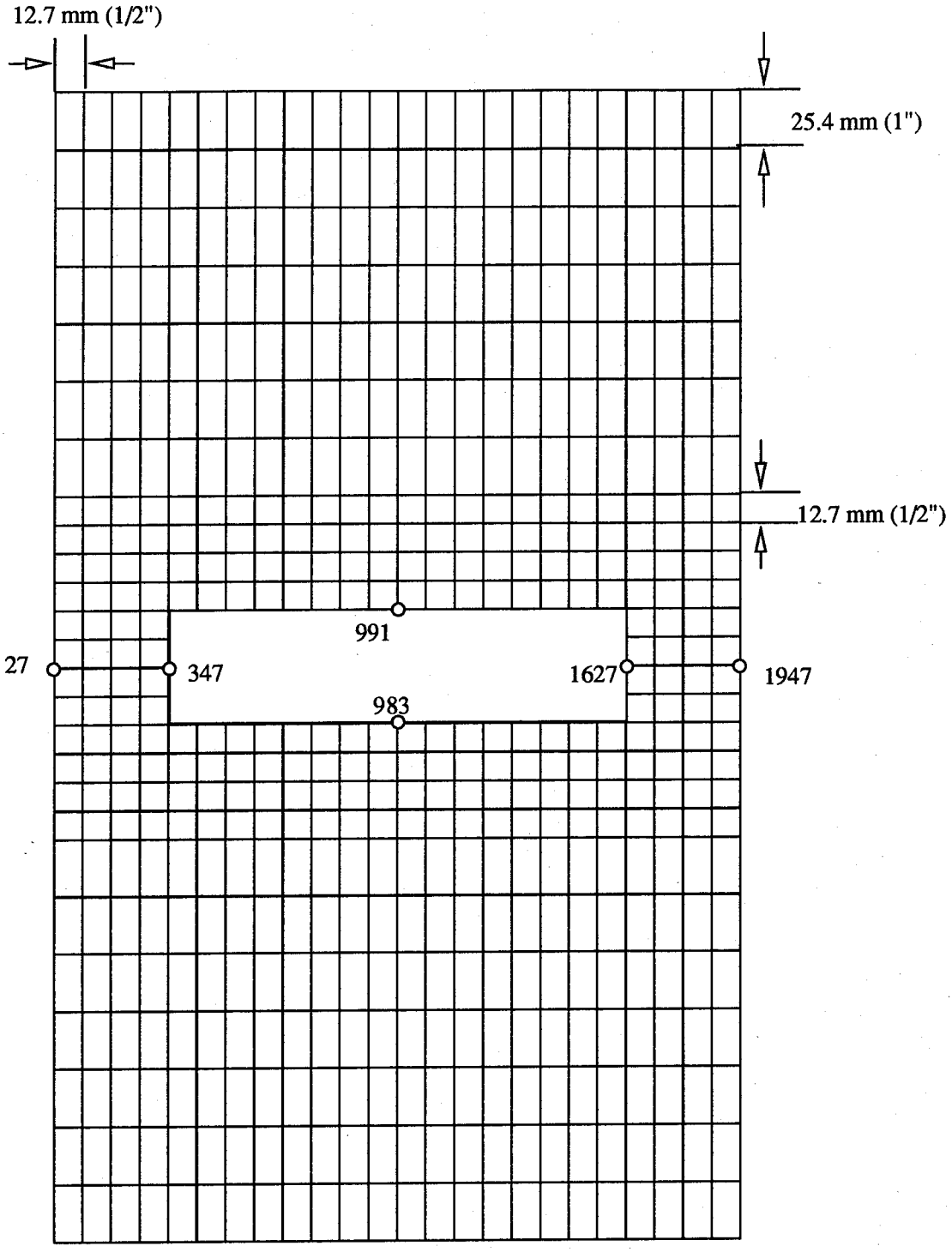

Figure 44. Finite-Element Mesh Used for 304.8 mm x 508 mm (12" x 20") Panel With 203.3 mm x 50.8 mm (8" x 2") Cutout

APPENDIX B

SAMPLE SHELL AND CLASSIC INPUT DECKS

SHELL and CLASSIC* Input Deck Sequence

* An astrix followed by an explanation indicates where the input Deck for CLASSIC differs from the one displayed for SHELL

Line 1	Title
Line 2	
IEL	Element type
	IEL = 2 cylindrical shell
NPE	Nodes per element
	NPE = 8
NANAL(1)	Nonlinear analysis
	NANAL(1) = 0
NANAL(2)	Symmetric laminate
	NANAL(2) = 2
NANAL(3)*	Large rotation
	NANAL(3) = 0

* (This is always 1 for Donnell)

IMESH	Automatic mesh generation
	IMESH = 1
NPRNT	Do not print elasticity matrices
	NPRNT = 0
NCUT (**Cutout**)	Number of elements to cutout

Line 3

INTYP	Displacement increment type INTYP = 1
NINC	Number of increments
IMAX	Maximum number of iterations
IRES	Do not update stiffness every iteration IRES = 0
TOL	Percent convergence tolerance

Line 4-5

TABLE(NINC)	Real number multiplicative factors of prescribed displacements

Line 6

NX	Number of elemental subdivisions in the x direction
NY	Number of elemental subdivisions in the y direction

Lines 7-14

DX(I)	Distance between nodes along the x direction

Lines 15-20

DY(I)	Distance between nodes along the y direction

Lines 21-30

(Cutout)	Assigned element numbers of cutout to be deleted These elements are not calculated in the stiffness of the panel

Line 31

LD	Load type parameter LD = 0
PO	Distributed load intensity PO = 0.0

Line 32

NBDY	Number of nodes with specified primary degrees of freedom (e.g. for this study the specified degrees of freedom at the top and bottom horizontal edge of panel and inside the cutout region)
Lines 33-77**	Specified degrees of freedom for top panel nodes (1 = prescribed and 0 = free)

** (The last two D.O.F. in each line are not included for CLASSIC)

Lines 78-122**	Specified degrees of freedom for bottom panel nodes
Lines 123-383**	Specified degrees of freedom for nodes which fall within the cutout area (excludes those nodes that fall on the cutout boundary)
Lines 384-404***	Values for the top panel nodes degrees of freedom (either zero or the prescribed displacement increment in inches)
Lines 404-425***	Values for the bottom panel nodes degrees of freedom

***(There are less values listed in CLASSIC because there are only 5 D.O.F. for the corner nodes)

Lines 425-517 ***	Values for the cutout nodes degrees of freedom. Set to zero.
(Cutout)	
Line 518	
NBSF	Number of point loads (zero)
	NBSF = 0
Line 519	
E1	Young's modulus along fibers
E2	Young's modulus transverse to fibers
G12	Shear modulus
NU12	Major Poisson's ratio
Line 520 ****	
G13	1-3 Shear Modulus
G23	2-3 Shear Modulus

****(This line is not included in CLASSIC)

Line 521	
NP	Number of plies
PT	Ply thickness
Lines 522-523	Ply orientation angle
Line 524	Radius of curvature
Line 525	Number of nodal forces to be calculated along the top edge of the panel

Lines 526-530 *****	Degree of Freedom number associated with loading direction (u), for each panel top edge node
*****(These numbers are different for CLASSIC because there are less D.O.F.)	
Line 531	Number of elements stresses to to be calculated for this study zero

```
1     12X20 [0/45/-45/90]2s 5" Cutout
2     2,8,0,2,0,1,0,0,100
3     1,18,80,0,.001
4     2.,4.,6.,8.,10.,12.,14.,16.,16.2,16.
5     16.6,16.8,17.,17.2,17.4,17.6,17.8,18
6     30,22
7     0.50,0.50,0.50,0.50,0.50,0.50,0.50,0
8     0.50,0.50,0.25,0.25,0.25,0.25,0.25,0
9     0.25,0.25,0.25,0.25,0.25,0.25,0.25,0
10    0.25,0.25,0.25,0.25,0.25,0.25,0.25,0
11    0.25,0.25,0.25,0.25,0.25,0.25,0.25,0
12    0.25,0.25,0.25,0.25,0.25,0.25,0.25,0
13    0.25,0.25,0.50,0.50,0.50,0.50,0.50,0
14    0.50,0.50,0.50,0.50
15    0.50,0.50,0.25,0.25,0.25,0.25,0.25,0
16    0.25,0.25,0.25,0.25,0.25,0.25,0.25,0
17    0.25,0.25,0.25,0.25,0.25,0.25,0.25,0
18    0.25,0.25,0.25,0.25,0.25,0.25,0.25,0
19    0.25,0.25,0.25,0.25,0.25,0.25,0.25,0
20    0.25,0.25,0.50,0.50
21    191,192,193,194,195,196,197,198,199,
22    221,222,223,224,225,226,227,228,229,
23    251,252,253,254,255,256,257,258,259,
24    281,282,283,284,285,286,287,288,289,
25    311,312,313,314,315,316,317,318,319,
26    341,342,343,344,345,346,347,348,349,
27    371,372,373,374,375,376,377,378,379,
28    401,402,403,404,405,406,407,408,409,
29    431,432,433,434,435,436,437,438,439,
30    461,462,463,464,465,466,467,468,469,
31    0,0.0
32    351
33    61,1,1,1,1,1,1,1
34    92,1,1,0,0,0,0,0
35    153,1,1,1,1,1,1,1
36    184,1,1,0,0,0,0,0
37    245,1,1,1,1,1,1,1
38    276,1,1,0,0,0,0,0
39    337,1,1,1,1,1,1,1
40    368,1,1,0,0,0,0,0
41    429,1,1,1,1,1,1,1
42    460,1,1,0,0,0,0,0
43    521,1,1,1,1,1,1,1
44    552,1,1,0,0,0,0,0
45    613,1,1,1,1,1,1,1
```

46 644,1,1,0,0,0,0,0
47 705,1,1,1,1,1,1,1
48 736,1,1,0,0,0,0,0
49 797,1,1,1,1,1,1,1
50 828,1,1,0,0,0,0,0
51 889,1,1,1,1,1,1,1
52 920,1,1,0,0,0,0,0
53 981,1,1,1,1,1,1,1
54 1012,1,1,0,0,0,0,0
55 1073,1,1,1,1,1,1,1
56 1104,1,1,0,0,0,0,0
57 1165,1,1,1,1,1,1,1
58 1196,1,1,0,0,0,0,0
59 1257,1,1,1,1,1,1,1
60 1288,1,1,0,0,0,0,0
61 1349,1,1,1,1,1,1,1
62 1380,1,1,0,0,0,0,0
63 1441,1,1,1,1,1,1,1
64 1472,1,1,0,0,0,0,0
65 1533,1,1,1,1,1,1,1
66 1564,1,1,0,0,0,0,0
67 1625,1,1,1,1,1,1,1
68 1656,1,1,0,0,0,0,0
69 1717,1,1,1,1,1,1,1
70 1748,1,1,0,0,0,0,0
71 1809,1,1,1,1,1,1,1
72 1840,1,1,0,0,0,0,0
73 1901,1,1,1,1,1,1,1
74 1932,1,1,0,0,0,0,0
75 1993,1,1,1,1,1,1,1
76 2024,1,1,0,0,0,0,0
77 2085,1,1,1,1,1,1,1
78 1,1,1,1,1,1,1,1
79 62,1,1,0,0,0,0,0
80 93,1,1,1,1,1,1,1
81 154,1,1,0,0,0,0,0
82 185,1,1,1,1,1,1,1
83 246,1,1,0,0,0,0,0
84 277,1,1,1,1,1,1,1
85 338,1,1,0,0,0,0,0
86 369,1,1,1,1,1,1,1
87 430,1,1,0,0,0,0,0
88 461,1,1,1,1,1,1,1
89 522,1,1,0,0,0,0,0
90 553,1,1,1,1,1,1,1

91 614,1,1,0,0,0,0,0
92 645,1,1,1,1,1,1,1
93 706,1,1,0,0,0,0,0
94 737,1,1,1,1,1,1,1
95 798,1,1,0,0,0,0,0
96 829,1,1,1,1,1,1,1
97 890,1,1,0,0,0,0,0
98 921,1,1,1,1,1,1,1
99 982,1,1,0,0,0,0,0
100 1013,1,1,1,1,1,1,1
101 1074,1,1,0,0,0,0,0
102 1105,1,1,1,1,1,1,1
103 1166,1,1,0,0,0,0,0
104 1197,1,1,1,1,1,1,1
105 1258,1,1,0,0,0,0,0
106 1289,1,1,1,1,1,1,1
107 1350,1,1,0,0,0,0,0
108 1381,1,1,1,1,1,1,1
109 1442,1,1,0,0,0,0,0
110 1473,1,1,1,1,1,1,1
111 1534,1,1,0,0,0,0,0
112 1565,1,1,1,1,1,1,1
113 1626,1,1,0,0,0,0,0
114 1657,1,1,1,1,1,1,1
115 1718,1,1,0,0,0,0,0
116 1749,1,1,1,1,1,1,1
117 1810,1,1,0,0,0,0,0
118 1841,1,1,1,1,1,1,1
119 1902,1,1,0,0,0,0,0
120 1933,1,1,1,1,1,1,1
121 1994,1,1,0,0,0,0,0
122 2025,1,1,1,1,1,1,1
123 625,1,1,0,0,0,0,0
124 626,1,1,0,0,0,0,0
125 627,1,1,0,0,0,0,0
126 628,1,1,0,0,0,0,0
127 629,1,1,0,0,0,0,0
128 630,1,1,0,0,0,0,0
129 631,1,1,0,0,0,0,0
130 632,1,1,0,0,0,0,0
131 633,1,1,0,0,0,0,0
132 666,1,1,0,0,0,0,0
133 667,1,1,1,1,1,1,1
134 668,1,1,0,0,0,0,0
135 669,1,1,1,1,1,1,1

136 670,1,1,0,0,0,0,0
137 671,1,1,1,1,1,1,1
138 672,1,1,0,0,0,0,0
139 673,1,1,1,1,1,1,1
140 674,1,1,0,0,0,0,0
141 675,1,1,1,1,1,1,1
142 676,1,1,0,0,0,0,0
143 677,1,1,1,1,1,1,1
144 678,1,1,0,0,0,0,0
145 679,1,1,1,1,1,1,1
146 680,1,1,0,0,0,0,0
147 681,1,1,1,1,1,1,1
148 682,1,1,0,0,0,0,0
149 683,1,1,1,1,1,1,1
150 684,1,1,0,0,0,0,0
151 717,1,1,0,0,0,0,0
152 718,1,1,0,0,0,0,0
153 719,1,1,0,0,0,0,0
154 720,1,1,0,0,0,0,0
155 721,1,1,0,0,0,0,0
156 722,1,1,0,0,0,0,0
157 723,1,1,0,0,0,0,0
158 724,1,1,0,0,0,0,0
159 725,1,1,0,0,0,0,0
160 758,1,1,0,0,0,0,0
161 759,1,1,1,1,1,1,1
162 760,1,1,0,0,0,0,0
163 761,1,1,1,1,1,1,1
164 762,1,1,0,0,0,0,0
165 763,1,1,1,1,1,1,1
166 764,1,1,0,0,0,0,0
167 765,1,1,1,1,1,1,1
168 766,1,1,0,0,0,0,0
169 767,1,1,1,1,1,1,1
170 768,1,1,0,0,0,0,0
171 769,1,1,1,1,1,1,1
172 770,1,1,0,0,0,0,0
173 771,1,1,1,1,1,1,1
174 772,1,1,0,0,0,0,0
175 773,1,1,1,1,1,1,1
176 774,1,1,0,0,0,0,0
177 775,1,1,1,1,1,1,1
178 776,1,1,0,0,0,0,0
179 809,1,1,0,0,0,0,0
180 810,1,1,0,0,0,0,0

181 811,1,1,0,0,0,0,0
182 812,1,1,0,0,0,0,0
183 813,1,1,0,0,0,0,0
184 814,1,1,0,0,0,0,0
185 815,1,1,0,0,0,0,0
186 816,1,1,0,0,0,0,0
187 817,1,1,0,0,0,0,0
188 850,1,1,0,0,0,0,0
189 851,1,1,1,1,1,1,1
190 852,1,1,0,0,0,0,0
191 853,1,1,1,1,1,1,1
192 854,1,1,0,0,0,0,0
193 855,1,1,1,1,1,1,1
194 856,1,1,0,0,0,0,0
195 857,1,1,1,1,1,1,1
196 858,1,1,0,0,0,0,0
197 859,1,1,1,1,1,1,1
198 860,1,1,0,0,0,0,0
199 861,1,1,1,1,1,1,1
200 862,1,1,0,0,0,0,0
201 863,1,1,1,1,1,1,1
202 864,1,1,0,0,0,0,0
203 865,1,1,1,1,1,1,1
204 866,1,1,0,0,0,0,0
205 867,1,1,1,1,1,1,1
206 868,1,1,0,0,0,0,0
207 901,1,1,0,0,0,0,0
208 902,1,1,0,0,0,0,0
209 903,1,1,0,0,0,0,0
210 904,1,1,0,0,0,0,0
211 905,1,1,0,0,0,0,0
212 906,1,1,0,0,0,0,0
213 907,1,1,0,0,0,0,0
214 908,1,1,0,0,0,0,0
215 909,1,1,0,0,0,0,0
216 942,1,1,0,0,0,0,0
217 943,1,1,1,1,1,1,1
218 944,1,1,0,0,0,0,0
219 945,1,1,1,1,1,1,1
220 946,1,1,0,0,0,0,0
221 947,1,1,1,1,1,1,1
222 948,1,1,0,0,0,0,0
223 949,1,1,1,1,1,1,1
224 950,1,1,0,0,0,0,0
225 951,1,1,1,1,1,1,1

226 952,1,1,0,0,0,0,0
227 953,1,1,1,1,1,1,1
228 954,1,1,0,0,0,0,0
229 955,1,1,1,1,1,1,1
230 956,1,1,0,0,0,0,0
231 957,1,1,1,1,1,1,1
232 958,1,1,0,0,0,0,0
233 959,1,1,1,1,1,1,1
234 960,1,1,0,0,0,0,0
235 993,1,1,0,0,0,0,0
236 994,1,1,0,0,0,0,0
237 995,1,1,0,0,0,0,0
238 996,1,1,0,0,0,0,0
239 997,1,1,0,0,0,0,0
240 998,1,1,0,0,0,0,0
241 999,1,1,0,0,0,0,0
242 1000,1,1,0,0,0,0,0
243 1001,1,1,0,0,0,0,0
244 1034,1,1,0,0,0,0,0
245 1035,1,1,1,1,1,1,1
246 1036,1,1,0,0,0,0,0
247 1037,1,1,1,1,1,1,1
248 1038,1,1,0,0,0,0,0
249 1039,1,1,1,1,1,1,1
250 1040,1,1,0,0,0,0,0
251 1041,1,1,1,1,1,1,1
252 1042,1,1,0,0,0,0,0
253 1043,1,1,1,1,1,1,1
254 1044,1,1,0,0,0,0,0
255 1045,1,1,1,1,1,1,1
256 1046,1,1,0,0,0,0,0
257 1047,1,1,1,1,1,1,1
258 1048,1,1,0,0,0,0,0
259 1049,1,1,1,1,1,1,1
260 1050,1,1,0,0,0,0,0
261 1051,1,1,1,1,1,1,1
262 1052,1,1,0,0,0,0,0
263 1085,1,1,0,0,0,0,0
264 1086,1,1,0,0,0,0,0
265 1087,1,1,0,0,0,0,0
266 1088,1,1,0,0,0,0,0
267 1089,1,1,0,0,0,0,0
268 1090,1,1,0,0,0,0,0
269 1091,1,1,0,0,0,0,0
270 1092,1,1,0,0,0,0,0

271 1093,1,1,0,0,0,0,0
272 1126,1,1,0,0,0,0,0
273 1127,1,1,1,1,1,1,1
274 1128,1,1,0,0,0,0,0
275 1129,1,1,1,1,1,1,1
276 1130,1,1,0,0,0,0,0
277 1131,1,1,1,1,1,1,1
278 1132,1,1,0,0,0,0,0
279 1133,1,1,1,1,1,1,1
280 1134,1,1,0,0,0,0,0
281 1135,1,1,1,1,1,1,1
282 1136,1,1,0,0,0,0,0
283 1137,1,1,1,1,1,1,1
284 1138,1,1,0,0,0,0,0
285 1139,1,1,1,1,1,1,1
286 1140,1,1,0,0,0,0,0
287 1141,1,1,1,1,1,1,1
288 1142,1,1,0,0,0,0,0
289 1143,1,1,1,1,1,1,1
290 1144,1,1,0,0,0,0,0
291 1177,1,1,0,0,0,0,0
292 1178,1,1,0,0,0,0,0
293 1179,1,1,0,0,0,0,0
294 1180,1,1,0,0,0,0,0
295 1181,1,1,0,0,0,0,0
296 1182,1,1,0,0,0,0,0
297 1183,1,1,0,0,0,0,0
298 1184,1,1,0,0,0,0,0
299 1185,1,1,0,0,0,0,0
300 1218,1,1,0,0,0,0,0
301 1219,1,1,1,1,1,1,1
302 1220,1,1,0,0,0,0,0
303 1221,1,1,1,1,1,1,1
304 1222,1,1,0,0,0,0,0
305 1223,1,1,1,1,1,1,1
306 1224,1,1,0,0,0,0,0
307 1225,1,1,1,1,1,1,1
308 1226,1,1,0,0,0,0,0
309 1227,1,1,1,1,1,1,1
310 1228,1,1,0,0,0,0,0
311 1229,1,1,1,1,1,1,1
312 1230,1,1,0,0,0,0,0
313 1231,1,1,1,1,1,1,1
314 1232,1,1,0,0,0,0,0
315 1233,1,1,1,1,1,1,1

316 1234,1,1,0,0,0,0,0
317 1235,1,1,1,1,1,1,1
318 1236,1,1,0,0,0,0,0
319 1269,1,1,0,0,0,0,0
320 1270,1,1,0,0,0,0,0
321 1271,1,1,0,0,0,0,0
322 1272,1,1,0,0,0,0,0
323 1273,1,1,0,0,0,0,0
324 1274,1,1,0,0,0,0,0
325 1275,1,1,0,0,0,0,0
326 1276,1,1,0,0,0,0,0
327 1277,1,1,0,0,0,0,0
328 1310,1,1,0,0,0,0,0
329 1311,1,1,1,1,1,1,1
330 1312,1,1,0,0,0,0,0
331 1313,1,1,1,1,1,1,1
332 1314,1,1,0,0,0,0,0
333 1315,1,1,1,1,1,1,1
334 1316,1,1,0,0,0,0,0
335 1317,1,1,1,1,1,1,1
336 1318,1,1,0,0,0,0,0
337 1319,1,1,1,1,1,1,1
338 1320,1,1,0,0,0,0,0
339 1321,1,1,1,1,1,1,1
340 1322,1,1,0,0,0,0,0
341 1323,1,1,1,1,1,1,1
342 1324,1,1,0,0,0,0,0
343 1325,1,1,1,1,1,1,1
344 1326,1,1,0,0,0,0,0
345 1327,1,1,1,1,1,1,1
346 1328,1,1,0,0,0,0,0
347 1361,1,1,0,0,0,0,0
348 1362,1,1,0,0,0,0,0
349 1363,1,1,0,0,0,0,0
350 1364,1,1,0,0,0,0,0
351 1365,1,1,0,0,0,0,0
352 1366,1,1,0,0,0,0,0
353 1367,1,1,0,0,0,0,0
354 1368,1,1,0,0,0,0,0
355 1369,1,1,0,0,0,0,0
356 1402,1,1,0,0,0,0,0
357 1403,1,1,1,1,1,1,1
358 1404,1,1,0,0,0,0,0
359 1405,1,1,1,1,1,1,1
360 1406,1,1,0,0,0,0,0

```
361     1407,1,1,1,1,1,1,1
362     1408,1,1,0,0,0,0,0
363     1409,1,1,1,1,1,1,1
364     1410,1,1,0,0,0,0,0
365     1411,1,1,1,1,1,1,1
366     1412,1,1,0,0,0,0,0
367     1413,1,1,1,1,1,1,1
368     1414,1,1,0,0,0,0,0
369     1415,1,1,1,1,1,1,1
370     1416,1,1,0,0,0,0,0
371     1417,1,1,1,1,1,1,1
372     1418,1,1,0,0,0,0,0
373     1419,1,1,1,1,1,1,1
374     1420,1,1,0,0,0,0,0
375     1453,1,1,0,0,0,0,0
376     1454,1,1,0,0,0,0,0
377     1455,1,1,0,0,0,0,0
378     1456,1,1,0,0,0,0,0
379     1457,1,1,0,0,0,0,0
380     1458,1,1,0,0,0,0,0
381     1459,1,1,0,0,0,0,0
382     1460,1,1,0,0,0,0,0
383     1461,1,1,0,0,0,0,0
384     -.0015,0.,0.,0.,0.,0.,0.,-.0015,0.,-
385     0.,0.,0.,0.,0.,0.,-.0015,0.,-.0015,0
386     0.,0.,0.,0.,0.,-.0015,0.,-.0015,0.,0
387     0.,0.,0.,0.,-.0015,0.,-.0015,0.,0.,0
388     0.,0.,0.,-.0015,0.,-.0015,0.,0.,0.,0
389     0.,0.,-.0015,0.,-.0015,0.,0.,0.,0.,0
390     0.,-.0015,0.,-.0015,0.,0.,0.,0.,0.,0
391     -.0015,0.,-.0015,0.,0.,0.,0.,0.,0.,-
392     0.,-.0015,0.,0.,0.,0.,0.,0.,-.0015,0
393     -.0015,0.,0.,0.,0.,0.,0.,-.0015,0.,-
394     0.,0.,0.,0.,0.,0.,-.0015,0.,-.0015,0
395     0.,0.,0.,0.,0.,-.0015,0.,-.0015,0.,0
396     0.,0.,0.,0.,-.0015,0.,-.0015,0.,0.,0
397     0.,0.,0.,-.0015,0.,-.0015,0.,0.,0.,0
398     0.,0.,-.0015,0.,-.0015,0.,0.,0.,0.,0
399     0.,-.0015,0.,-.0015,0.,0.,0.,0.,0.,0
400     -.0015,0.,-.0015,0.,0.,0.,0.,0.,0.,-
401     0.,-.0015,0.,0.,0.,0.,0.,0.,-.0015,0
402     -.0015,0.,0.,0.,0.,0.,0.,-.0015,0.,-
403     0.,0.,0.,0.,0.,0.,-.0015,0.,-.0015,0
404     0.,0.,0.,0.,0.,0.,0.,0.,0.,0.,
405     0.,0.,0.,0.,0.,0.,0.,0.,0.,0.,
```

406 0.,0.,0.,0.,0.,0.,0.,0.,0.,0.,
407 0.,0.,0.,0.,0.,0.,0.,0.,0.,0.,
408 0.,0.,0.,0.,0.,0.,0.,0.,0.,0.,
409 0.,0.,0.,0.,0.,0.,0.,0.,0.,0.,
410 0.,0.,0.,0.,0.,0.,0.,0.,0.,0.,
411 0.,0.,0.,0.,0.,0.,0.,0.,0.,0.,
412 0.,0.,0.,0.,0.,0.,0.,0.,0.,0.,
413 0.,0.,0.,0.,0.,0.,0.,0.,0.,0.,
414 0.,0.,0.,0.,0.,0.,0.,0.,0.,0.,
415 0.,0.,0.,0.,0.,0.,0.,0.,0.,0.,
416 0.,0.,0.,0.,0.,0.,0.,0.,0.,0.,
417 0.,0.,0.,0.,0.,0.,0.,0.,0.,0.,
418 0.,0.,0.,0.,0.,0.,0.,0.,0.,0.,
419 0.,0.,0.,0.,0.,0.,0.,0.,0.,0.,
420 0.,0.,0.,0.,0.,0.,0.,0.,0.,0.,
421 0.,0.,0.,0.,0.,0.,0.,0.,0.,0.,
422 0.,0.,0.,0.,0.,0.,0.,0.,0.,0.,
423 0.,0.,0.,0.,0.,0.,0.,0.,0.,0.,
424 0.,0.,0.,0.,0.,0.,0.,0.,0.,0.,
425 0.,0.,0.,0.,0.,0.,0.,0.,0.,0.,
426 0.,0.,0.,0.,0.,0.,0.,0.,0.,0.,
427 0.,0.,0.,0.,0.,0.,0.,0.,0.,0.,
428 0.,0.,0.,0.,0.,0.,0.,0.,0.,0.,
429 0.,0.,0.,0.,0.,0.,0.,0.,0.,0.,
430 0.,0.,0.,0.,0.,0.,0.,0.,0.,0.,
431 0.,0.,0.,0.,0.,0.,0.,0.,0.,0.,
432 0.,0.,0.,0.,0.,0.,0.,0.,0.,0.,
433 0.,0.,0.,0.,0.,0.,0.,0.,0.,0.,
434 0.,0.,0.,0.,0.,0.,0.,0.,0.,0.,
435 0.,0.,0.,0.,0.,0.,0.,0.,0.,0.,
436 0.,0.,0.,0.,0.,0.,0.,0.,0.,0.,
437 0.,0.,0.,0.,0.,0.,0.,0.,0.,0.,
438 0.,0.,0.,0.,0.,0.,0.,0.,0.,0.,
439 0.,0.,0.,0.,0.,0.,0.,0.,0.,0.,
440 0.,0.,0.,0.,0.,0.,0.,0.,0.,0.,
441 0.,0.,0.,0.,0.,0.,0.,0.,0.,0.,
442 0.,0.,0.,0.,0.,0.,0.,0.,0.,0.,
443 0.,0.,0.,0.,0.,0.,0.,0.,0.,0.,
444 0.,0.,0.,0.,0.,0.,0.,0.,0.,0.,
445 0.,0.,0.,0.,0.,0.,0.,0.,0.,0.,
446 0.,0.,0.,0.,0.,0.,0.,0.,0.,0.,
447 0.,0.,0.,0.,0.,0.,0.,0.,0.,0.,
448 0.,0.,0.,0.,0.,0.,0.,0.,0.,0.,
449 0.,0.,0.,0.,0.,0.,0.,0.,0.,0.,
450 0.,0.,0.,0.,0.,0.,0.,0.,0.,0.,

451 0.,0.,0.,0.,0.,0.,0.,0.,0.,0.,
452 0.,0.,0.,0.,0.,0.,0.,0.,0.,0.,
453 0.,0.,0.,0.,0.,0.,0.,0.,0.,0.,
454 0.,0.,0.,0.,0.,0.,0.,0.,0.,0.,
455 0.,0.,0.,0.,0.,0.,0.,0.,0.,0.,
456 0.,0.,0.,0.,0.,0.,0.,0.,0.,0.,
457 0.,0.,0.,0.,0.,0.,0.,0.,0.,0.,
458 0.,0.,0.,0.,0.,0.,0.,0.,0.,0.,
459 0.,0.,0.,0.,0.,0.,0.,0.,0.,0.,
460 0.,0.,0.,0.,0.,0.,0.,0.,0.,0.,
461 0.,0.,0.,0.,0.,0.,0.,0.,0.,0.,
462 0.,0.,0.,0.,0.,0.,0.,0.,0.,0.,
463 0.,0.,0.,0.,0.,0.,0.,0.,0.,0.,
464 0.,0.,0.,0.,0.,0.,0.,0.,0.,0.,
465 0.,0.,0.,0.,0.,0.,0.,0.,0.,0.,
466 0.,0.,0.,0.,0.,0.,0.,0.,0.,0.,
467 0.,0.,0.,0.,0.,0.,0.,0.,0.,0.,
468 0.,0.,0.,0.,0.,0.,0.,0.,0.,0.,
469 0.,0.,0.,0.,0.,0.,0.,0.,0.,0.,
470 0.,0.,0.,0.,0.,0.,0.,0.,0.,0.,
471 0.,0.,0.,0.,0.,0.,0.,0.,0.,0.,
472 0.,0.,0.,0.,0.,0.,0.,0.,0.,0.,
473 0.,0.,0.,0.,0.,0.,0.,0.,0.,0.,
474 0.,0.,0.,0.,0.,0.,0.,0.,0.,0.,
475 0.,0.,0.,0.,0.,0.,0.,0.,0.,0.,
476 0.,0.,0.,0.,0.,0.,0.,0.,0.,0.,
477 0.,0.,0.,0.,0.,0.,0.,0.,0.,0.,
478 0.,0.,0.,0.,0.,0.,0.,0.,0.,0.,
479 0.,0.,0.,0.,0.,0.,0.,0.,0.,0.,
480 0.,0.,0.,0.,0.,0.,0.,0.,0.,0.,
481 0.,0.,0.,0.,0.,0.,0.,0.,0.,0.,
482 0.,0.,0.,0.,0.,0.,0.,0.,0.,0.,
483 0.,0.,0.,0.,0.,0.,0.,0.,0.,0.,
484 0.,0.,0.,0.,0.,0.,0.,0.,0.,0.,
485 0.,0.,0.,0.,0.,0.,0.,0.,0.,0.,
486 0.,0.,0.,0.,0.,0.,0.,0.,0.,0.,
487 0.,0.,0.,0.,0.,0.,0.,0.,0.,0.,
488 0.,0.,0.,0.,0.,0.,0.,0.,0.,0.,
489 0.,0.,0.,0.,0.,0.,0.,0.,0.,0.,
490 0.,0.,0.,0.,0.,0.,0.,0.,0.,0.,
491 0.,0.,0.,0.,0.,0.,0.,0.,0.,0.,
492 0.,0.,0.,0.,0.,0.,0.,0.,0.,0.,
493 0.,0.,0.,0.,0.,0.,0.,0.,0.,0.,
494 0.,0.,0.,0.,0.,0.,0.,0.,0.,0.,
495 0.,0.,0.,0.,0.,0.,0.,0.,0.,0.,

```
496     0.,0.,0.,0.,0.,0.,0.,0.,0.,0.,
497     0.,0.,0.,0.,0.,0.,0.,0.,0.,0.,
498     0.,0.,0.,0.,0.,0.,0.,0.,0.,0.,
499     0.,0.,0.,0.,0.,0.,0.,0.,0.,0.,
500     0.,0.,0.,0.,0.,0.,0.,0.,0.,0.,
501     0.,0.,0.,0.,0.,0.,0.,0.,0.,0.,
502     0.,0.,0.,0.,0.,0.,0.,0.,0.,0.,
503     0.,0.,0.,0.,0.,0.,0.,0.,0.,0.,
504     0.,0.,0.,0.,0.,0.,0.,0.,0.,0.,
505     0.,0.,0.,0.,0.,0.,0.,0.,0.,0.,
506     0.,0.,0.,0.,0.,0.,0.,0.,0.,0.,
507     0.,0.,0.,0.,0.,0.,0.,0.,0.,0.,
508     0.,0.,0.,0.,0.,0.,0.,0.,0.,0.,
509     0.,0.,0.,0.,0.,0.,0.,0.,0.,0.,
510     0.,0.,0.,0.,0.,0.,0.,0.,0.,0.,
511     0.,0.,0.,0.,0.,0.,0.,0.,0.,0.,
512     0.,0.,0.,0.,0.,0.,0.,0.,0.,0.,
513     0.,0.,0.,0.,0.,0.,0.,0.,0.,0.,
514     0.,0.,0.,0.,0.,0.,0.,0.,0.,0.,
515     0.,0.,0.,0.,0.,0.,0.,0.,0.,0.,
516     0.,0.,0.,0.,0.,0.,0.,0.,0.,0.,
517     0.,0.,0.,0.,0.,0.,0.
518     0
519     19.7e6,1.579e6,0.925e6,0.276,
520     0.925e6,0.462e6
521     16,0.00539
522     0.,45.,-45.,90.,0.,45.,-45.,90.,90.,
523     45.,0.,90.,-45.,45.,0.
524     12.0
525     45
526     271,338,610,677,949,1016,1288,1355,1
527     1966,2033,2305,2372,2644,2711,2983,3
528     3389,3661,3728,4000,4067,4339,4406,4
529     5017,5084,5356,5423,5695,5762,6034,6
530     6440,6712,6779,7051,7118,7390,7457,7
531     0
```

APPENDIX C

ADDITIONAL NUMERICAL/EXPERIMENTAL AXIAL LOAD VERSUS DISPLACEMENT CURVES

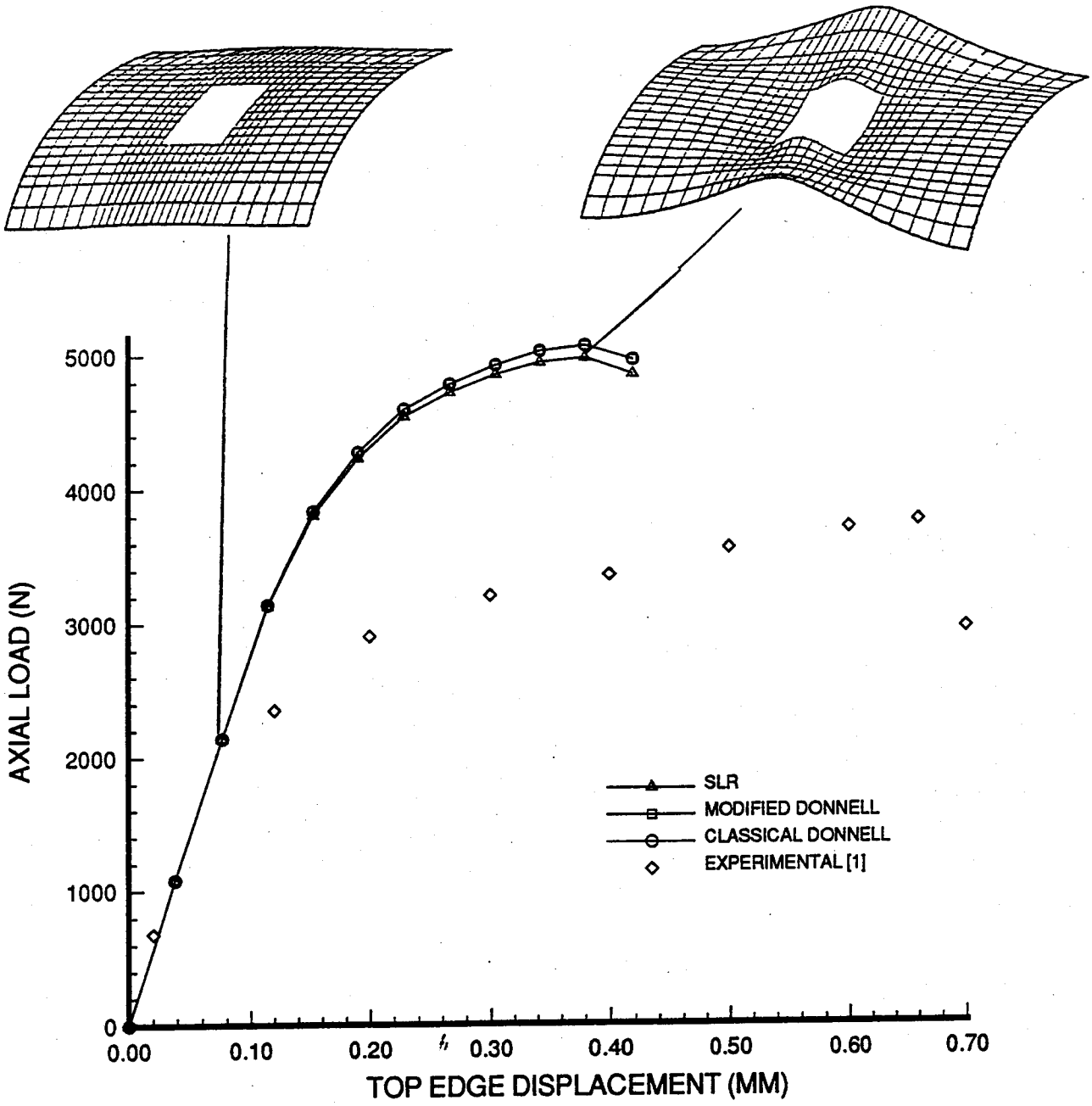

Figure 45: Load vs. Top Edge Displacement, Comparing Experimental to SLR, Modified Donnell, and Classical Donnell, 101.6 mm x 101.6 mm (4" x 4") Cutout, 304.8 mm x 508 mm (12" x 20") Panel [0/45/-45/90]s

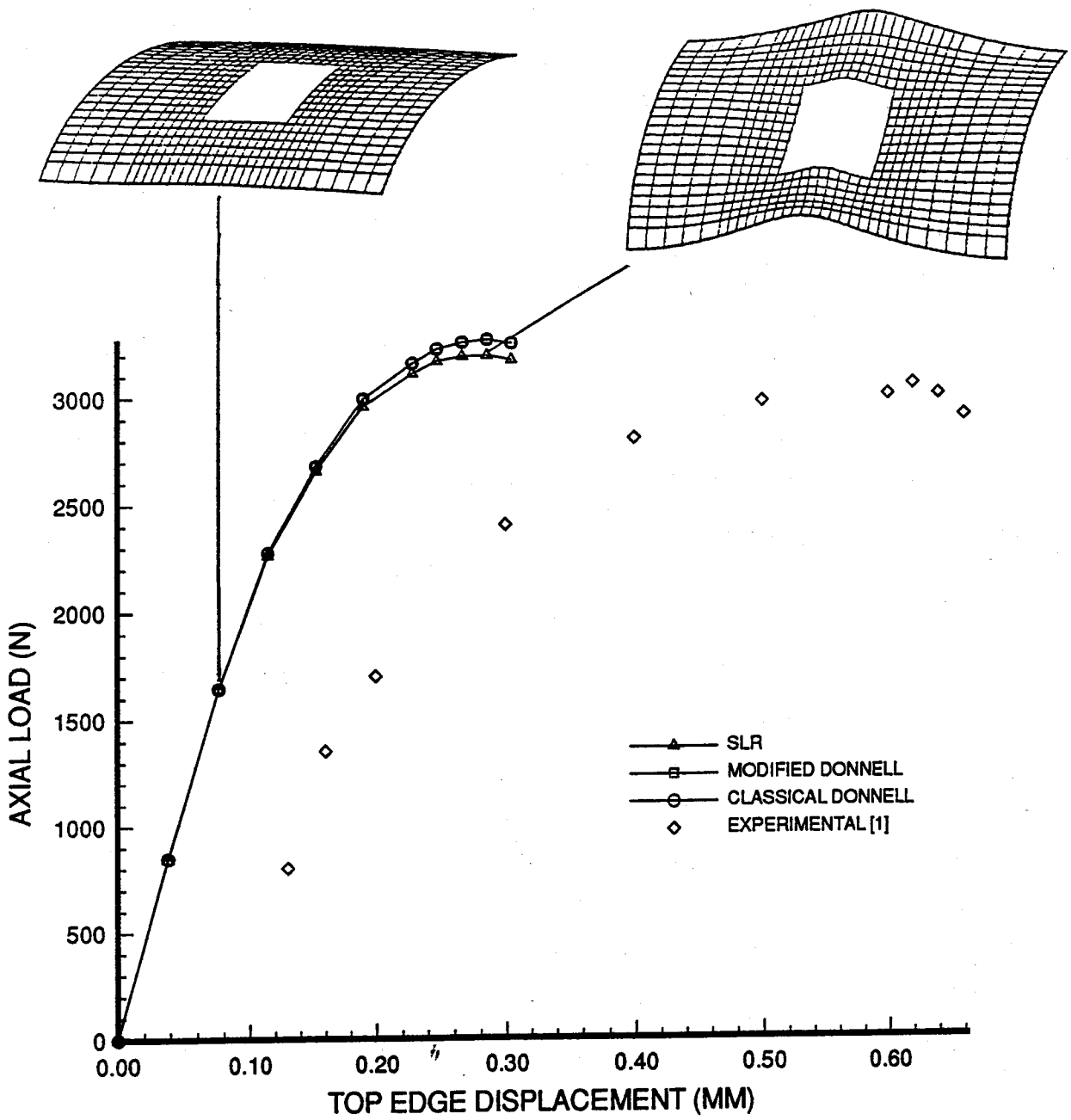

Figure 46: Load vs. Top Edge Displacement, Comparing Experimental to SLR, Modified Donnell, and Classical Donnell, 127 mm x 127 mm (5" x 5") Cutout, 304.8 mm x 508 mm (12" x 20") Panel [0/45/-45/90]s

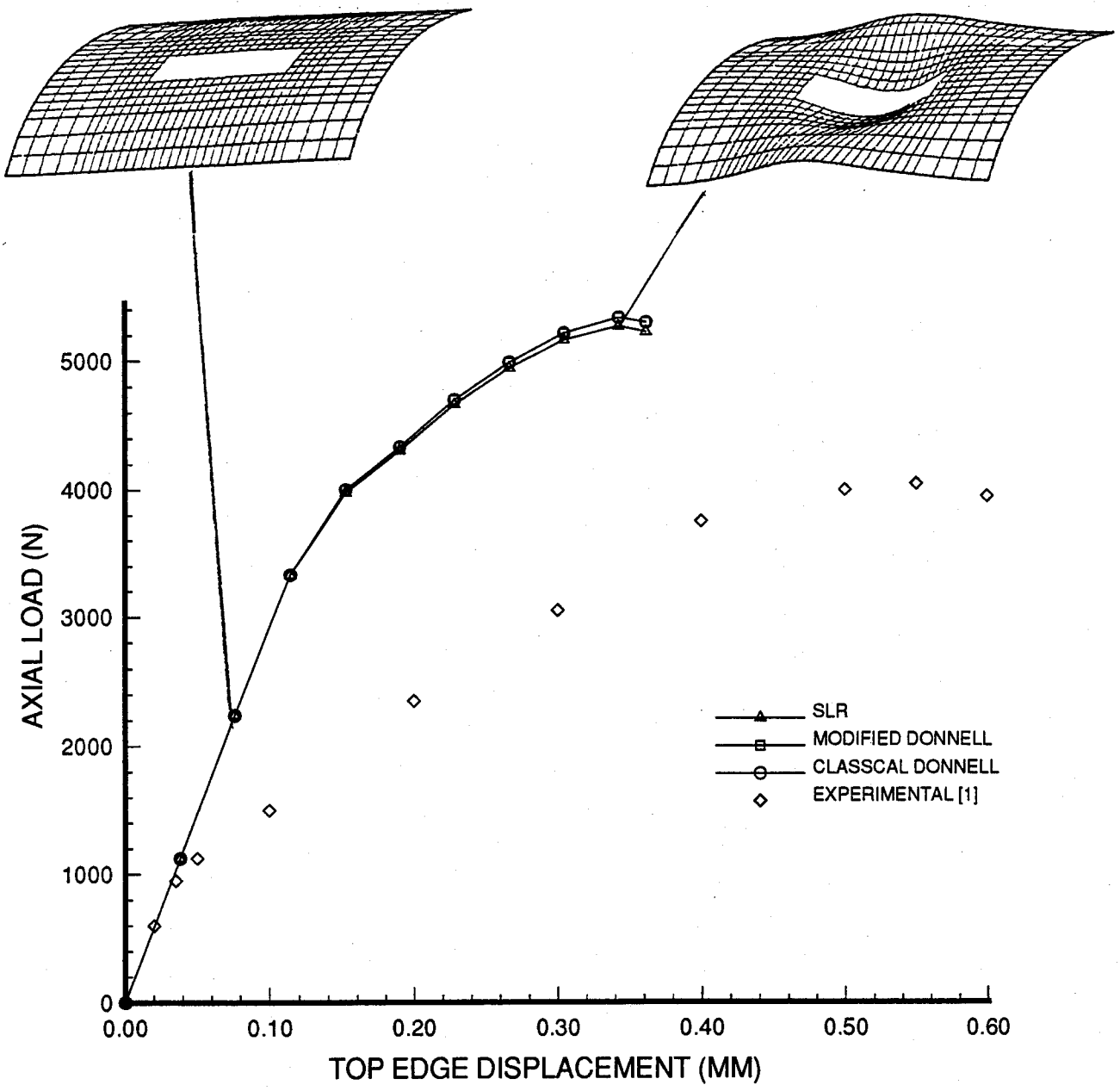

Figure 47: Load vs. Top Edge Displacement, Comparing Experimental to SLR, Modified Donnell, and Classical Donnell, 50.8 mm x 203.2 mm (2" x 8") Cutout, 304.8 mm x 508 mm (12" x 20") Panel [0/45/-45/90]s

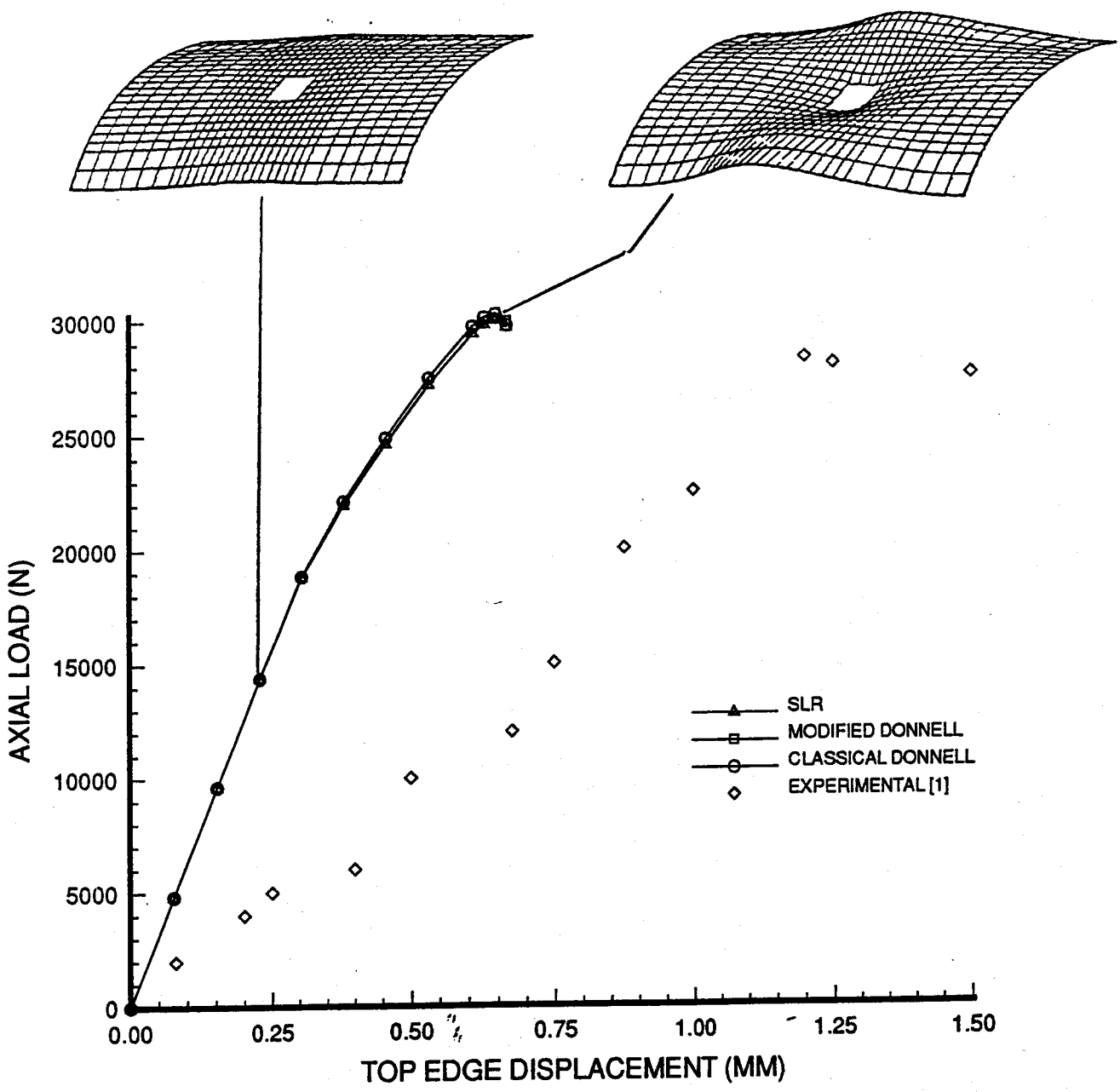

Figure 48: Load vs. Top Edge Displacement, Comparing Experimental to SLR, Modified Donnell, and Classical Donnell, 50.8 mm x 50.8 mm (2" x 2") Cutout, 304.8 mm x 508 mm (12" x 20") Panel [0/45/-45/90]2s

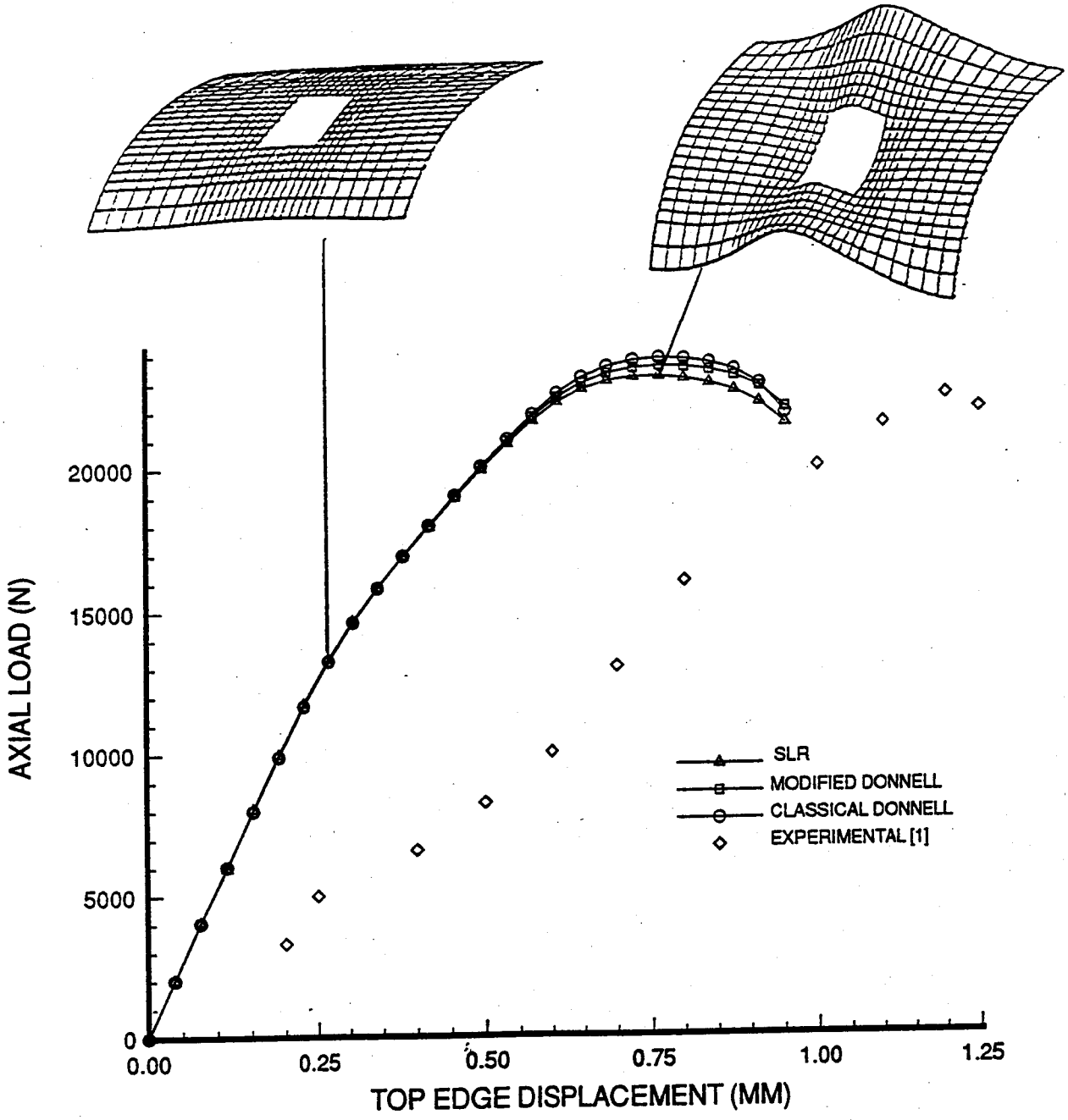

Figure 49: Load vs. Top Edge Displacement, Comparing Experimental to SLR, Modified Donnell, and Classical Donnell, 101.6 mm x 101.6 mm (4" x 4") Cutout, 304.8 mm x 508 mm (12" x 20") Panel [0/45/-45/90]2s

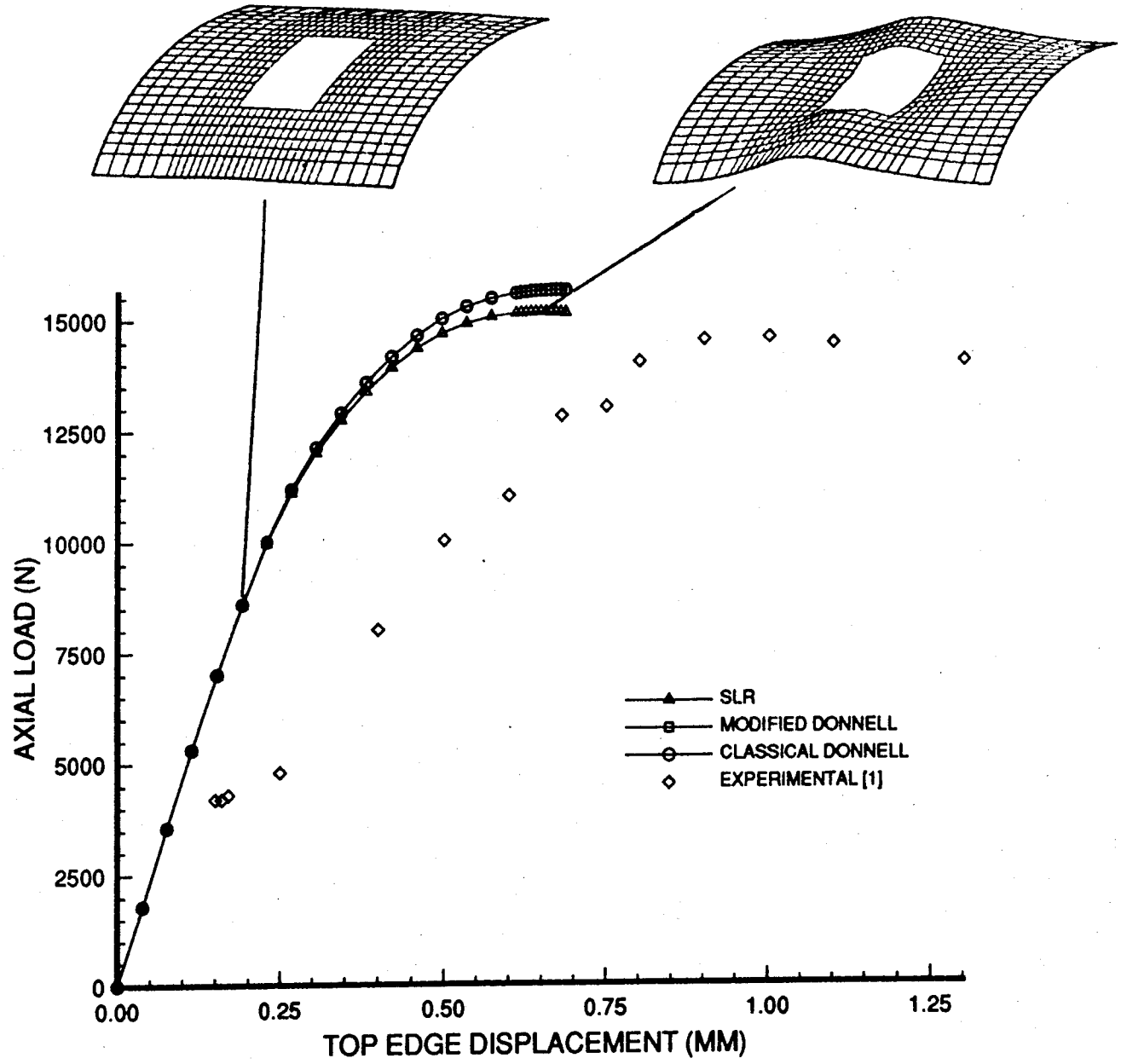

Figure 50: Load vs. Top Edge Displacement, Comparing Experimental to SLR, Modified Donnell, and Classical Donnell, 127 mm x 127 mm (5" x 5") Cutout, 304.8 mm x 508 mm (12" x 20") Panel [0/45/-45/90]2s

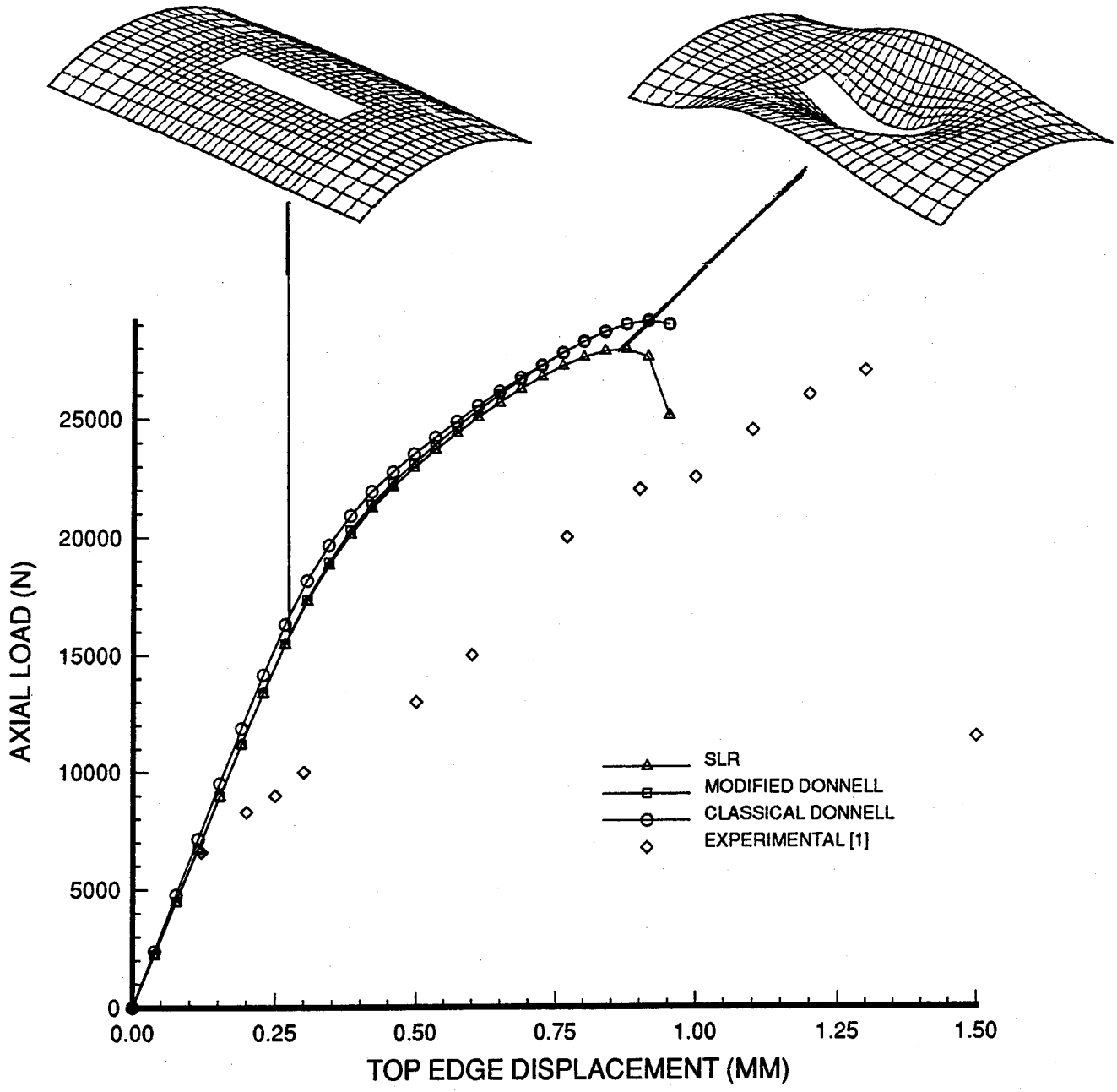

Figure 51: Load vs. Top Edge Displacement, Comparing Experimental to SLR, Modified Donnell, and Classical Donnell, 50.8 mm x 202.3 mm (2" x 8") Cutout, 304.8 mm x 508 mm (12" x 20") Panel [0/45/-45/90]2s

Vita

Lieutenant Christopher P. Chaplin was born on 17 January 1971 in Denver, Colorado. He graduated from Shawnee Mission South High School in Overland Park, Kansas in 1989 and attended the U.S. Air Force Academy. In June 1993 he graduated with a Bachelor of Science in Astronautical Engineering. Upon graduation, he received a regular commission in the USAF and served his first tour of duty as a masters student at the School of Engineering at the Air Force Institute of Technology in June 1993.

Permanent Address: 10246 Russell
Overland Park, KS 66212

REPORT DOCUMENTATION PAGE

Form Approved
OMB No. 0704-0188

1. AGENCY USE ONLY *(Leave blank)*	2. REPORT DATE	3. REPORT TYPE AND DATES COVERED
	December 1994	Master's Thesis

4. TITLE AND SUBTITLE
THE COLLAPSE OF COMPOSITE CYLINDRICAL PANELS WITH VARIOUS THICKNESS USING FINITE ELEMENT ANALYSIS

5. FUNDING NUMBERS

6. AUTHOR(S)
Christopher P. Chaplin, 2Lt., USAF

7. PERFORMING ORGANIZATION NAME(S) AND ADDRESS(ES)
Air Force Institute of Technology, WPAFB, OH 45433-6583

8. PERFORMING ORGANIZATION REPORT NUMBER
AFIT/GA/ENY/94D-4

9. SPONSORING / MONITORING AGENCY NAME(S) AND ADDRESS(ES)
Dr. Arnold Mayer
WL/FIV
Wright-Patterson AFB, OH 45433

10. SPONSORING / MONITORING AGENCY REPORT NUMBER

11. SUPPLEMENTARY NOTES

12a. DISTRIBUTION / AVAILABILITY STATEMENT
Approved for public release; distribution unlimited

12b. DISTRIBUTION CODE

13. ABSTRACT *(Maximum 200 words)*

This study compared numerical collapse results of graphite/epoxy cylindrical panels with free vertical edges undergoing axial compression for three different shell theories. Symmetric quasi-isotropic laminates were investigated using solid panels and panels with five different centralized cutouts with three thicknesses. The theories compared in the study were the Simplified Large displacement moderate Rotation (SLR) theory, the Donnell Cylindrical Shell (Modified Donnell) theory, and the Classical Donnell theory. The purpose of the study was to determine when large rotations and through-the-thickness shear become important in the numerical collapse analysis of cylindrical composite shells. By observing cases where the numerical collapse results for each of the three theories differed noticeably (>3%), it could be determined when large rotations and through-the-thickness shear were important. The effects of large rotations were noticed in nearly all of the panels with large cutouts (>3% panel area). Large rotations were also found to be important for thicker panels with either no cutout or a small cutout. The effects of through-the-thickness shear were only noticed in the thickest panels with large cutouts.

14. SUBJECT TERMS
Composites, Shells, Cylindrical Panels, Cutouts, Finite Elements, Nonlinear Analysis, Transverse Shear, Geometric Instability, Collapse, Graphite/Epoxy

15. NUMBER OF PAGES
133

16. PRICE CODE

17. SECURITY CLASSIFICATION OF REPORT	18. SECURITY CLASSIFICATION OF THIS PAGE	19. SECURITY CLASSIFICATION OF ABSTRACT	20. LIMITATION OF ABSTRACT
Unclassified	Unclassified	Unclassified	UL